

G E O L O G I C A U L T R A I E C T I N A

Mededelingen van de
Faculteit Aardwetenschappen
Universiteit Utrecht
no. 217

**THE ALKALI-SILICA REACTION:
MINERALOGICAL AND GEOCHEMICAL
ASPECTS OF SOME DUTCH CONCRETES
AND NORWEGIAN MYLONITES.**

Maarten A.T.M. Broekmans

ISBN 90 - 5744 - 074 - 1

**THE ALKALI-SILICA REACTION:
MINERALOGICAL AND GEOCHEMICAL
ASPECTS OF SOME DUTCH CONCRETES
AND NORWEGIAN MYLONITES.**

De alkali-silica reactie: mineralogische en geochemische aspecten van
enige Nederlandse betonnen en Noorse mylonieten.
(met een samenvatting in het Nederlands)

Alkali-silika reaksjonen: mineralogiske og geokjemiske aspekter fra
noen nederlandske betonger og norske mylonitter.
(med en sammendrag på norsk)

Proefschrift

Ter verkrijging van de graad van doctor aan de Universiteit van Utrecht
op gezag van de Rector Magnificus, Professor doctor W.H. Gispen,
ingevolge het Besluit van het College voor Promoties
in het openbaar te verdedigen op maandag 18 februari 2002
des namiddags 16.15 uur

door
MARINUS ANTONIUS THOMAS MARIA BROEKMANS,
geboren op 16 mei 1963 te Rotterdam.

promotor: Professor doctor R.D. Schuiling, faculteit Aardwetenschappen

dit proefschrift werd mede mogelijk gemaakt met financiële steun van
de Nederlandse Rijkswaterstaat en
Norges geologische undersøkelse

**Veel herder dan in stael, in koper oft pourphier,
Heb' ick dit werck volbroght,**

soo dat de loop der Jaren,
Noch d'Water, noch de Windt, noch oock Mulsiberscharen,
Dat selfde nimmermeer en sullen scheynden fier:

Als mynen lesten dagh my sal doen slapen schier,
Dan en sal Vander Noot niet al gaen inder baren:
Want siet zijn boeck sal dan synen naem bat verklaren
Dan Marmer of Pourphier, al en ist maer papier

Het welck dan over alle jeughdigh, cloeck t'allen tyden,
Sal vlighen (wiet benijdt) om dat ick my gheveughdt
Heb' tot dat eerlijck werck, d'welck den Musen gheneughdt.

Musa wel aen, vlieghdt op, en boodschapt met verblyden,
Inden hemel, dat ick alree heb overwonnen,
Deur uulie jonste goedt, deur d'werck med u begonnen.

Sonnet by Jan van der Noot
Dutch poet, 1538-ca.1596

Aan mijn ouders

Abstract

Chapter 1 of this thesis provides a brief outline of ASR history in general, followed by a summary on the history of ASR in the Netherlands. The first contributions date from 1957 and 1962, but the problem only regains attention 30 years later when ASR is rediscovered in the early 1990's. First regarded as a curiosity, a considerable research effort is paid from the mid-1990's until present. Subsequently, a brief history on the Norwegian situation is provided, where ASR was speculated for the first time in 1962. Extensive mapping of field structures was conducted from 1990-1993 in Southern Norway, and in 1993-1996 in Northern Norway. This has resulted into a number of Masters and PhD-theses at the Technical University of Trondheim. Currently, Norwegian ASR research is coordinated by the Forum on Alkali-Reactions In Norway with the acronym FARIN.

Chapter 2 presents results from detailed petrographic and geochemical analysis of concrete from Dutch structures Heemraadsingel, Wolput and Vlijmen-Oost on main road A59 and from structure KW5 at Zaltbommel. Petrographic results imply that not only chert but also sand-/siltstone is violently alkali-reactive and might release alkalies. Geochemical results further suggest a strong correlation between the amount of damage and the bulk alkali concentration. The results presented here serve as a basis for the work presented in following Chapters on concrete from Heemraadsingel and KW5 at Zaltbommel. Both structures have been sacrificed to science by the Dutch Ministry of Transport and Water Works who owned the structures.

Chapter 3 discusses results from petrographic analysis and chloride profiles of concrete from former structures Heemraadsingel and KW5 at Zaltbommel. Five (3+2) complete vertical cross-sections of the decks were each divided in 16 equal parts. The amount of damage was rated according to a damage rating index (DRI) and plotted as a 16-section depth profile of chloride concentrations. There is a striking coincidence between the DRI and the chloride content, even though the latter is generally very low. This is attributed to infiltration of dissolved deicing salt along the crack fabric, implying that the concrete is accessible for fluids.

Chapter 4 presents alkali concentrations measured by XRF on bulk concrete, and by ICP-AES after selective acid digestion on the cement paste, in 16-section depth profiles on the very same samples as in Chapter 3. The alkali concentration of the aggregate material is calculated by subtraction XRF minus ICP-AES. The results show no straight-forward coincidence between DRI and alkali-content. This is attributed to the fact that alkalies derived from the paste on one site (local depletion) may infiltrate concrete elsewhere (local enrichment). Alternatively, the paste may be locally enriched in alkalies derived from clay minerals and/or mica from the aggregate material.

Chapter 5 presents element maps for K, Na, Ca, Si, Fe, and S, for intact and ASR-cracked chert, and intact and ASR-cracked sandstone. Intact chert appears dense and inaccessible, whereas in cracked chert K, Na and Ca enter the grain margin through the initial porosity or through the ASR-induced crack, while Si is extruded from the grain. In intact sandstone, Ca enters the initial pore fabric and K and Na seem immobile. In the ASR-cracked sandstone Ca enters the grain, however, K, Na, and Si are all extruded through the crack in a gel plug. In all situations, Fe and S appear immobile. It is argued that the extruded K and Na may have been released by interstitial (diagenetic) clay minerals.

Chapter 6 presents crystallinity indices $<1-10$ for handpicked quartz from Norwegian mylonites (8.5-10.2), and for bulk Ohio cherts (1.8-7.3) and Dutch cherts ($<1-7.1$). Results are compared with previously published data on the very same samples, including DTA/TGA and expansion testing data. No universal, consistent correlation between the crystallinity index and other data appears to be present, and it is argued that the crystallinity index in its current definition may be affected by many different and unquantified parameters in the crystal lattice.

Finally, Chapter 7 reviews several parameters controlling or affecting silica dissolution under geological conditions from the viewpoint of undesired silica dissolution in alkali-silica reaction attacked concrete.

Samenvatting in het Nederlands

Hoofdstuk 1 van dit proefschrift schetst in grote lijnen de historie van ASR, gevolgd door een korte samenvatting van de geschiedenis van ASR in Nederland. De eerste bijdragen dateren van 1957 en 1962, maar het probleem krijgt pas aandacht als 30 jaar later in het begin van de 1990's ASR herontdekt wordt. Van het midden der 90'er jaren tot heden wordt aan ASR uitgebreid aandacht besteedt. Vervolgens wordt een korte historie van de Noorse ASR-situatie geschetst, waarin in 1962 voor het eerst daarover gespeculeerd werd. Van 1990-1993 zijn zuid-Noorse constructies gekarterd, van 1993-1996 noord-Noorse. Een en ander is uitgemond in een aantal afstudeer- en promotie-onderzoeken aan de Technische Universiteit van Trondheim. Heden wordt Noors ASR-onderzoek gecoördineerd door het Forum voor Alkali-Reacties In Noorwegen met het acronym FARIN.

Hoofdstuk 2 presenteert resultaten van gedetailleerd petrografisch en geochemisch onderzoek aan beton van constructies Heemraadsingel, Wolput en Vlijmen-Oost in de A59, en van KW5 te Zaltbommel. Petrografisch onderzoek geeft aan dat niet alleen chert maar ook zand-/siltsteen hevig alkali-reactief is, en eventueel alkali loslaat. Resultaten van geochemisch onderzoek suggereren een sterke samenhang tussen de hoeveelheid schade en de bulk alkali concentratie. De hier gepresenteerde resultaten dienen als basis voor verder werk op beton van Heemraadsingel en KW5 te Zaltbommel in navolgende Hoofdstukken. Beide genoemde constructies zijn door voormalig eigenaar Rijkswaterstaat aan de wetenschap geofferd.

Hoofdstuk 3 bediscussieert resultaten van petrografische analyse en chlorideprofielen van beton van Heemraadsingel en KW5 te Zaltbommel. Vijf (3+2) complete rijdek-doorsneden zijn daartoe verdeeld in 16 gelijke delen. De hoeveelheid schade is geïndexeerd (DRI), en geplot als een chloride-diepteprofiel met 16 secties. De samenhang tussen DRI en chloride-diepteprofiel is in het oog springend, hoewel het chloridegehalte in het algemeen laag is. Dat wordt toegedragen aan de infiltratie van dooizout langs het scheurmaaksel, ergo is het beton toegankelijk voor vloeistoffen.

Hoofdstuk 4 presenteert alkaliconcentraties volgens XRF voor bulk beton, en volgens ICP-AES na selectieve zuur-ontsluiting van de cement pasta, in diepteprofielen van 16 secties van dezelfde monsters als in Hoofdstuk 3. Het alkaligehalte van de toeslag is berekend uit het verschil XRF minus ICP-AES. De resultaten wijzen niet op een rechttoe-rechtaan samenhang tussen DRI en alkaligehalte. Dit wordt toegewezen aan het lokaal uitloggen van alkali (verarming) dat elders infiltreert (aanrijking). Een alternatief kan zijn dat de cementpasta lokaal aangerijkt is met alkali uit kleimineralen en/of mica uit de toeslag.

Hoofdstuk 5 geeft elementverdelingen voor K, Na, Ca, Si, Fe, en S, in intacte en door ASR gescheurde chert, en intacte en door ASR gescheurde zandsteen. Intacte chert lijkt ondoordringbaar voor elementen van buitenaf, terwijl in gescheurde chert K, Na en Ca binnendringen via de poriën en/of de scheur, en Si als gel geëxtrudeerd wordt. In intacte zandsteen treedt Ca binnen langs de korrelgrenzen en lijken K en Na immobiel. In de door ASR gescheurde zandsteen treedt Ca ook zo binnen, echter K, Na, en Si worden allen in een gel-plug langs de scheur geëxtrudeerd. Fe en S lijken in alle gevallen immobiel. Er wordt aangevoerd dat de geëxtrudeerde K en Na afkomstig kan zijn van interstitiële (diagenetische) kleimineralen in de zandsteen.

Hoofdstuk 6 geeft kristalliniteitsindices $<1-10$ voor hand gezuiverde kwarts van Noorse mylonieten (8.5-10.2), en voor bulk Ohio cherts (1.8-7.3) en Nederlandse cherts ($<1-7.1$). Resultaten worden vergeleken met eerder gepubliceerde data van dezelfde monsters, inbegrepen DTA/TGA en expansietests. Een universele consequente samenhang tussen kristalliniteitsindex en de overige data lijkt niet aanwezig, en er wordt beargumenteerd dat de kristalliniteitsindex in de huidige definitie afhankelijk is van verschillende en niet-gekwantificeerde parameters in het kwarts kristalrooster.

Tenslotte geeft Hoofdstuk 7 een overzicht van diverse parameters die het oplossen van silica onder geologische omstandigheden kunnen beïnvloeden, in samenhang met ongewenst oplossen van silica zoals in door de alkali-silica reactie aangetast beton.

Sammendrag på norsk

Kapittel 1 skisserer ASR'ens historie i store trekk, fulgt av en sammendrag om ASR-historien in Nederland. De første bidragene er fra 1957 og 1962, men problemet får først ny oppmerksomhet 30 år senere etter ASR'ens gjenoppdagelse i begynnelsen av 1990'årene. Til tross at det i første omgang ble betraktet som kuriositet ble det utført en betydelig mengde forskning på ASR fra midt i 90-tallet opp til nå. Etter det følger en kort sammendrag om den norske ASR-situasjonen, der det ble spekulert om for første gang i 1962. Fra 1990-1993 ble det kartlagt sør-norske konstruksjoner, fra 1993-1996 nord-norske. Dette har ført til et antall hovedfag- og doktoravhandlinger ved det Norske Tekniske og Naturvitenskapelige Universitetet i Trondheim. Per dag i dag koordineres norsk ASR-forskning gjennom Forum for Alkali-Reaksjoner I Norge som lytter til akronymet FARIN.

Kapittel 2 gir detaljerte petrografiske og geokjemiske resultater fra betong fra konstruksjonene Heemraadsingel, Wolput og Vlijmen-Oost i hovedvei A59, og fra KW5 ved Zaltbommel. Petrografiske forskning antyder at ikke bare chert men også sand-/siltstein er kraftig alkali-reaktive, og eventuelt slipper ut alkalier. Geokjemiske resultater suggererer en klar sammenheng mellom skademengden og bulk alkalikonsentrasjon. De her resultater brukes gjennom resten av avhandlingen i følgende Kapitler på betong fra Heemraadsingel og KW5 te Zaltbommel. Begge konstruksjoner ble ofret til vitenskapet av tidligere eieren, 'det nederlandske Veidirektoratet' Rijkswaterstaat.

Kapittel 3 diskuterer resultatene fra petrografiske analyse og kloridprofiler av betong fra Heemraadsingel og KW5 te Zaltbommel. Fem (3+2) fullstendige brodekke seksjoner ble delt opp i 16 like deler. Skademengden ble indeksert etter et nytt skjema (DRI) og plottet som en kloridprofil i 16 seksjoner. Sammenhengen mellom DRI og kloridprofilen er iøynefallende, selv om kloridkonsentrasjonene er i gjennomsnittet lave. Dette skyldes til infiltrasjon av veisalt gjennom sprekke mønsteret, som antyder at betongen er tilgjengelig for fluider.

Kapittel 4 gir alkalikonsentrasjoner fra XRF i bulk betong, og fra ICP-AES etter deloppslutning av sementstein i syre, i 16 seksjoners dypdeprofiler fra samme prøvene som i Kapittel 3. Tilslagsmaterialets alkaliinnhold ble beregnet som forskjellen XRF minus ICP-AES. Resultatene antyder ikke en rett frem sammenheng mellom DRI og alkaliinnhold. Dette vies til lokal utlutning av alkali (forarming) som infiltrerer ellers (anrikning). Et alternativ kan være at sementpastaen ble anrikt med alkalier fra leirmineraler eller/og mika i tilslagsmaterialet.

Kapittel 5 gir elementfordelinger for K, Na, Ca, Si, Fe, og S, i hel og ASR-oppsprukket chert, og i hel og ASR-oppsprukket sandstein. Hel chert virker ugjennomtrengelig for elementer utenfra, mens i oppsprukket chert K, Na, og Ca trenger inn gjennom porer eller/og sprekken, og Si skvises ut som gel. I hel sandstein trer Ca inn langs korn grensene, og K og Na virker immobil. Ca trenger på lik måte inn i ASR-oppsprukket sandstein, men derimot blir K, Na og Si alle skviset ut i en gel-plugg. Fe og S virker i alle situasjoner immobil. Det argumenteres at K og Na kan stamme fra diagenetiske leirmineraler i sandsteinens porer.

Kapittel 6 gir kristallinitetsindekser $<1-10$ for håndplukkete kvartser fra norske mylonitter (8.5-10.2), bulk Ohio chert (1.8-7.3) og nederlandske chert ($<1-7.1$). Resultatene sammenlignes med tidligere publiserte data på de samme prøvene, DTA/TGA og ekspansjonsforsøk inkludert. En universell konsekvent sammenheng mellom kristallinitetsindeks og øvrige data synes ikke, og det argumenteres at kristallinitetsindeksen i sin nåværende definisjon kan påvirkes av flere ulike og ikke-kvantifiserte parametere i kvartsenes kristallgitter.

Til slutt gir Kapittel 7 en oversikt fra diverse parametere som kan påvirke oppløsning av silika under geologiske forhold, sett i lyset av uønsket oppløsning av silika i av alkali-silika reaksjonen angrepet betong.

Table of Contents

Abstract	7
Samenvatting in het Nederlands	8
Sammendrag på norsk	9
General Introduction	15
1 The history of ASR	15
2 The Dutch history of ASR	15
2.1 Before 1991	
2.2 After 1991	
2.3 National guidelines	
2.4 Recent Dutch developments in structure assessment	
2.5 Recent Dutch developments in aggregate assessment	
3 The Norwegian history of ASR	20
4 Thesis history	22
ASR in Four Dutch Viaducts:	
Petrographic Characterization and	
Bulk Geochemistry	23
1 Introduction	23
2 Sample extraction and handling	24
3 Analytical methods	25
3.1 Petrography	
3.2 Chemistry	
4 Results	26
4.1 Petrography	
4.2 Geochemistry	
5 Interpretation and discussion	30
5.1 General	
5.2 Silica dissolution in natural systems	
5.3 Silica dissolution in concrete by ASR	
6 Conclusions	32
A Simple and Straight-forward Damage Rating Index	
and its Correlation with Infiltrated Chloride	47
1 Introduction	47
2 Sampling and experimental methods	48
2.1 Sampling	
2.2 Petrography	
2.3 Ion-selective electrode	

3	Results	50
	3.1 Data presentation	
	3.2 Petrographic observations	
	3.3 Cracks and crack distribution	
4	Discussion	51
	4.1 Cracks and crack distribution	
	4.2 Correlation of DRI with chloride content	
	4.3 The central portion of core BB246	
5	Conclusions	53
Origin and Mobility of Alkalies in		
Two Dutch ASR-concretes:		
Correlation with the Damage Rating Index		55
1	Introduction	55
2	Experimental methods	56
	2.2 Geochemistry	
3	Results	57
	3.1 Petrographic observations	
	3.2 Na ₂ O-equivalents (Na ₂ O _{eq} 's)	
	3.3 Reverse calculation of the cement content	
4	Discussion	59
	4.1 Trends in the alkali profiles	
	4.2 Reverse calculation of the cement content	
	4.3 Statistical analysis	
	4.4 Trends in the scattergraphs, and a speculative model	
	4.5 Reactive aggregate constituents	
5	Conclusions	63
Microscale Element Distribution		
Around Chert and Sandstone		65
1	Introduction	65
2	Experimental methods	66
3	Results	66
	3.1 Data presentation	
	3.2 Figure 1/Plate 13: intact chert	
	3.3 Figure 2/Plate 14: cracked chert	
	3.4 Figure 3/Plate 15: intact sandstone	
	3.5 Figure 4/Plate 16: cracked sandstone	
4	Discussion	71
5	Conclusions	72
On the Crystallinity Indices		
of Some Norwegian Mylonites,		
and Some Ohio and Dutch Cherts		75
1	Introduction	75
2	Samples	76
3	Analytical techniques	76
	3.1 General	
	3.2 Sample preparation	
	3.3 X-ray diffractometry (XRD)	
	3.4 Differential thermal analysis/thermogravimetric analysis (DTA/TGA)	

4	Results	79
	4.1 Data presentation	
	4.2 X-ray diffraction	
	4.3 Differential thermal analysis	
5	Discussion	80
	5.1 Crystallinity index	
	5.2 Quartz crystallinity	
	5.3 Quartz alkali-reactivity	
6	Conclusions and suggestions for further research	84
Silica Dissolution Related to the		
Alkali-Silica Reaction: A Review 91		
1	Introduction	91
2	Silica in the geological environment	91
	2.1 Silica polymorphs and varieties	
	2.2 Silica dissolution controls	
3	Comparison with silica in the concrete environment	99
	3.1 Geological vs. ambient conditions	
	3.2 Silica dissolution	
4	Conclusions	102
Summary 107		
Acknowledgments 109		
References 111		
Curriculum Vitae 125		
Color Plates 127		

General Introduction

1 The history of ASR

Stanton explicitly describes the alkali-silica reaction for the first time in 1940 in a legendary article entitled “Expansion of concrete through reaction between cement and aggregate.” [1]. The title immediately explains the classical model for the alkali-silica reaction: certain aggregate constituents react with alkalis from the cement paste, forming an alkali-silica gel that expands and breaks up the concrete. Though initially regarded as a curiosity, ASR was soon identified in many large structures, including large dams, ship locks, parking houses, main roads, pavements, et cetera, basically all over the world. However, earlier reports of interactions between cement and aggregate material do exist, even as early as from 1923 [2].

It was also soon recognized that the alkali-silica reaction was not restricted to one particular rock type nor region, and expansion testing was introduced already in the mid-forties, followed by the introduction of aggregate testing methods and assessment criteria, in many different countries all over the globe. During the same period, many experiments were conducted in the laboratory in an attempt to understand the intricacies and peculiarities of deleterious silica dissolution and gel formation under ASR conditions [eg. 3,4,5]. Thus, it was found that expansion was not merely a function of the alkali content, but rather of the ratio between contents of alkali and reactive aggregate. At a given ratio that may be different for different aggregate materials, experimental expansion reaches a maximum. This knowledge laid the foundation for the later pessimum concept. However, up til today it has proven difficult to transcript experimental results in terms of daily practice, for a complexity of reasons.

The following is for a large part based upon the extensive ‘Alkali-aggregate reactions in concrete: an annotated bibliography 1939-1991’, which provides an overview of world literature on ASR, listing more than two-thousand two-hundred (annotated) references [6].

2 The Dutch history of ASR

2.1 Before 1991

A thorough literature survey reveals that the first Dutch contribution to ASR knowledge dates from 1957, from the hand of Bosschaert [7]. He arguments against the general Dutch attitude back then that the use of different aggregate material together with a different cement composition provides adequate prevention for ASR. However, Bosschaert warns that in the long run, the particular combination of Dutch materials might also prove susceptible to deleterious ASR, with the state of knowledge he back then recognized as being full of voids and gaps. The article urges for caution in selecting (aggregate) materials and strongly recommends collaboration between civil engineers and mineralogists [8]. This is most probably the first publication to recognize ASR in Dutch concrete though without applying thin section petrography, and the author makes plausible arguments that the damage described by another article may be attributed to ASR too [9].

The next Dutch contribution to ASR-literature dates from 1962 [10] and is also listed in Diamonds' bibliography [6]. The article bears the more general character of a review. Of the European countries only Denmark is referred to have alkali-reactive aggregate, whereas Great-Britain is mentioned to be free of such deleterious materials. Furthermore, the article provides first experimental expansion data on Dutch aggregate materials.

The authors explicitly state that only opal expands significantly, and that the expansion of all other investigated materials (chalcedony, flint, siliceous) is negligible, even after two years of exposure to Portland cement. Expansion maximum (pessimum) is reported to occur at around 2.5% content of opaline silica and was also found to correlate with grain size, in good agreement with previous results by others. Fluvial sands from the Meuse river were found innocuous. In their final summary, the authors state "...the crypto-crystalline forms of SiO₂ are inaccurately marked as deleterious...". Their final conclusion "It is highly unlikely that ... the Dutch aggregate material contains (alkali) reactive constituents." could perhaps be held responsible for the fact that ASR was neglected in the Netherlands for almost three subsequent decades.

In 1980, a PhD-thesis by a Dutch author discussing the influence of blast furnace slag cement on ASR and/or sulphate corrosion is published by the Technical University of Aachen in Germany [11]. Most of the positive effects are attributed to the immobilization of alkalis and to the different porosity distribution of slag cement. In 1988, more than thirty years after the first Dutch article by Bosschaert, Flemish author De Ceukelaire reports ASR as the most likely cause for the deterioration of a then 20-some year old structure [12]. Alkali-silica reaction of porous chert in the fine aggregate was held responsible for the damage. The pre-tensioned viaduct in the peripheral highway around the Belgian capitol Brussels had hand wide cracks over almost its entire length, and was demolished in the night of April 27, 1995 using explosives.

The proceedings of the 8th International Conference on Alkali-Aggregate Reactions in Concrete held in Kyoto, Japan in 1989 contain two contributions by Flemish authors Soers and Meyskens [13] and Van Gemert [14], as well as two papers co-authored by Larbi [15,16], at that time a PhD-student at the Technical University of Delft. With the same (co-) author Hudec, Larbi published two more papers on rapid testing of the alkali-reactivity potential of rocks [17,18], in 1989 and 1990, respectively.

In 1990, Flemish authors Soers and Meyskens published a general overview on Belgian ASR in the Dutch periodical *Cement* [19]. At the time of writing, ASR had been recognized in some twenty-five Belgian structures, including both in-situ poured and prefabricated concrete, and some structures had been replaced already. Their subtitle "Extended quality control a necessity" in fact reaffirms the original suggestions published in the same periodical in 1957 [7]. However, none of the papers mentioned above confirms a Dutch occurrence of ASR.

2.2 *After 1991*

The first time that ASR in Dutch concrete was unequivocally confirmed by petrography dates from 1991 [20]. This article is not listed in [6] and nor are [12,19], somewhat strange as they were all published in the same periodical as [7] in 1957 and [10] in 1962. The article describes ASR as the main cause for the deterioration in a two-lane viaduct in a local road near Schoonhoven. The damage consisted of intensive surface cracking and leaching of the concrete with the concomitant formation of lime stalactites. The reluctant identification of

ASR as the primary cause for the damage was partly due to limited access to the structure for a appropriate structural assessment and sample extraction.

Porous chert is reported as the main alkali-reactive constituent in the coarse aggregate, though alkali-silica reaction products also have been observed in cracks in sericitic sandstone (ie. containing fine-grained muscovite). Macroscopic cracks were assumed not to run very deep from the surface, and a more thorough assessment of the (macroscopic) crack fabric was considered useful and said to be included in further research [p.11 in 20]. However, later publications by the same author with various co-authors do neither contain nor refer to such data [21,22].

Until some time after its discovery, the Schoonhoven ASR-case was considered an isolated and incidental curiosity. The article furthermore reaffirms the general conviction of the immunity of Dutch concrete for deleterious ASR [p.11 in 20] that apparently had persisted despite suggestions made in 1957 [7]. In 1962, this immunity was attributed to lack of alkali-silica reactive constituents in Dutch aggregate material [10; see above]. The article describing the Schoonhoven ASR-case cannot subscribe to this argument and rather attributes this (suddenly only relative) immunity mainly to the extensive use of cements with a high slag content together with the less extensive use of high water/cement-ratio concrete mixes. However, data supporting these statements have not been found published yet [20,21].

2.3 *National guidelines*

In March 1991, the same year as when the Schoonhoven ASR-case was first published, the Dutch legislative organisation ‘Civieltechnisch Centrum voor Uitvoering van Research en Regelgeving’ CUR established technical committee B56 named ‘Alkali-silica reaction in concrete’, with its initial objectives defined as [23]:

1. Identification of aggregate materials for Dutch concrete which are potentially ASR-deleterious, depending on winning location, through literature investigations and interviews,
2. To draft procedures for the assessment of the alkali-reactivity potential of aggregate materials for Dutch concrete,
3. To draft guidelines for the production of durable concrete with the use of potentially alkali-reactive aggregate materials, and finally
4. Communicating knowledge acquired with bullet points 1,2 and 3.

After “...undisputed occurrences of Dutch ASR had become known to the committee...” [ipse dixit p57 in 23], these were changed into the much more pragmatic objectives:

1. What causes the damage, and
2. How to prevent future damage.

In 1994, the B56 CUR-committee published CUR-recommendation 38 entitled ‘Measures to prevent damage by the alkali-silica reaction (ASR) in concrete’ [24], which in the accompanying article [23] is stated to provide an answer to the latter of both objectives. The recommendation is based upon data (unpublished) acquired from investigated ‘ASR-damaged structures’ in the Netherlands. The criteria from CUR-recommendation 38 are not to be used to assess data from existing structures, though this is not explicitly excluded in the recommendation’s applicability statement [§2 in 24]. Moreover, CUR-recommendation 38 was said to be based upon just that kind of data [p.60 in 23].

Furthermore, CUR-recommendation 38 provides four methods for assessing aggregate material prior to use in concrete, including:

1. Long-term experience with the use of that material in concrete,
2. Microscopic analysis of the mineralogical composition,
3. Experiments with mortar bars or concrete prisms, and/or
4. Chemical determination of the reactivity.

Long-term experience will only provide warranty against potential alkali-reactivity if unequivocally can be demonstrated that the aggregate material indeed has been exposed to ASR-conditions. Since these conditions are poorly defined (if at all), the only proof that the material has been exposed to such conditions is the presence of actually reacted alkali-reactive material. However, the latter concludes that the aggregate material is alkali-reactive and should therefore be rejected.

Furthermore, CUR-recommendation 38 failed to provide references to standard methods for bullets 2-4, nor does it provide acceptance/rejection criteria. To fill that omission, CUR-recommendation 38 was supplemented with two documents from the Ministry of the Flemish Community, Department of the Environment and Infrastructure [25,26]. The older document is a circular providing criteria for the maximum content of potentially alkali-reactive grains including porous chert, chalcedony and opal, differentiated for both coarse and fine aggregate materials. It furthermore provides an outline of the counting procedure [25]. The younger document is merely a code of conduct describing the procedures to follow for construction works [26].

Together with the stated criteria for maximum alkali-content of the cement and the final concrete mixture [both in 25 and 24], this should in principle guarantee that ASR would not occur in concrete produced following these guidelines. The Flemish circular explicitly states that ‘coarse-grained sandstone’ is considered innocuous to ASR. This is in contrast with earlier observations on Dutch concrete [20,21, 27,28,29,30], even from before the circular was supplemented to CUR-recommendation 38.

2.4 *Recent Dutch developments in structure assessment*

In 1992, three viaducts named Heemraadsingel, Hoogeindse Rondweg, and Wolput respectively, and one tunnel named HertogJanstraat, all in or over Dutch main road A59 were assessed [31]. The overall conclusion from petrographic analysis of cores extracted from two structures was that ASR did occur in structure Heemraadsingel, and that the tunnel HertogJanstraat *might* contain some grains of alkali-reactive aggregate [see 31]. The other structures were not included in the petrographic analyses.

The concrete structure Wolput was reinvestigated early Summer 1994, when the Dutch road authorities had reserved budget for rehabilitation of the structure. This time, ten cores for petrographic analysis on thin sections were extracted from locations spread over the entire structure, from both cracked and uncracked surface areas. The surface cracking was observed to be confined to certain parts of the structure, seemingly leaving large areas unaffected. However, all thin sections contained either reactive aggregate grains and/or silica-gel filled cracks, without exception, a sign that alkali-reactive aggregate grains were near [32]. Thus, the one justified conclusion had to be that ASR was present in all main parts of the structure, and that the strength of the concrete and the structure as a whole had been reduced by ASR-induced cracking to some degree which could not yet be quantified.

According to personal communication with the Dutch road authorities, Wolput was not the worst ASR-affected structure [33]. There were a few more significantly affected structures, and more importantly, with the knowledge at that time it was impossible to make a reliable estimate of the strength reduction. In 1995, this led to the establishment of a new CUR-committee C106 entitled “Structural aspects of the alkali-silica reaction in concrete structures”. Its main objectives were defined as:

1. Collecting knowledge on and experiences with ASR regarding structural aspects and (remaining) service life,
2. Drafting of procedures for the assessment of potentially ASR-affected structures,
3. Publishing the above procedures as an official CUR-recommendation.

Technical input to CUR-committee C106 was provided by pilot studies on structures Heemraadsingel, Wolput and Vlijmen-Oost that were commenced in 1996. These included both structural assessment [34,35] and detailed petrographic analysis and subsequent geochemical characterization [27,29]. Data on other structures (eg. KW5 at Zaltbommel) and (respective) concrete compositions were made accessible to the committee as they became available. Some of the obtained results were submitted at the 11th International Conference on Alkali-Aggregate Reactions in Concrete, held on June 11-16, 2000 in Québec, Canada [36,37,38].

The 1992 ISE-procedure for the assessment of potentially ASR-affected structures [39] was reassessed by the C106 committee to comply with Dutch building practice and ASR-experience [40]. At the time of publication of this thesis, a CUR-recommendation guiding the assessment of (potentially) ASR-attacked structures is in its final editing stages, and publication is expected within short.

2.5 Recent Dutch developments in aggregate assessment

Apart from the developments in structural civil engineering of ASR-structures, there are recent developments in the assessment of aggregate materials, with respect to analytical methods and the drafting of procedures and criteria, mainly based upon and supported by data on concrete from existing structures. In March 2000, CUR established a new research committee VC62 entitled “Alkali-silica reaction in concrete”, to produce a revision of the existing CUR-recommendation 38, with a detailed report to support the revised recommendation. Initially, the revised recommendation was scheduled for publication before June 1, 2001.

The project plan was ambitious and addressed several topics to resolve the ASR-problem:

1. Drafting an overview of current available ASR-specific knowledge on which subsequent research items will be specified in more detail,
2. Characterization of the alkali-reactivity potential of Dutch aggregate material,
3. Assessment and characterization of field structures in terms of CUR-recommendation 38,
4. ASR-mitigation by added blast-furnace slag and/or pulverized fly-ash, and
5. Alkali-attribution from internal and/or external resources.

Some of these topics alone would be worth a PhD-study and had thus to be restricted to very specific questions to meet the initial deadline. The overview as intended in bullet point 1 has recently been published in a report [41].

In February 2001, a one-day workshop followed by a one-day seminar was held at the Technical University of Delft, organized by the Dutch Ministry of Transport. The workshop critically assessed the reliability of (point) counting methods and counting statistics, reliability of sample extraction and sample size procedures and methods, and the identification of potentially alkali-reactive aggregate constituents. The subsequent seminar informed authorities and executives from the aggregate producing industry on the outcomes of the technical workshop sessions the day before, indicating the need for further research and discussion to reach general consensus.

A second two-day workshop was organized on 2-3 October 2001, with participants from all over Europe, USA and Canada. The workshop also included a half-day guided tour to a few Dutch concrete structures with ASR. Discussions addressed the applied different criteria for the minimum content of blast-furnace slag and/or pulverized fly-ash and/or the maximum alkali-content, and their combinations.

Per time of writing this thesis, a draft-revision of the current CUR-recommendation 38 is in the final stages of editing by CUR-committee VC62 members. The definitive revision will be published as a new CUR-recommendation which is expected early 2002.

3 The Norwegian history of ASR

The first Norwegian publication on ASR dates from 1962 when Musæus writes his graduation thesis on the topic during his studies at the University of Trondheim [42], however, he leaves the origin and nature of the observed alkali-silica gel unattended. In 1967, mortar bar experiments conducted by concrete legend Gunnar Idorn indicated that basaltic sands from Oslo apparently were alkali-reactive [43], though these have never been reported as deleterious in real life. Idorn also confirmed the ASR observed by Musæus in phyllites as being genuine, but unfortunately omits to relate his thin section observations to the scale of the structure as a whole.

The next contribution then dates from 1978, when ASR is presumed to be responsible for damage observed in an indoor swimming pool basin and a concrete foundation [44]. When the article was first published it received much scepticism, however, ASR was confirmed three years later in a report on the rehabilitation of the swimming pool [45].

A graduation thesis from the Norsk Teknisk Høyskole (NTH) in Trondheim on accelerated mortar bar testing experiments on Norwegian aggregate materials from 1986 remained unpublished [46]. In 1989, the Norwegian Water and Energy Administration (NVE) published a report on alkali-reactions in Norwegian concrete dams [47]. They investigated twenty-two power dams all of which had significant cracking. Nine dams were assessed in depth by petrographic analysis; ASR was diagnosed in eight of the dams. One year later, a final report mentions many more power dams to suffer severe cracking and further investigation is highly recommended [48].

From 1988 through 1991 several more reports dealing with diverse aspects of ASR were published, as well as a few more graduation theses from NTH that remained unpublished [eg. 49]. Together, these studies comprised a major research project running during the same period to investigate the alkali-aggregate reaction in southern Norway. Several instances were involved in the project, including Trondheim-based Sintef and the Geological Survey of Norway (NGU). Data from these studies were summarized in the PhD-thesis by Jensen [50, and references therein]. A similar project on ASR in the northern

parts of Norway ran from 1993 through 1996; results were published in a series of Sintef reports [51,52,53].

After 1991, the number of Norwegian publications on ASR really takes off, though the majority of publications are authored in Norwegian as research reports and contributions to Nordic periodicals. The proceedings of the International Conference on Alkali-Aggregate Reactions in Concrete (1992: London/UK, 1996: Melbourne/AU, 2000: Québec/CA) also contain several Norwegian contributions. Many deal with the examination and assessment of aggregate material and/or mortar bar testing. Two contributions stand out: the PhD-thesis by Jensen mentioned above because it provides an excellent overview of (southern) Norwegian ASR [50]. The other one is the PhD-thesis by Wigum that deals with some material properties, classification and testing of Norwegian cataclastic rocks [54], providing important tools in aggregate material assessment for ASR prevention.

Wigum introduced a point-counting method for thin sections to assess the alkali-reactivity potential of Norwegian mylonites. He establishes a correlation between the diameter of quartz grains within mylonite grains, which parameter may be translated by potential reaction surface [55]. The research path that Wigum had initiated in Norway was continued in 1996 as a pilot study for the NORMIN2000 project [56]. The pilot study recommended to concentrate ASR research on three issues:

1. Petrography as a method for aggregate assessment,
2. Accelerated mortar bar expansion testing, and
3. Assessment of field structures.

Expert committees were established for each issue.

In the same year, a national guideline was published by the Norwegian concrete society (Norsk Betongforening) [57], providing criteria for the maximum allowable alkali content of bulk concrete, cement and added fly-ash or silica fume. It also describes testing methods for aggregate materials and provides criteria for individual constituents, the maximum content, and how to deal with blended aggregate materials. The guideline has been known for a while to be outdated at certain points, however, its status remains unchanged until a revised version will be published.

The NORMIN2000 main ASR-project was commenced early 1997 and finished as scheduled by the end of 1998. The final report was published in March 1999 [58] and contains a picture atlas of (Norwegian) aggregate materials, including both potentially reactive and innocuous rock types. The document contains a wealth of all kinds of data related to ASR, but after ample discussion the petrography expert committee found that despite the contribution of the newly obtained data, there were still many voids in essential knowledge. Time and money were lacking to fill in these voids within the running main project for NORMIN2000. Thus, to institutionalize Norwegian ASR-research and to ensure its continuity, a research forum was established in March 1999 with the name FARIN, which acronym stands for Forum for Alkali-Reactions In Norway [59,60]. FARIN has continued research on petrographic analysis of aggregate materials, concentrating on point counting statistics, reliability and uniformity of obtained data, education and accreditation of (future) petrographers, and the revision of the current national guideline for ASR-prevention [57].

4 Thesis history

The idea to pursue this PhD-research gradually took shape during the first few years of the authors' employment at Nebest BV, Groot-Ammers, in the period from 1993-1995.

Routine thin section analysis on deteriorated (often ASR-suspect) structures revealed that some cherts seemed alkali-reactive and some not, and likewise for sandstones. This rose questions as to whether this was to be attributed to the nature of thin sections being a thin slice of rock, or to the specific properties of the alkali-reactive grains, or both. Grant NM95064 from the Dutch research program "PBTS-materiaaltechnologie 1995" was used for the geochemical characterization of a number of (Dutch) concrete samples, aggregate materials, cements, and other materials used in concrete production [61].

The Dutch aggregate materials proved to be very rich in silica (from 88-98wt% SiO₂, typically >94wt%), typical for mature (reworked) sediment. Petrographic analysis showed that the content of acid soluble constituents in the aggregate material is negligible. Thus, to separate cement paste from aggregate materials in geochemical characterization, selective acid dissolution could be used. Furthermore, post-processing of analytical results was expected to be easier for bulk concrete could be represented in a fair first approximation as a mixture of quartz aggregate and cement. This was a clear advantage as compared to Norwegian aggregate that may contain a significant amount of acid soluble constituents. Some results from detailed petrographic analysis and geochemical characterization have been published in previous contributions [28,29]. The combined results from both disciplines strongly suggested some correlation between the amount of cracking and the alkali-content of the bulk concrete, which the Dutch Ministry of Transport and Water Works 'Rijkswaterstaat' considered worth to investigate in further detail. To further improve sample representativity and data reliability, new samples would preferably have to be larger than the ones previously extracted, and thus sample availability posed a problem. In Norway, Wigum met similar problems during his PhD-research [62].

In 1999, Rijkswaterstaat 'fortunately' decided to sacrifice two structures to science, for four point bending strength testing on large beams cut from the structures. After the testing, several sets of cores were extracted from the seemingly unaffected ends of the bent beams. These are the cores that have been investigated in this thesis.

ASR in Four Dutch Viaducts: Petrographic Characterization and Bulk Geochemistry

Synthesized from:

Broekmans, MATM, and Jansen, JBH (1997): ASR in impure sandstone: mineralogy and chemistry. In: Sveinsdóttir, EL (editor): Proceedings of the 6th Euroseminar on Microscopy Applied to Building Materials, Reykjavik, Iceland: 161-76;

Broekmans, MATM, and Jansen, JBH (1998): Silica dissolution in impure sandstone: application to concrete. In: Vriend, SP, and Zijlstra, JJP (editors): Proceedings of the Conference on Geochemical Engineering: Current Applications and Future Trends. Journal of Geochemical Exploration, Special Volume (62): 311-8; and:

Broekmans, MATM, and Jansen, JBH (1998): Possibility of enhanced silica dissolution in concrete as in diagenetically altered sandstone. NGU-Bulletin (433): 42-3.

1 Introduction

In 1992, the concrete structures Heemraadsingel, Wolput, and Vlijmen-Oost in and over the A59 main road were tentatively investigated, of which only Wolput was suspect to ASR. In 1994, an in-depth assessment was made of this structure, prior to its planned rehabilitation. However, the conclusion reached was that even though the structure seemed only partially affected, ASR was also present in superficially uncracked, supposedly healthy parts. The Dutch Ministry of Transport and Water Works 'Rijkswaterstaat' pointed out that Wolput was not the structure worst affected by ASR. During a quick survey along the A59 road including some forty structures, many more were found to show signs of deterioration potentially caused by ASR.

This initiated the establishment of CUR-committee C106 "Structural aspects of alkali-silica reaction in concrete structures" in 1995, with its mission defined as "to draft a procedure for the assessment of the bearing capacity of concrete structures with ASR". Internationally, several procedures to assess existing structures subject to ASR have been developed. CUR-C106 has chosen to reconcile the ISE-procedure [63] to fit the Dutch building tradition. In other European countries, similar assessment procedures are currently under development [64,56,58].

In 1996, a pilot study was conducted on the same three structures mentioned above, to gather data on the civil engineering as well as mineralogical and geochemical properties of the concrete. Mechanical data have been reported in [65], and later large-scale experimental results on beams cut from Heemraadsingel have been published in [66,36].

In 1999, a twin deck viaduct on the former Dutch main road A2 became obsolete due to major reconstruction works. During demolition of one deck, the presence of ASR was identified, and in consequence the second deck was sacrificed to science. That deck was sampled in a way similar to the three structures mentioned previously.

Traditionally, chert as a form of microporous and poorly crystalline silica was assumed to be the main cause of ASR in Dutch concrete [21], although later research clearly revealed that other aggregate constituents could also be subject to a deleterious ASR [67], as has long been known from other countries [eg. 68,69,50,54]. Moreover, suggestions for a characterization of Dutch aggregate materials with regard to ASR had already been proposed as early as 1957 [7], and some preliminary experiments with Dutch chert had been done as early as 1962 [10].

The identification of reactive materials in this particular concrete was therefore considered of major importance, as well as eventually occurring alkali-release. Though OPC (as used in these concretes) ordinarily usually contain enough alkalies to initiate deleterious ASR, alkalies introduced from other resources may potentially help initiate, enhance or sustain ASR. Thus, eventual alkali-release by aggregate material was included in the research.

Mineralogical and geochemical data were first presented to the CUR-C106 committee [27] and subsequently published in [28,29,30]. In essence, this chapter comprises an updated and revised merger of [28] and [29]. A summary of the assessment procedures followed, in-situ and laboratory experiments as well as an outline of a monitoring program conducted on several structures on the A59 main road is given in [70].

2 Sample extraction and handling

Three grades of ASR-damaged concrete were selected, judged from surficial appearance. Thus, concrete cores were drilled from areas with no visible surficial cracking and from the worst cracked area on the structure. Finally, cores were extracted from areas with cracking intermediate between the extremes.

Typically, the worst cracked concrete has a moist surface with pendant stalactites up to 120mm in length. Though stalactites are in principle not diagnostic for ASR, they are indicative of significant fluid transport. The surface is densely map-cracked with cracks up to 3mm in width. Intermediately attacked concrete does not carry stalactites and contains fewer and thinner cracks up to 0.5mm wide. The least cracked concrete displays no deep cracks at all, and only occasionally a very thin surface craquelé.

In all, nine cores of $\varnothing 100$ mm by at least 400 mm length and weighing ~ 7.5 kg each were extracted by careful drilling, using a securely fixed boom stand to reduce introduction of new cracks. To avoid contamination by adhering sludge, drilled cores were immediately rinsed with minimal water as they came out. However, some slurry did adhere to the cores from the Zaltbommel structure, indicating inadequate rinsing. Prior to further preparation, the lowermost 100mm of each core (~ 1.8 kg) was carefully removed by near-dry diamond cutting for the purpose of geochemical analysis.

Though care was taken to avoid reinforcement steel, this wasn't always possible. The mesh width of the reinforcement net is 100mm, and on more than one occasion, a second mesh was present or eventually pieces of steel L-profile, apparently intended for construction purposes only.

Subsequently, the remainder of the core was vacuum impregnated with UV-fluorescent epoxy resin, and then cut lengthwise with a diamond blade. Locations for fluorescence-dyed epoxy impregnated $20\mu\text{m}$ thin sections of 30×45 mm were selected, after visual examination

of each set of halved cores. During all transport, unimpregnated cores were wrapped in a damp cloth to prevent desiccation and secured against impact and bending.

Cores BB212-4 were extracted from structure Heemraadsingel (Figure 1), cores BB215-7 from structure Wolput (Figure 2), and cores BB218-20 from structure Vlijmen-Oost (Figure 3). All these structures were/are located on main road A59. Cores BB240-2 were extracted from the KW5 structure near Zaltbommel (Figure 4), located on a now abandoned part of main road A2. Details on exact sampling procedures are provided elsewhere [27,71].

None of these structures contain (-ed) a post-tensioning system; they are (were) all passive. Detailed building documentation on reinforcement configuration is lacking and/or has gone lost, possibly during when the entire A59 main road changed owner, from local authorities to national. All structures appear to have a conventional cage-formed reinforcement, remarkably enough completely lacking vertical rebars [66]. Thus, their shear strength capacity fully depends on the tensile strength of the concrete [ipse dixit 36]. In 1998, structure Wolput has partly been reinforced with vertical rods in 732 drilled holes, on average 6 bars per square meter [70].

3 Analytical methods

3.1 Petrography

Core halves have been investigated with a Zeiss DRC stereo-microscope in plain light, thin sections were studied with a Zeiss Axioskop using incident and transmitted (polarized) illumination, and fluorescence. Determination of contents was done by grid-counting of core halves for coarse aggregate using a 10mm square grid and averaging 5 counts, and by point-counting thin sections for fine aggregate and cement paste, point counting 1500 points per 30×45mm thin section and averaging 3 counts. Air void content was determined by observation in low-angle stray light and subsequent size-classification. Petrographical methods are essentially described in [72,73].

Originally [28,29], the amount of ASR-damage was rated after assessing the number of cracks per unit surface of each impregnated halved core, which then was classified per structure as ‘freshest’ for concrete with the least amount of cracking, ‘moderate’ for cores with an intermediate amount of cracking, and ‘severe’ for the worst cracked cores. This rating system is used in the interpretation of the geochemical data.

3.2 Chemistry

Each $\varnothing 100 \times 100 \text{mm}$ / $\sim 1.8 \text{kg}$ subsample was crushed $< 3 \text{mm}$ in a steel jaw and subsequently pulverized in a vibratory disc mill with a tungsten carbide vessel. After powdering, each sample was homogenized by mixing and stirring and finally aliquotted with a split-sieve. All analyses were controlled by incorporating doubles, blanks, and internal standards into the analytical procedures. For each analysis, a separate aliquot was taken. The careful sample preparation and the application of established geochemical techniques virtually precludes analytical artefacts due to sample handling and/or contamination [74].

Powdered samples were digested in Li-borate flux [75] and analyzed for major element concentrations in bulk material by X-ray fluorescence (XRF) [76]. Loss on ignition (LOI) was determined gravimetrically by weighing before and after ignition at 950°C . Another amount of powder was dissolved in *aqua regia* (concentrated $1\text{HNO}_3 : 3\text{HCl}$) at room

temperature. After four hours, the solution was filtered, evaporated and redissolved in dilute nitric acid. The final solution was then introduced into the ICP-AES instrument [77]. In doing so, only the acid-soluble part of the bulk material is analysed. Silica is unstable in *aqua regia* and was hence not analysed. Total-C and total-S contents of the bulk were determined by Leco; bulk chloride-contents by ion-selective electrode (ISE) after digestion in dilute nitric acid [78].

4 Results

4.1 Petrography

Data presentation

Full core petrography and fluorescence have been integrated with thin section petrography, described in the paragraphs below. Petrographical results are tabulated in Table 1 at the end of this chapter. Color images of the cores in fluorescent illumination after cutting off the part for geochemical analysis are printed in Plates 1-4. Later research by this author on concrete from structures Heemraadsingel and Zaltbommel used an improved method to rate the damage [79, and Chapter 3]. The samples in this study (BB212-4 and BB240-2, respectively) have been re-evaluated with this improved method, and these results are included in Table 1 for comparison.

Texture and fabric

Pebbles and air voids are unevenly distributed throughout the concrete. Circular air bubbles tend to adhere to the surface of coarse aggregate or to cluster in the paste. The air void reported in Table 1 seems high, but is actually due to a few large irregular air voids, not due to the use of an air entraining agent.

Coarse aggregate may form clusters but without honeycombing, and flat or elongate grains occasionally may have a preferential orientation. The D_{\max} as observed in the halved cores was 24mm. Some areas seem to lack coarse aggregate, possibly due to demixing during emplacement. Kidney-shaped voids on the underside of aggregate grains are bordered by fining-upward sequences in the cement paste directly under it, and probably result from microbleeding in a water-rich mixture. Occasionally, the actual feeder channel may be seen. The concrete also contains sigmoidal *en echelon* cracks along the outer surface due to deformation of settled but still semi-plastic concrete. Despite the small flaws present the concrete can be said to be of average moderate quality.

The crack distribution varies locally within a single core with respect to crack width, density per unit surface and orientation. The mean direction of the macroscopic cracks approximately coincides with the average long axes of coarse aggregate, which hence dominates the crack fabric. Microscopic cracks may either be ASR-related or alternatively induced by hydration shrinkage. Cracks from early semi-plastic deformation or from pre-ASR-initiation are partly remineralised with ettringite and/or portlandite and may have been healed completely [80]. ASR-related cracks also contain calcite, gypsum, and/or crystallized ASR-gel.

Coarse aggregate

The material consists of well rounded gravel of variable composition, the majority being (vein-) quartz, finely grained sand-/siltstone with neogenic quartz overgrowths, and diagenetically compacted sand-/siltstone annex low-grade metamorphic quartzite. The material also contains small amounts of chert (ie., <5vol%) as well as some heavily retrograded spilitic basalt and minor carbonate. Siltstone and chert may contain

pseudomorphs of mixed iron (hydro-) oxides after pyrite. The material is typical for fresh-water deposited sedimentary material from the Belgian Ardennes. Scarcely available building information informs that the aggregate material was taken out from local nearby resources during the construction period [70, and references therein].

In fine grained sand-/siltstones, detrital quartz grains with 'dusted' cores are overgrown with clear, inclusion-free neogenic quartz, which cements the grains together. Ancient quartz grain cores and neogenic rims are optically continuous. The internal fabric of sandstone is more or less equi-angular, and some overgrowths of quartz appear to be subhedral. Similar syntactic rims also occur on epidote and tourmaline. Detrital and/or heavy minerals are concentrated along original sedimentary foresets and may or may not include augitic clinopyroxene, hornblende clinoamphibole, mica, tourmaline, monazite, zircon, and some epidote or clinozoisite. Fine grained opaque minerals are mostly concentrated along stylolite surfaces.

Albite does occur but seems rare, although some may go undetected because of its optical resemblance to quartz, on account of the absence of twinning. Potassium feldspar is also rare and always kaolinitized or sericitized to various degrees. Prehnite and phyllosilicates like glauconite and vermicular chlorite are clearly of prograde diagenetic or low metamorphic origin. Solitary flakes of chlorite are most probably retrograded (altered) detrital biotite.

Diagenetically compacted sand-/siltstone annex low-grade metamorphic quartzite contain sutured grain contacts (Plate 5 & 6). Occasionally, the internal fabric may resemble a mylonite structure in some orientations, except that the sandstone/quartzite structure is not lined. Stylolites are quite common, indicating pressure-dissolution compaction, with local concentration of opaque and/or very dark fine grained minerals. This type of sand-/siltstone annex quartzite is alkali-reactive. The sand-/siltstone retains some relict sedimentary features whereas the quartzite does not, although this may be a cross-sectional effect, that a thin section only contains a thin slice of material and does not show features eventually present in other parts of the grains outside the slice [81].

In these alkali-reactive sand-/siltstones, boundaries between neighbouring quartz individuals appear accentuated when observed in plane polarized light (Plate 5a & 6a). Under fluorescent illumination (Plate 5c), however, the view compares with that of other sandstone in having normal boundary contrast, thus ruling out an uncommonly high interstitial porosity. Eventually occurring interstitial minerals are beyond optical resolution (Plate 6), and may even include ASR-gel. Diagenetic sand-/siltstone and low-grade quartzite are known to quite commonly contain neogenic interstitial clay minerals [82].

Microporous chert is also subject to alkali-silica reaction ranging from slight to severe, ie. from crazing of the surface to wide cracks extending into the surrounding cement paste. The cracking and gel formation seem to be constrained to the grain margin, and essentially consists of spalling off thin shards. Gel may be extruded into the surrounding cement paste along the cracks, and parts of the grains' interior may be missing.

The chert grains are not homogeneous. Their interior shows local variations in fossil content (sponge needles, foraminifera, radiolarians, etc.), in porosity, in color due to variable limonite content (also see Chapter 6), in internal grain size and degree of recrystallization. An eventual coincidence between chert type and reaction pattern does not

appear from the current observations, but may be due to the relatively few grains observed and the large number of variable parameters.

However, in all of the investigated concretes, compacted sandstone/quartzite with accentuated grain boundaries typically appears to be more violently alkali-reactive than any of the cherts, with extensive internal cracking extending into the cement paste, and usually with gel extrusion (Plates 5 & 6; also see Plates 13-16). Opposite areas of crack walls do not exactly fit, suggesting that part of the grains' interior has been consumed up to 15vol%, especially in grains with stylolites. The bulk porosity of reactive sandstone/quartzite is similar to that of non-reactive material, except directly adjacent to the tip of (detrital) muscovite flakes where it is clearly higher in drop-shaped areas (Plate 5c & 6c). This occurs consistently in all investigated samples containing this type of alkali-reactive aggregate. These areas seem to be 'drained' by ASR-induced cracks (Plate 5c). The alkali-reactivity of micaceous sandstones in Dutch concrete has been confirmed lately by a great number of petrographic analyses [73].

Fine aggregate

The bulk of this consists of well rounded grains of (vein-) quartz and/or sandstone, occasionally with neogenic syntactic rims. Main accessories are potassium feldspar, plagioclase ($An_{<40}$), clinopyroxene and -amphibole (augitic and actinolitic, respectively), occasional flakes of muscovite or biotite, some single grains of epidote and/or clinozoisite, glauconite, apatite, zircon and/or monazite, and barite. Chert, micro-agate, calcsilicate rock, and occasionally fragments of both fine- and coarse-grained calcite also occur in very minor quantities, ie. a few grains in all thin sections together. The winning locations of this material are unknown.

Cement paste

All concretes were made using a relatively coarse grained ordinary Portland cement class A. Aluminate and alite relicts are colorless, belite is light brown with a lamellar or striated substructure [eg. 74]. The ferrite content of concrete from Wolput seems a bit lower than both other structures. In all pastes, ferrite is dark moss-green translucent in thin parts. Though the origin of the cement remains unresolved, the Dutch producer ENCI is the most likely resource, according to building traditions at the time of construction.

In Wolput and Vlijmen-Oost, the Portland cement contains minor quantities of pulverized fuel ash (PFA), and most likely, no other mineral additives have been added. The PFA consists of colorless, brownish and nearly opaque cenospheres and plerospheres of which the largest are easily recognizable in the paste. It is quite possible that the PFA was not intentionally added to the paste, but that the particles stem from 'ash fall-out' from pulverized coal used in firing the cement kiln.

The initial PFA-content is difficult to determine due to the high degree of hydration of the majority of all fly ash particles, but would not exceed 10wt% relative to cement [73]. Furthermore, the variation in mineralogical and geochemical composition of individual fly ash particles is quite large [83], thus the composition of the relicts as observed in the current paste is most likely not representative for the initial PFA-bulk.

The relatively coarse grainsize of the cement implies a comparatively low water demand, however, that may or may not have been affected by the low content of PFA present. On average, the paste fluorescence implies an effective water/cement ratio of circa 0.55 varying

from ≤ 0.35 to ≥ 0.60 , with a high degree of hydration. Clinker relicts may have hollow cores due to completed hydration, ie. Hadley-holes [84,85].

4.2 Geochemistry

Data presentation

Results from XRF analysis of bulk material are given in Table 2, after the main text of this Chapter. Data are presented in weight percent oxides, chloride in parts per million. Columns 2 and 2d provide duplicate analyses. The column ‘Total ICP-set’ totals only the elements analyzed with ICP-AES. Table 3 provides from ICP-AES analysis after partial digestion in *aqua regia*, recalculated to oxides in bulk material. For example, sample BB213 contains 0.07wt% of acid-soluble Na_2O conform ICP-AES, as compared to 0.22wt% in all conform XRF. Thus, circa two thirds of all the Na_2O present are apparently acid-insoluble.

Na_2O -equivalents in weight percentages are calculated as $\text{Na}_2\text{O} + (0.658 \cdot \text{K}_2\text{O})$, for bulk concrete from XRF data and for the acid-soluble part from ICP-AES data. Their difference (XRF minus ICP-AES) is attributed to aggregate material, and is included in Table 2. These weight percentage Na_2O -equivalents are visualized in Plate 7, arranged per structure.

The weight percentages Na_2O -equivalents were then recalculated into $\text{kg} \cdot \text{m}^{-3}$, assuming a specific weight of $2350 \text{kg} \cdot \text{m}^{-3}$ for structures Heemraadsingel, Wolput and Vlijmen-Oost [65], and $2400 \text{kg} \cdot \text{m}^{-3}$ for the Zaltbommel structure, respectively [71].

The ratio $\text{Na}_2\text{O}/\text{K}_2\text{O}$ is used to test leaching behavior. This ratio should remain constant with increasing ASR-damage whether calculated from XRF or ICP-AES data, on the prime condition that Na and K behave identical.

Bulk concrete

Analytical totals by XRF of all samples are always close to 100wt% (Table 2), duplicate analyses (BB214 and BB214d, respectively) are mutually in good agreement. Compositional variations are attributed to variations in aggregate, cement, and air content as eg. in Table 1. Thus, a higher SiO_2 -content (\sim aggregate) coincides with a lower CaO-content (\sim cement), reflecting small variations in cement/aggregate ratio. In all four structures, Na_2O -equivalents for decrease with increasing amount of ASR-deterioration, which pleases for the overall stripping of the concrete for alkalis. However, the inconsistent $\text{Na}_2\text{O}/\text{K}_2\text{O}$ ratio suggests that Na_2O might very well act differently from K_2O (Table 4).

Acid-soluble part of bulk concrete

The acid soluble part of the bulk concrete basically consists of cement paste, including relic fly ash particles. The contribution of acid-soluble compounds in the aggregate material can be neglected. According to detailed thin section petrography, acid-soluble constituents like carbonate, (altered) pyrite, and diagenetic and/or retrograde minerals are by volume only very subordinate in the total aggregate material. ASR-gel will be leached for soluble elements, whereas the Si-part of the gel remains in the residue since it is not stable in an *aqua regia* solution. Although all of these constituents are readily soluble in *aqua regia*, eventually incongruently [86], they only occur in very subordinate quantities. Hence, contamination of the readily acid-soluble cement paste by dissolved aggregate material is negligible. Geochemical analysis of the solid residue after digestion in *aqua regia* verified that the main element composition of that residue was within analytical error of fresh aggregate material [61]. Duplicate analyses are in good mutual agreement (Table 3).

The results in column 'total ICP-set' (Table 3) as calculated from actual ICP-AES data are consistently lower than the correspondent data calculated from XRF-results. Elemental concentrations by ICP-AES are generally lower than the matching bulk XRF-concentrations, implying that the elements are mainly consolidated in an *aqua regia*-insoluble compound. A higher ICP-AES-concentration than with XRF may however be due to the different procedures for the correction of matrix effects [77; and references therein].

The Na₂O-equivalents of the acid soluble part do not correlate with the ASR-grade. However, if these values of the acid soluble part (by ICP-AES) are subtracted from the matching values for bulk concrete (by XRF), then the results essentially represent Na₂O-equivalents of the acid *insoluble* complements only (XRF minus ICP-AES). This may be translated with the aggregate material. As appears from Plate 7, there is no uniform correlation of the acid-insoluble material with ASR-grade.

5 Interpretation and discussion

5.1 General

The volume of a typical core section for geochemical characterization is a bit variable around 1ℓ, roughly equal to 2.0-2.3kg. According to relevant ASTM-norms [87], the minimum size for a representative sample of aggregate material with a D_{max} of 25mm is 50kg, ie. roughly >20× larger than the samples in this study. With the observed D_{max} of 24mm, this would then be the appropriate sample size. If the material also contains fine aggregate like this concrete, then the minimum sample size increases by another 10kg to 30kg. This large ASTM-sample size is intended to meet potential compositional variations in a polymict material, containing eg. and gabbro and granite and schist.

However, Dutch aggregate material in the samples from this study consists mainly of sandstone and siltstone, pebbles of white quartz, and eventually some chert as typical for a mature coarse sediment from these realms. Individual sand- and siltstone grains may have different accessory minerals but still this does not emerge even from meticulous pointcounting data of bulk aggregate material (unpublished data). According to a thorough mathematical review of point counting statistics [88], this implies that the content of accessory minerals is less than analytical error (ie. uncertainty) and can hence be neglected.

As a corollary to that, geochemical variations in bulk material due to variations in the mineralogical composition of individual aggregate grains are less than in material for which the ASTM-rule was designed. Hence, representative sample size can be much smaller without compromising the integrity of geochemical results.

Apart from these technical issues, there is undeniably a practical aspect of sample preparation. Preparing a 2.0-2.3kg sample already proved a challenge with the accessible comminution equipment, each sample requiring four subsequent crushing and pulverizing steps and thorough homogenization between each two steps.

Preliminary experiments with splitting of a crushed sample and subsequent further preparation of the partial sample resulted in unreliable data. After further experimenting, this could be attributed to a discontinuous grainsize distribution of the final product. Whereas the coarse fragments in the intermediate crushed product almost exclusively consisted of aggregate grains, the fine fraction in the same intermediate product consisted mainly of cement paste dust, practically inhibiting splitting prior to further preparation. Thus, crushing and pulverizing steps might be executed on partial samples for practical

purposes, but homogenization should involve the whole sample. There would have been no equipment accessible to homogenize 60kg samples.

5.2 *Silica dissolution in natural systems*

An overview of seven fundamental geochemical and/or mineralogical qualities that may increase the solubility of quartz has been summarized in [89]. While there are certainly more ways to increase quartz solubility, those seven seem most viable for a deleterious alkali-silica reaction in concrete. Additionally, it seems very possible that a combination of these qualities may be effective in one given aggregate material (eg., chert), but not in another of a different geological origin (eg., mylonite). This makes the whole issue of different geochemical and/or mineralogical qualities worthy on investigation.

The solubility of silica species is enhanced by increasing pressure and/or temperature. At ambient conditions, silica solubility rises with increasing basicity above pH=9, but crystalline and amorphous silica behave distinctly. Between pH4 and pH9, silica solubility is negatively affected by dissolved sodium and potassium salts, and especially by calcium and magnesium salts [90].

The dissolution behavior of silica is to an important degree also determined by the size of individual particles. Fine grained amorphous silica dissolves relatively easily under high-pH conditions [91, and references therein]. Large particles have a small surface curvature and vice versa, which property directly relates to the surface free energy. This directly influences silica solubility and promotes growth of silica with low surface energy, ie. 'large, round quartz particles' at the expense of 'fine grained, angular silica', particularly when the silica is poorly crystalline as eg. in chert, or in intensively deformed rocks. The same issue also obtains for quartz precipitation at the tip of microcracks [92,89, and Chapter 7].

Chert is a fine grained variety of silica formed under ambient, diagenetic or low-grade metamorphic conditions, with variations in microstructural, mineralogical and chemical composition [93]. Potentially alkali-reactive cherts consist of loosely stacked, very fine particles of silica, resulting in a high internal microporosity and large surface area, often combined with bad particle crystallinity. All of these features promote silica solubility in chert. Sandstone however is much coarser grained, less microporous, and better crystalline than chert. Thus, sandstone should theoretically be less prone to undesired silica dissolution under ASR-conditions than chert.

Despite the afore-said assertions, alkali-reaction appears less violent in chert, and much more abundant in sandstone with accentuated grain boundaries and sutured grain contacts, which are lacking in non-reactive sandstone. ICP-AES chemistry reveals that the alkali content of the acid soluble part is roughly one-third of the bulk material, even when least affected by leaching via ASR-induced cracking [50,94]. Apparently, some constituent, mechanism or process in sandstone effectively enhances silica dissolution.

Recent articles [95,96] describe and model respectively the effects of confining pressure and the presence of phyllosilicates on silica dissolution in sandstone under low grade diagenetic conditions. One study describes detrital mica flakes, partly embedded in quartz [95]. Using the E-module of muscovite, the flakes rigidity is calculated to be so low that mechanical penetration into the quartz is certainly no option. From cathode-luminescence, the author demonstrates that the intruded quartz grains are detrital, and not neogenic overgrowths.

BSE images reveal slightly more space at the mica-quartz interface near the mica tips, than at the 001-faces of the same grains.

Reference [95] also reports on sutured quartz-quartz interfaces between exclusively detrital grains, where clay minerals seem consistently present, according to K-Al element mapping. The author recommends redefinition of pressure-solution as clay/mica-induced (quartz) dissolution. In other words, the authors of [95,96] conclude that silica dissolution is apparently enhanced by some little understood catalytic interaction of (detrital) mica and/or (neogenic) clay minerals by locally affecting the pore fluid pH. Similar effects have been reported previously from natural systems [97,98,99], and perhaps from concrete [100]. Biotite with portlandite precipitated along tips and cleavage planes has recently been reported from Dutch OPC concrete [101], also suggesting a pH effect on its environment.

5.3 Silica dissolution in concrete by ASR

The Na₂O-equivalents calculated for acid-insoluble alkali calculated as “XRF minus ICP-AES” in Plate 7 suggest that the alkali-depletion trends as observed are clearly dominated by (acid-insoluble) aggregate, and not by the acid-soluble part, ie. the cement paste. Relative to bulk concrete, the alkali depletion amounts from ~23% for Vlijmen-Oost to ~30% for Heemraadsingel and Wolput, in contrast to only ~15% for Zaltbommel.

The main part of the total alkali is consolidated in the (acid-insoluble) aggregate; the cement paste contains 25% (BB220) up to 40% (BB215) of the total alkali present, of all structures in this study. Corollary, if it is exclusively alkali from the paste that is available for leaching, then at least 60wt% to well over 100wt% of the cement paste would have to be stripped of all alkali to obtain a bulk alkali depletion of 15-30%. This would then require pervasive and penetrative access to the paste and complete alteration to liberate all that alkali. This obviously contradicts the petrographical observations in this study. The only plausible explanation remaining is that part of the leached alkali is provided by the largest alkali reservoir present, ie. the aggregate material.

The observation of a sedimentary detrital mica flake (Plate 5 & 6) within a dumbbell shaped area of higher porosity that appears to be drained by ASR-induced cracks (Plate 5c & 6c) is also suggestive of some interaction near the tips of that mica flake. This phenomenon has been frequently observed in alkali-reactive sandstone grains from all structures in this study, and in other structures as well. In addition, the accentuated grain boundaries phenomenon is common in most Dutch alkali-reactive sandstones (Plate 5 & 6).

The petrographic features of the alkali-reactive sandstone in this study remarkably resemble those in natural diagenetic sandstones [95,96], in which micas and/or interstitial clay minerals appear to have enhanced the dissolution of silica. In the concrete from this study, internal porosity of alkali-reactive sandstones is markedly increased near mica grains, while the observation of accentuated grain boundaries without enhanced microporosity suggests the presence of an interstitial fine grained clay mineral precipitate. All these observations together suggest that the alkali-silica reaction of sandstone is enhanced by mica and possibly the presence of clay minerals.

6 Conclusions

1. General Dutch experience indicates that as a rule, sandstone is less prone to silica dissolution than chert, assumedly due to larger interior grain size and higher crystallinity. The present petrographic study, however, has revealed a converse situation in which sandstone with detrital mica is much more alkali-reactive than chert in the same concrete. This has been confirmed by later observations on Dutch concrete [73]. The sandstone may also contain sub-microscopic clay minerals at grain boundaries. Interstitial porosity of sandstone by UV-fluorescence is clearly enhanced in areas directly adjacent to detrital mica.
2. Recent literature argues that diagenetic dissolution of silica in natural sandstones is significantly enhanced by a catalytic interaction of mica or interstitial clay minerals. The observed ASR-features in our concrete closely resemble the dissolution phenomena described for such natural sandstones.
3. Comparing geochemical results of bulk concrete (XRF) with the acid-soluble part (ICP-AES) prove that most of the alkali is contained within the aggregate material, and that approximately one-third of the alkali resides in the acid-soluble cement paste. The Na_2O -equivalents of the bulk correlate qualitatively with the relative crack density of the impregnated cores. The inconsistent variation of $\text{Na}_2\text{O}/\text{K}_2\text{O}$ with increasing damage suggests that sodium and potassium behave differently in ASR and/or in leaching.
4. Investigation by electron microprobe is required to unravel the micro-details of the ASR-process and to better understand the individual behavior of Na and K.

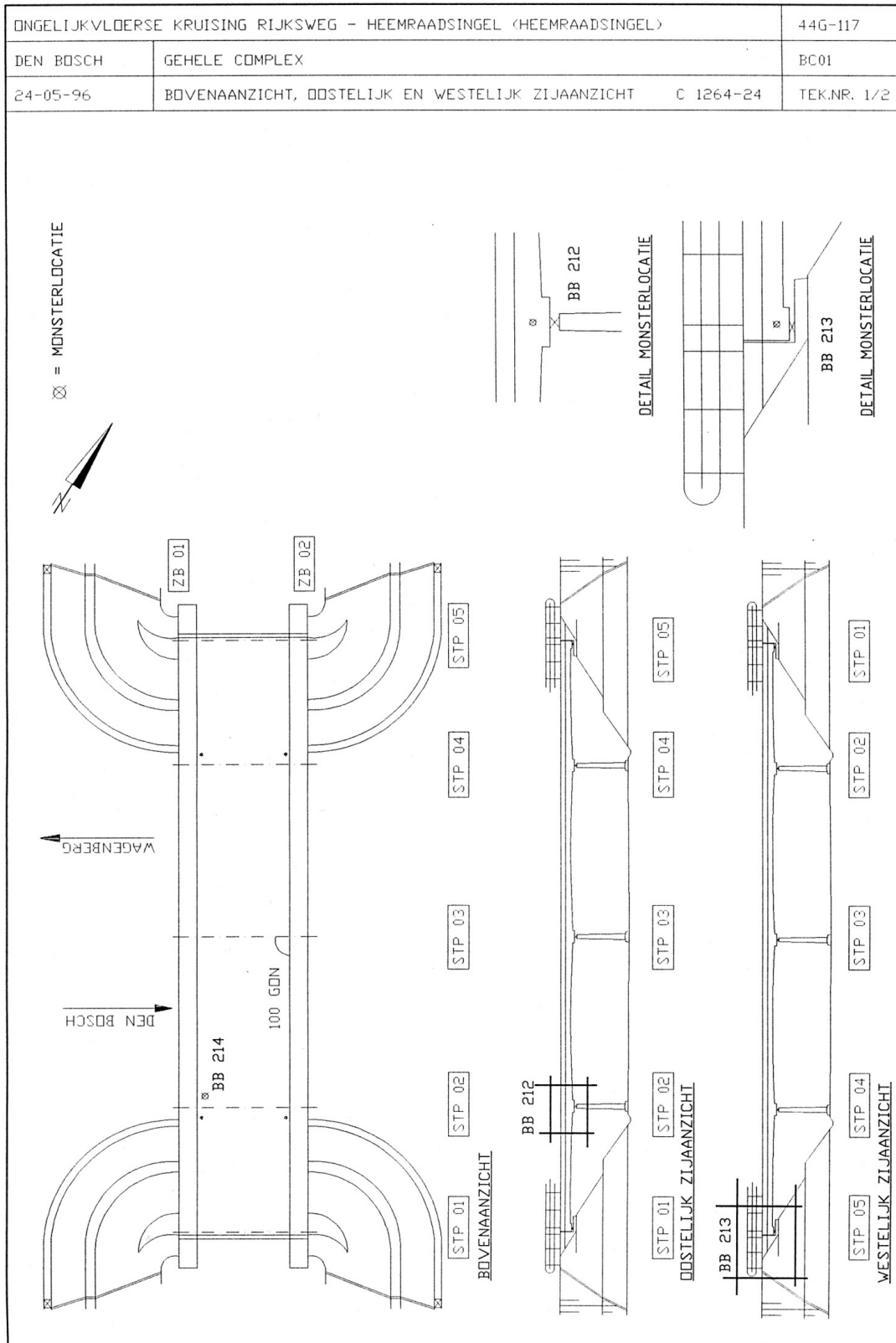


Figure 1a: Assessment drawing of structure Heemraadsingel. Courtesy Nebest BV [27]. Overall length: 48.5m.

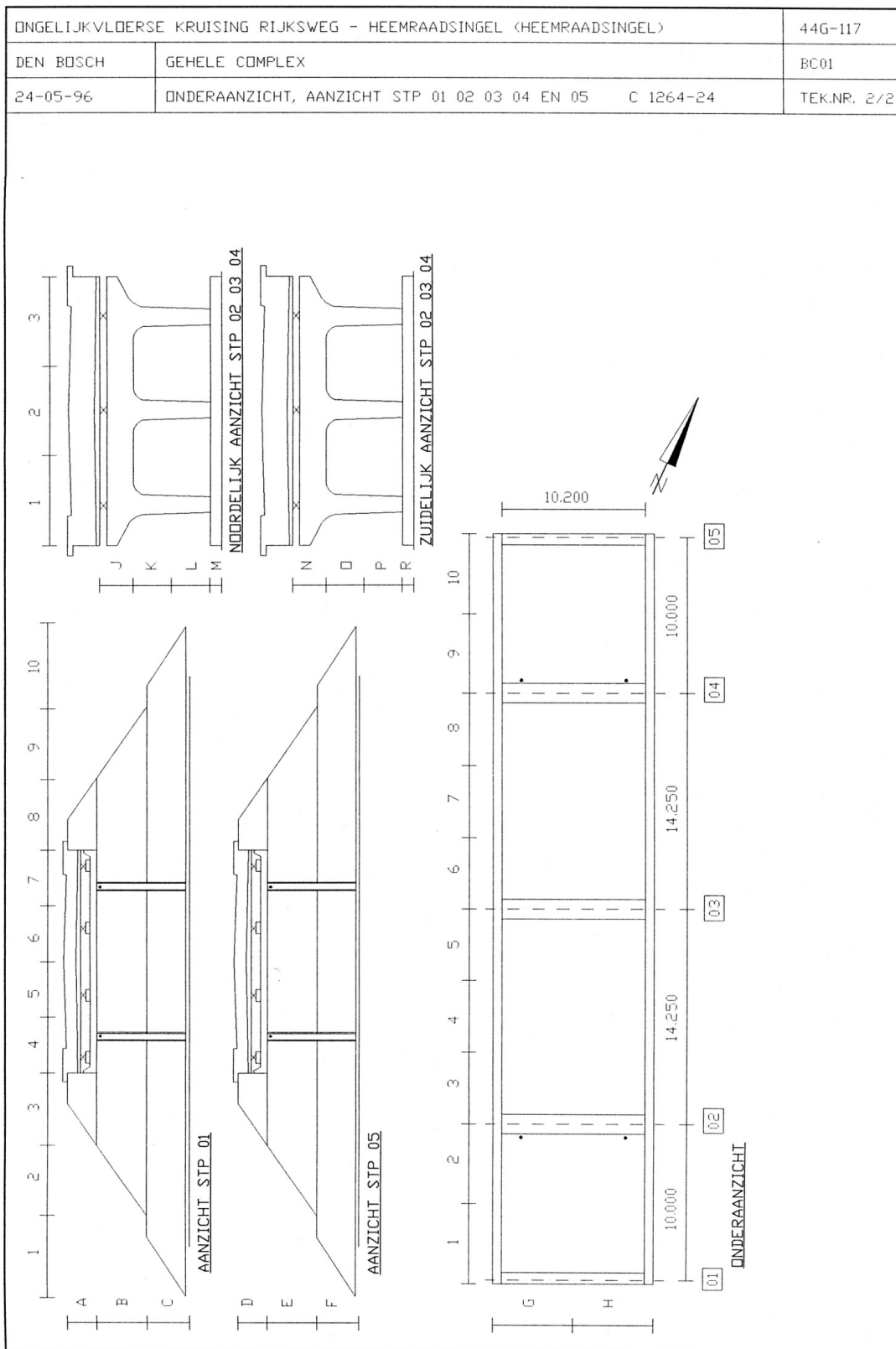


Figure 1b: Assessment drawing structure Heemraadsingel. Courtesy Nebest BV [27].

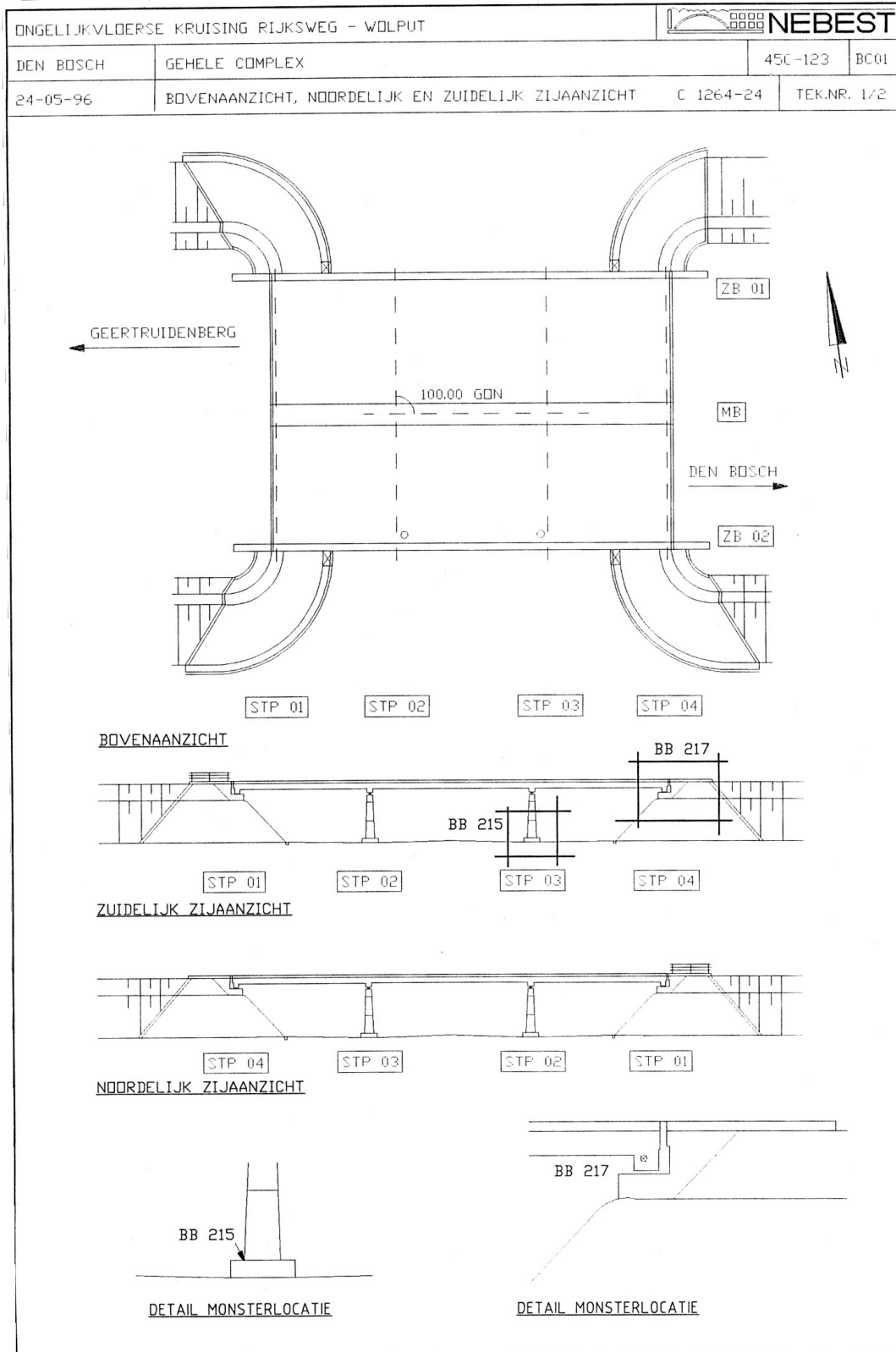


Figure 2a: Assessment drawing structure Wolput. Courtesy Nebest BV [27]. Overall length 32.6m.

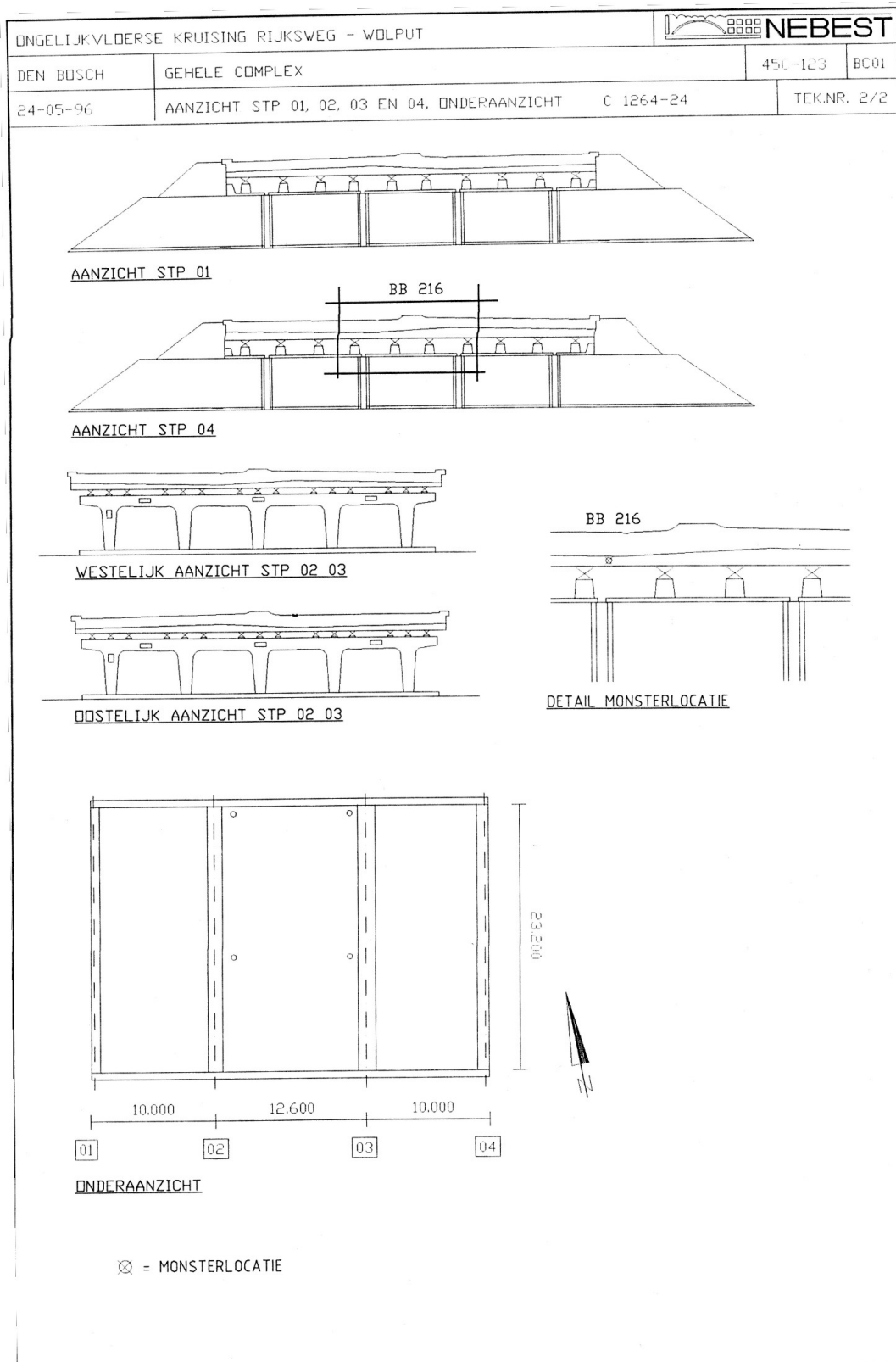


Figure 2b: Assessment drawing structure Wolput. Courtesy Nebest BV [27].

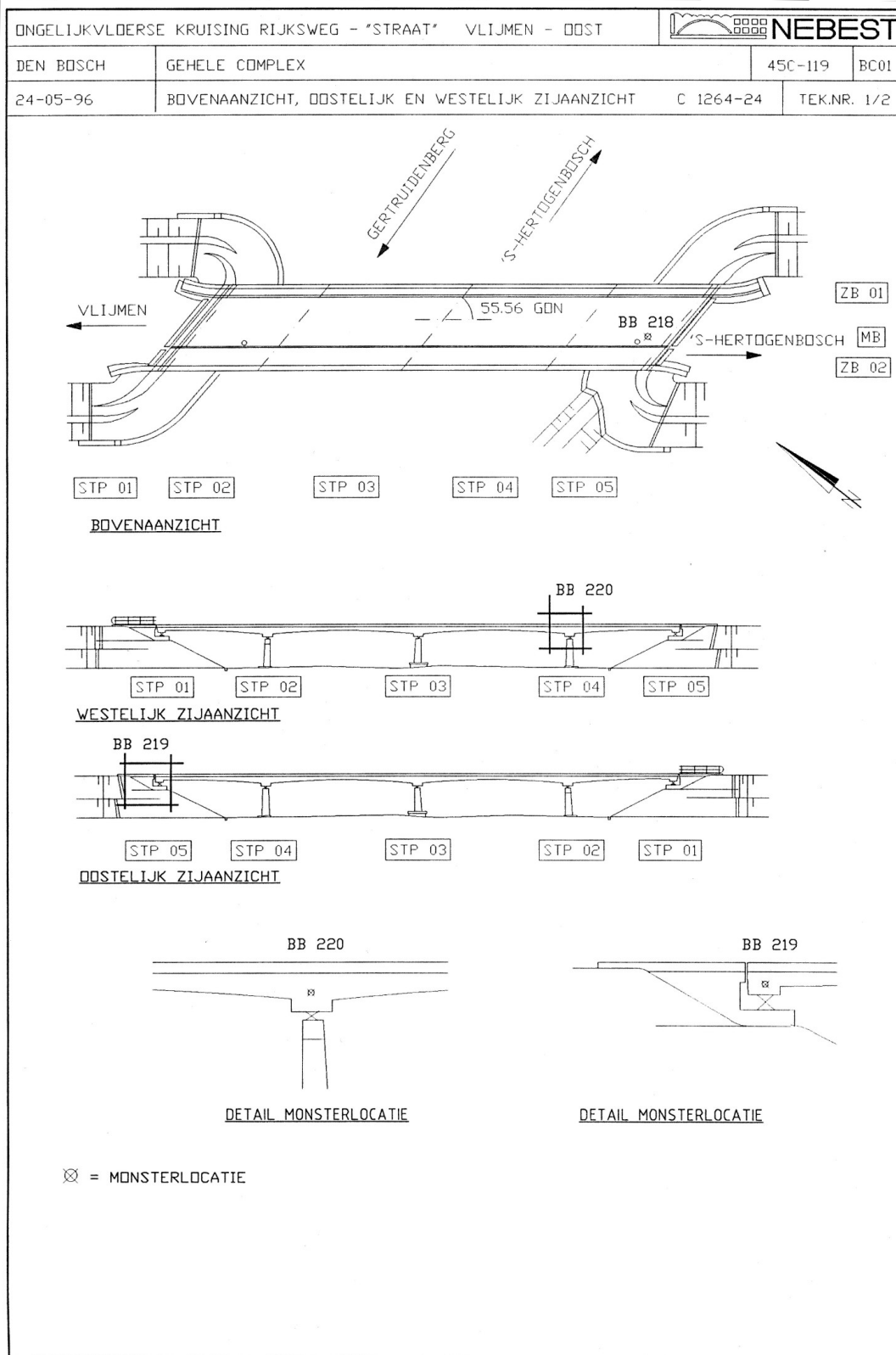


Figure 3a: Assessment drawing structure Vlijmen-Oost. Courtesy Nebest BV [27]. Overall length 68.4m.

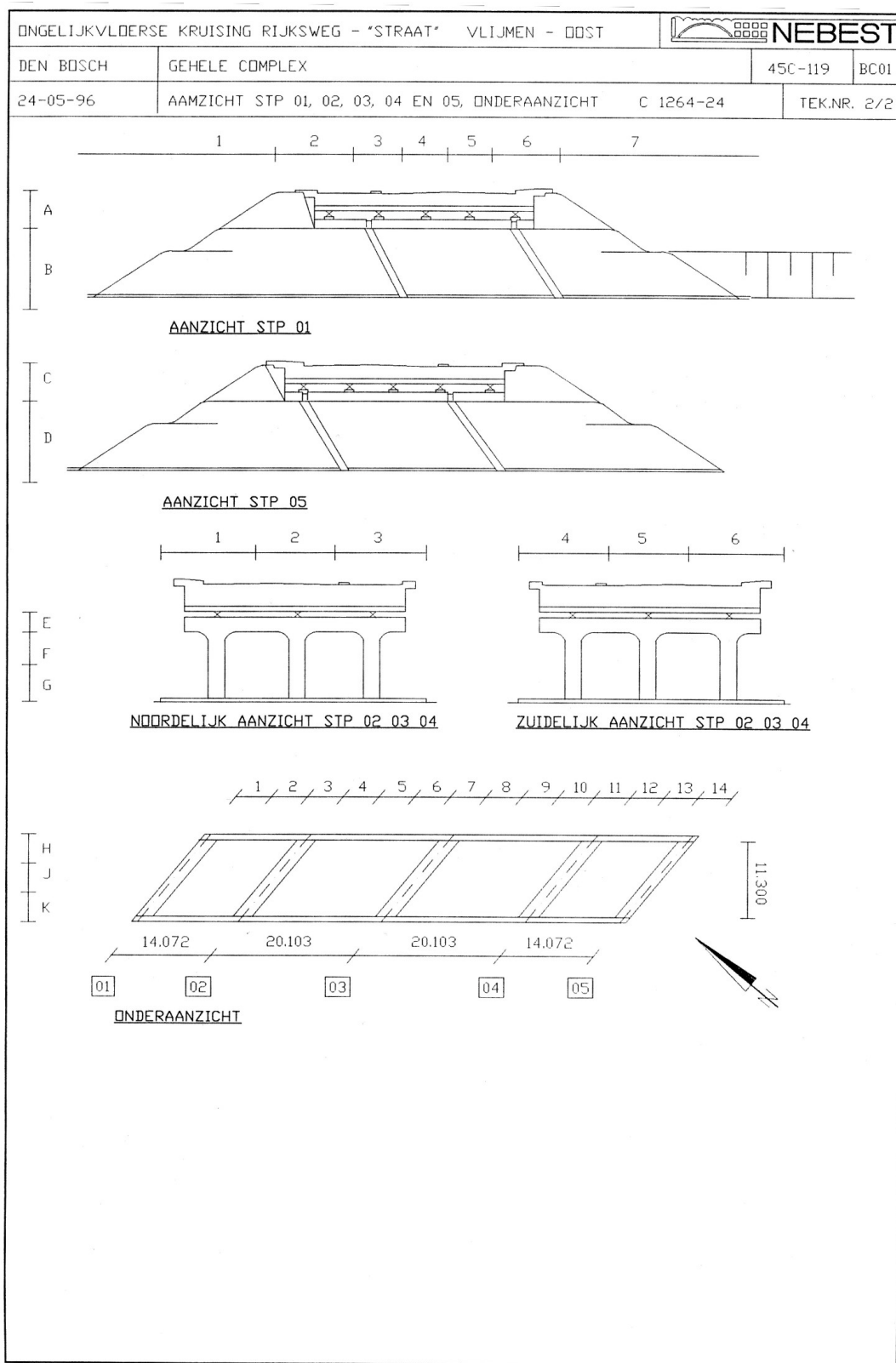


Figure 3b: Assessment drawing structure Vlijmen-Oost. Courtesy Nebest BV [27].

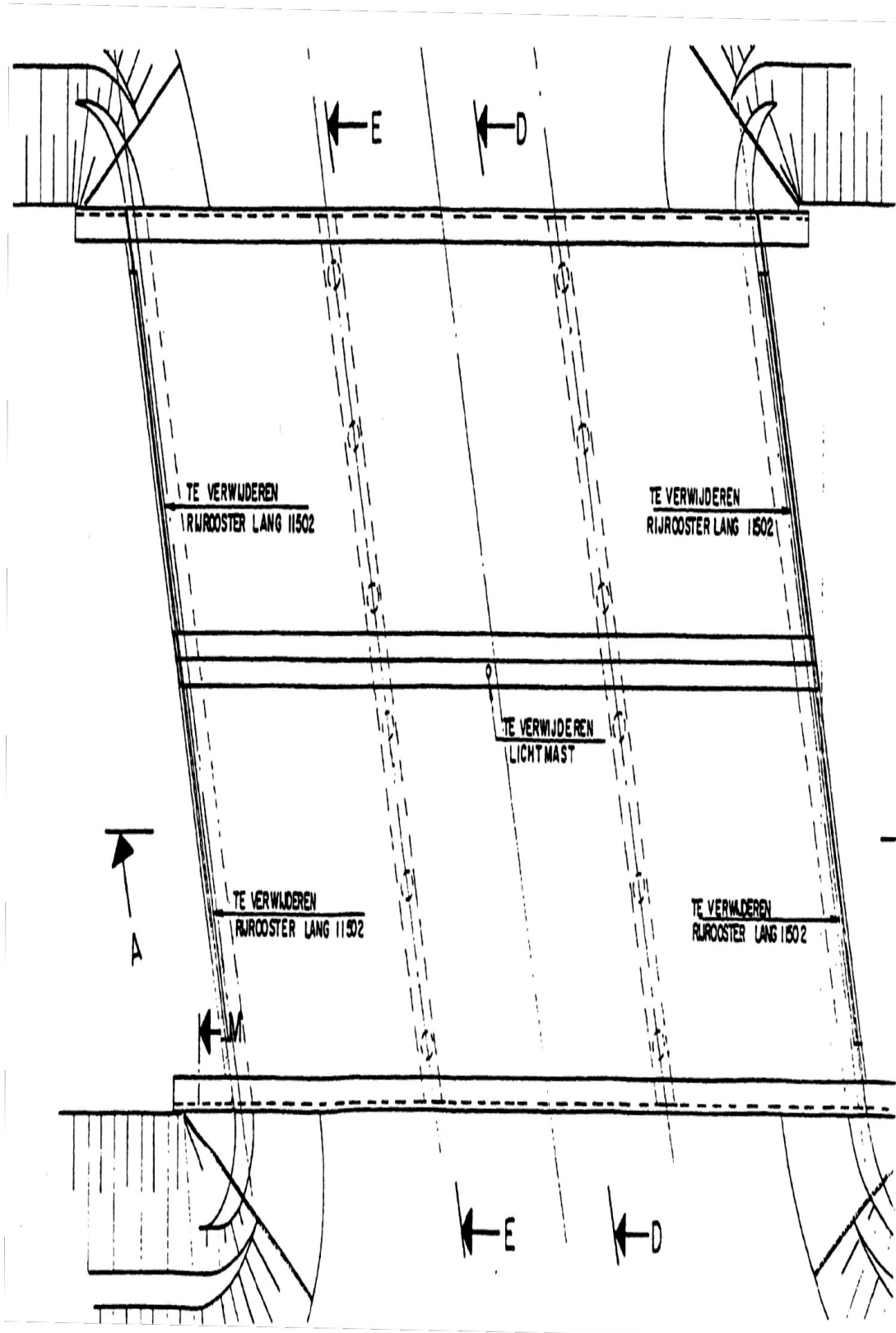


Figure 4a: Drawing of structure KW5 at Zaltbommel.

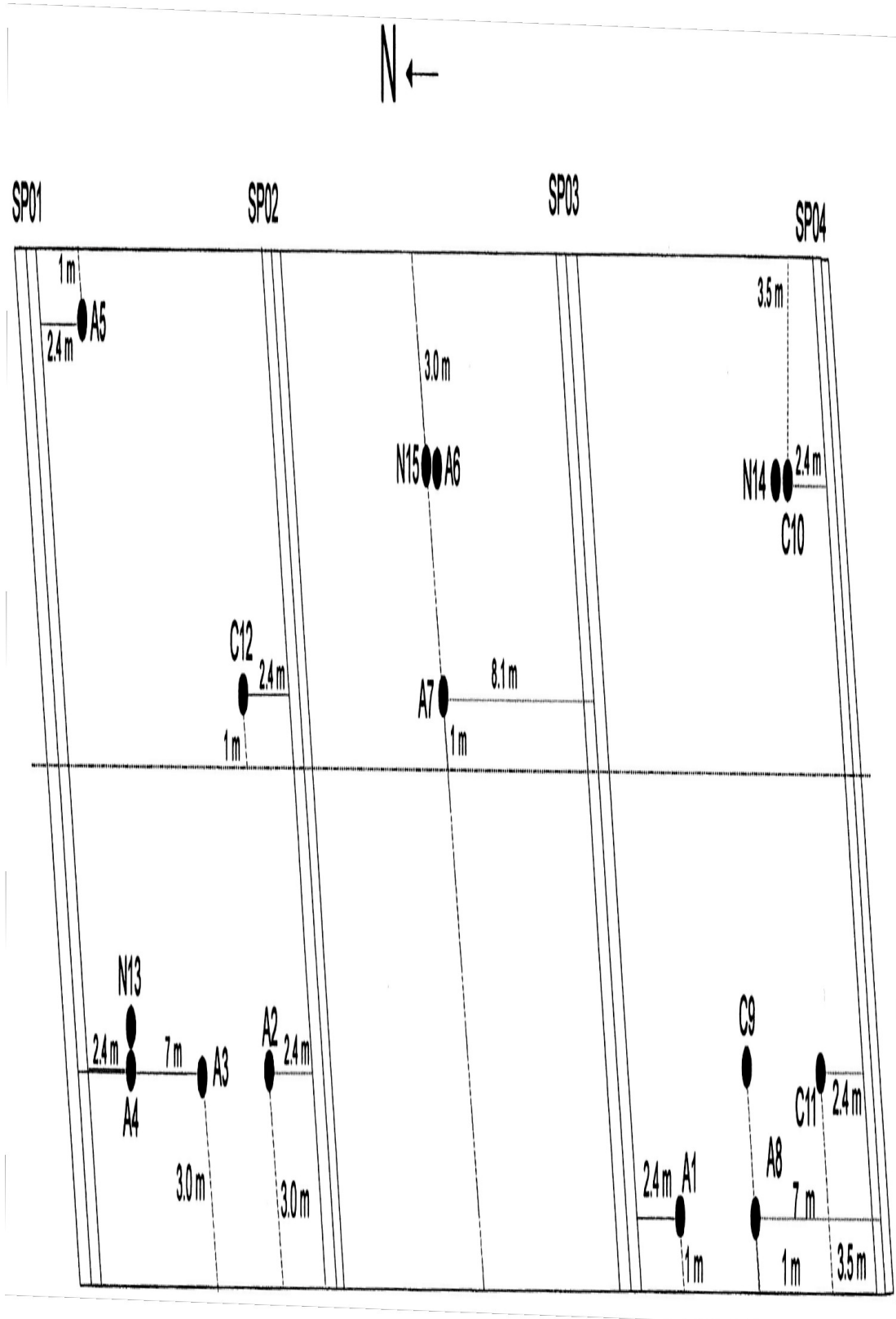


Figure 4b: Drawing of structure KW5 at Zaltbommel.
 Sampling sites BB240=N15, BB241=N13, BB242=N14.

TABLE 1: Volume percentages of constituents by petrography of handspecimen and thin sections. ASR-susceptible: percentage relative to bulk concrete.

<i>coarse aggregate</i>	<i>Heemraadsingel</i>				<i>Wolput</i>				<i>Vijmen-Oost</i>				<i>Zalbornmel</i>			
	BB213	BB214	BB212	BB215	BB217	BB216	BB218	BB219	BB220	BB240	BB242	BB241				
sample no.	44.8	39.6	45.3	35.6	40.1	39.4	36.0	41.6	39.9	47.3	50.5	50.8				
modus	1.2	1.6	1.2	1.2	0.4	1.4	1.8	2.0	2.4	1.46	1.64	2.02				
2σ	7	6	7	5	7	6	5	6	7	7	7	4				
ASR-susceptible																
<i>fine aggregate</i>																
modus	27.4	33.4	30.9	34.0	34.3	33.5	29.6	29.1	34.4	20.5	22.3	20.5				
2σ	0.6	0.8	0.6	1.6	1.2	0.8	0.4	0.6	0.6	0.5	0.5	0.4				
<i>cement paste</i>																
fly ash (wt%-cement)	0	0	0	≤10	≤10	≤10	≤10	≤10	≤10	≤10	≤10	≤10				
total modus	19.2	18.3	16.5	21.9	20.4	22.0	24.3	20.7	21.6	22.4	19.9	19.6				
2σ	1.0	0.8	0.8	0.8	0.8	1.2	0.8	0.8	0.8	0.5	0.7	0.6				
<i>air voids</i>																
≥2 mm	7.4	4.3	4.2	3.9	2.1	2.1	2.5	3.3	0.6	3.0	3.4	2.0				
2σ	0.6	0.4	0.6	0.4	0.4	0.4	0.4	0.4	0.2	0.2	0.3	0.4				
≤2 mm	1.2	4.4	3.1	4.6	3.2	3.1	7.7	5.3	3.4	2.1	2.0	2.2				
2σ	0.4	0.6	0.4	0.6	0.4	0.2	0.6	0.4	0.4	0.4	0.4	0.6				
<i>crack classification</i>																
structure surface	none	s	c	s	none	c	nv	c	vc	[71]	[71]	[71]				
core, uppermost	none	c	vc	s	c	vc	lp	s	vc	l	s	vc				
core, lowermost	vl	s	vc	l	c	vc	none	l	vc	none	l	vc				
thin section	none	c	l	l	l	vc	l	s	c	l	s	vc				
ASR-grade	fre	mod	sev	fre	mod	sev	fre	mod	sev	fre	mod	sev				
ASR-grade [79]	1	2	3	1	2	3	1	2	3	1	2	3				

(v)=clearly; s=some; (v)=some; (v)=little; nv=none visible; fre=freshest; mod=moderate; sev=severe.

TABLE 2: Weight percentages of oxides in bulk concrete, by XRF, total-C and total-S with Leco; Cl⁻ with ISE; LOI by weighing before and after ignition.

structure	Heenraadsingel						Wolput						Vlijmen-Oost						Zaibommel									
	BB213	BB214	BB214¶	BB212	BB215	BB217	BB216	BB218	BB219	BB220	BB240	BB242	BB241	BB213	BB214	BB214¶	BB212	BB215	BB217	BB216	BB218	BB219	BB220	BB240	BB242	BB241		
ASR-grade	fre	mod	mod	sev	fre	mod	sev	fre	mod	sev	fre	mod	sev	fre	mod	sev	fre	mod	sev	fre	mod	sev	fre	mod	sev	fre	mod	sev
ASR-grade [79]	1	2	2	3	1	2	3	1	2	3	1	2	3	1	2	3	1	2	3	1	2	3	1	2	3	1	2	3
Na ₂ O	0.22	0.16	0.16	0.1	0.16	0.18	0.16	0.25	0.13	0.12	0.19	0.16	0.18	0.25	0.13	0.12	0.19	0.16	0.18	0.19	0.16	0.18	0.19	0.16	0.18	0.19	0.16	0.18
K ₂ O	0.65	0.58	0.56	0.53	0.71	0.53	0.53	0.47	0.52	0.47	0.69	0.53	0.53	0.47	0.52	0.47	0.69	0.53	0.53	0.47	0.52	0.47	0.69	0.53	0.53	0.47	0.52	0.47
CaO	10.7	9.83	9.78	11.0	9.01	8.9	8.81	11.4	8.97	11.9	10.8	10.9	11.4	8.97	11.9	11.4	10.8	10.9	11.4	10.8	10.9	11.4	10.8	10.9	11.4	10.8	10.9	11.4
MgO	0.62	0.43	0.44	0.55	0.15	0.17	0.21	0.24	0.22	0.19	0.25	0.28	0.24	0.22	0.19	0.25	0.28	0.24	0.24	0.25	0.28	0.24	0.25	0.28	0.24	0.25	0.28	0.24
MnO	0.03	0.01	0.01	0.02	<0.01	<0.01	<0.01	0.02	0.01	0.01	0.03	0.02	0.02	0.01	0.01	0.01	0.03	0.02	0.02	0.03	0.02	0.02	0.03	0.02	0.02	0.03	0.02	0.02
Fe ₂ O ₃ -total	1.68	0.98	0.96	1.54	1.21	1.05	1.29	1.8	2.18	1.43	1.67	1.65	1.75	1.8	2.18	1.43	1.67	1.65	1.75	1.67	1.65	1.75	1.67	1.65	1.75	1.67	1.65	1.75
Al ₂ O ₃	3.24	2.58	2.56	2.62	2.91	2.95	3.14	3.08	2.9	2.8	2.65	2.93	2.66	3.08	2.9	2.8	2.65	2.93	2.66	2.65	2.93	2.66	2.65	2.93	2.66	2.65	2.93	2.66
SiO ₂	75.3	79.4	79.6	76.3	79.5	79.8	79.6	75.7	78.5	75.2	77.9	78.1	77.9	75.7	78.5	75.2	77.9	78.1	77.9	77.9	78.1	77.9	77.9	78.1	77.9	77.9	78.1	77.9
TiO ₂	0.21	0.16	0.16	0.15	0.17	0.14	0.21	0.2	0.15	0.15	0.15	0.17	0.14	0.2	0.15	0.15	0.15	0.17	0.14	0.15	0.15	0.15	0.15	0.17	0.14	0.15	0.15	0.14
P ₂ O ₅	0.05	0.04	0.03	0.04	0.07	0.06	0.07	0.09	0.07	0.08	0.07	0.07	0.09	0.07	0.07	0.08	0.07	0.07	0.09	0.07	0.07	0.08	0.07	0.07	0.09	0.07	0.07	0.08
LOI	7.45	6.00	5.85	7.3	6.4	6.5	6.2	6.9	6.45	7.75	5.15	4.70	5.20	6.9	6.45	7.75	5.15	4.70	5.20	5.15	4.70	5.20	5.15	4.70	5.20	5.15	4.70	5.20
SO ₃	0.35	0.30	0.35	0.35	0.23	0.28	0.25	0.14	0.1	0.14	0.30	0.30	0.30	0.14	0.1	0.14	0.30	0.30	0.30	0.30	0.30	0.30	0.30	0.30	0.30	0.30	0.30	0.30
Cl (ppm)	90	90	80	100	90	100	370	100	110	160	134	123	127	100	110	160	134	123	127	100.0	99.9	100.5	100.0	99.9	100.5	100.0	99.9	100.5
total	100.6	100.5	100.5	100.6	100.5	100.5	100.6	100.3	100.2	100.3	100.0	100.0	100.5	100.3	100.2	100.3	100.0	100.0	100.5	100.0	99.9	100.5	100.0	99.9	100.5	100.0	99.9	100.5
total ICP-set	17.5	14.8	14.7	16.6	14.4	13.9	14.5	17.7	15.2	17.3	16.3	16.6	16.8	17.7	15.2	17.3	16.3	16.6	16.8	16.3	16.6	16.8	16.3	16.6	16.8	16.3	16.6	16.8
CO ₂	0.62	0.55	0.66	0.95	0.62	1.06	0.73	1.1	0.81	1.03	1.14	1.06	1.25	1.1	0.81	1.03	1.14	1.06	1.25	1.14	1.06	1.25	1.14	1.06	1.25	1.14	1.06	1.25
H ₂ O*	6.83	5.45	5.19	6.35	5.78	5.44	5.47	5.8	5.64	6.72	4.01	3.64	3.95	5.8	5.64	6.72	4.01	3.64	3.95	4.01	3.64	3.95	4.01	3.64	3.95	4.01	3.64	3.95
Fe ²⁺ /Fe ³⁺	0.12	0.10	0.10	0.13	0.17	0.19	0.16	0.17	0.14	0.18	0.14	0.20	0.13	0.17	0.14	0.18	0.14	0.20	0.13	0.14	0.20	0.18	0.14	0.20	0.13	0.14	0.20	0.13

¶ = duplicate analysis; < = detection limit; * = (re-)calculated

TABLE 3: Weight percentages of oxides by ICP-AES after selective digestion of bulk concret in *aqua regia*.

structure	Heemraadsingel						Wolput			Vlijmen-Oost			Zaltbommel		
	BB213	BB214	BB214d	BB212	BB215	BB217	BB216	BB218	BB219	BB220	BB240	BB242	BB241		
ASR-grade	fre	mod	mod	sev	fre	mod	severe	fre	mod	sev	fre	mod	sev		
ASR-grade [79]	1	2	2	3	1	2	3	1	2	3	1	2	3		
Na ₂ O	0.07	0.07	0.05	0.07	0.07	0.07	0.07	0.05	0.05	0.04	0.05	0.04	0.05		
K ₂ O	0.24	0.20	0.19	0.25	0.28	0.19	0.14	0.17	0.23	0.10	0.24	0.17	0.22		
CaO	9.97	9.26	9.03	10.4	8.18	8.34	8.08	10.8	8.52	10.7	8.76	9.67	9.40		
MgO	0.66	0.51	0.49	0.66	0.21	0.23	0.25	0.30	0.28	0.25	0.20	0.23	0.20		
MnO	0.02	0.01	0.01	0.02	0.01	0.01	0.01	0.02	0.01	0.01	0.01	0.01	0.01		
Fe ₂ O ₃ -total	1.50	0.92	0.87	1.44	1.09	0.99	1.17	1.63	1.99	1.27	1.24	1.34	1.30		
Al ₂ O ₃	1.49	1.19	1.17	1.55	1.29	1.42	1.46	1.61	1.55	1.46	1.277	1.42	1.30		
TiO ₂	0.03	0.03	0.03	0.03	0.03	0.03	0.03	0.03	0.03	0.03	0.03	0.03	0.03		
P ₂ O ₅	0.05	0.02	0.02	0.05	0.07	0.07	0.07	0.09	0.09	0.09	0.07	0.07	0.07		
total ICP-set	14.0	12.2	11.9	14.5	11.2	10.5	11.3	14.7	12.8	14.0	11.8	12.9	12.5		

2d = duplicate analysis of 2; <=detection limit; #/=not determined; *=(re-)calculated

TABLE 4: Na₂O-equivalents in weight percentages and in kg·m⁻³, and ratios of Na₂O over K₂O, by XRF for bulk material, by ICP-AES for acid-soluble, Acid-insoluble alkali calculated as "XRF minus ICP-AES".

structure	Heemraadsingel						Wolput						Vlijmen-Oost						Zaltbommel							
	BB213	BB214	BB214d	BB212	BB216	BB217	BB215	BB217	BB216	BB218	BB219	BB220	BB240	BB242	BB241	fre	mod	sev	fre	mod	sev	fre	mod	sev		
ASR-grade	fre	mod	mod	sev	sev	mod	fre	mod	sev	fre	mod	sev	fre	mod	sev	1	2	3	1	2	3	1	2	3		
ASR-grade [79]	1	2	2	3	3	2	1	2	3	1	2	3	1	2	3											
<i>in wt%</i>																										
by XRF	0.648	0.542	0.528	0.449	0.627	0.529	0.479	0.419	0.559	0.472	0.419	0.644	0.575	0.548												
by ICP-AES	0.228	0.202	0.175	0.235	0.254	0.195	0.132	0.096	0.162	0.201	0.096	0.208	0.152	0.195												
acid-insoluble alkali	0.420	0.340	0.353	0.214	0.373	0.334	0.347	0.323	0.397	0.271	0.323	0.436	0.423	0.353												
<i>in kg·m⁻³</i>																										
													2350 kg·m ⁻³ [65]													
by XRF	15.2	12.7	12.4	10.6	14.7	12.4	11.3	9.85	13.1	11.1	9.85	15.5	13.8	13.2												
by ICP-AES	5.34	4.75	4.11	5.52	5.97	4.58	3.10	2.26	3.81	4.72	2.26	4.99	3.65	4.68												
acid-insoluble alkali	9.86	7.95	8.30	5.08	8.73	7.82	8.20	7.59	9.29	6.38	7.59	10.5	10.2	8.50												
<i>Na₂O/K₂O</i>																										
by XRF	0.338	0.276	0.286	0.189	0.225	0.340	0.245	0.234	0.532	0.250	0.234	0.275	0.254	0.321												
by ICP-AES	0.292	0.350	0.263	0.280	0.250	0.368	0.286	0.300	0.294	0.217	0.300	0.208	0.235	0.227												
acid-insoluble alkali	0.366	0.237	0.243	0.107	0.209	0.323	0.231	0.216	0.666	0.276	0.216	0.311	0.304	0.382												

A Simple and Straight-forward Damage Rating Index and its Correlation with Infiltrated Chloride

Adapted from:

Broekmans, MATM (2001): A simple and straight-forward damage rating index and its correlation with infiltrated chloride. In: Stamatakis, M, Georgali, B, Fragoulis, D, and Toumbakari, EE (editors): Proceedings of the 8th Euroseminar on Microscopy Applied to Building Materials, Athens, Greece: 93-99.

1 Introduction

A question often asked by the administering authorities when delivering a report on a damaged concrete structure is: "And how bad is it?". equally often, the answer rings: "Er, ... pretty bad.", leaving the authority to decide whether that actually means 'still pretty' or 'really bad'. Thus, the demand for a more objective way of grading or classifying concrete damage in materialographic terms is evident, even as an interim step towards a precise quantification.

The idea of a (semi-) quantitative classification scheme for grading the amount of damage is certainly not novel, and in the past, different workers have applied and/or combined several techniques [102,103,104]. Generally, while combined methods are quite accurate since they assess and cross-correlate different damage aspects, they are also time-consuming and elaborate for that very reason. The use of customized (ie. not off-the-shelf) research instrumentation and the laborious nature of the methodology may have contributed to the fact that such academic methods in large measure have never become integrated with the standard procedures of most engineering consultancies.

Directly related to the amount of damage is the question of whether to regard an ASR-damaged concrete as an open or a closed system for fluid exchange with the environment. Irrespective of their origin, cracks obviously provide easy pathways for fluids to enter or leave the concrete. A quick check of the keyword index to the year 2000 (volume 30) of Cement & Concrete Research [105] reveals only eight papers specifically referring to cracks, crack width and crack detection, out of a total of circa two-hundred and fifty contributions, omitting discussions, obituaries and book reviews, ie. ~3%. Though this number by no means is representative for crack research *sensu lato* (articles dealing with crack mechanics, initiation, the effect of cracks on fluid transport and the like are more likely to find their way into other journals), it does illustrate the scarcity in literature references on quantification of concrete damage in terms of cracking.

Obviously, analysis of crack fabrics does not seem very popular, perhaps due to immanent issues like how to account for differences in crack interconnectivity and crack length? Additionally, concrete is generally considered a closed system, despite a handful of cracks that are in daily practice often designated as 'irrelevant' or 'only unsightly'. This chapter investigates samples from two different structures to test these assumptions.

2 Sampling and experimental methods

2.1 Sampling

Five core suites, each suite consisting of two cores of $\varnothing 100\text{mm}$ and $\varnothing 170\text{mm}$, respectively, were drilled in the closest possible conjunction from the very ends of large beams (size order: $8 \times 0.5\text{m}$) that had been used in four-point bending shear strength testing [36]. The original orientation of the extracted cores was vertical, and each core comprises a complete cross-section of one of the bridge decks. Sampling locations are illustrated in Figures 1 and 2 at the end of this Chapter.

Special attention was given to careful handling of the $\varnothing 100\text{mm}$ cores as these were intended for detailed impregnation fluorescence petrography and crack analysis. Core suites BB243-5 were extracted from two beams that were cut from structure Heemraadsingel, core suites BB246-7 were both extracted from a beam cut from structure KW5 near Zaltbommel. Both structures have been demolished after the beams were cut out.

TABLE 1: Sample dimensions $\varnothing 170\text{mm}$ cores.

<i>structure</i>	<i>Heemraadsingel</i>			<i>Zaltbommel</i>	
core suite	BB243	BB244	BB245	BB246	BB247
<i>full cores</i>					
length (mm)	750	750	600	750	650
height (mm)	45	42	35	45	38
<i>per disc</i>					
volume (ℓ)	1. 021	0. 953	0. 794	1. 021	0. 863
weight (kg)	2. 40	2. 24	1. 87	2. 40	2. 03

2.2 Petrography

All $\varnothing 100\text{mm}$ cores were impregnated with epoxy resin containing a fluorescent dye. Generally, the Danish Prøvningsmetode TI-B 5 [106] was followed with some minor adaptations, to minimize the chance of preparation artefacts. After thorough hardening of the resin, the core was cut lengthwise. Up to seven locations were selected per core half for preparation of fluorescent thin sections. Impregnated core halves were studied with a Zeiss DRC stereomicroscope; thin sections were studied with a Zeiss Axioskop-50 petrographical microscope equipped with polarized transmitted illumination and fluorescent incident illumination, prior to geochemical characterization.

The damage was indexed according to a simple rating system here called DRI, which is based on the observation of macroscopic cracks visible in blacklight in epoxy-impregnated $\varnothing 100\text{mm}$ cores, slabbed lengthwise. The classification scheme for the DRI is given in Table 2 below. Examples for each DRI-value are illustrated in Plate 8. The DRI was assessed for 16 areas (BB244: 17) per impregnated $\varnothing 100\text{mm}$ core, each area precisely corresponding to the disc sections as used in geochemical analysis.

TABLE 2: Damage rating index (DRI) classification criteria.

<i>DRI</i>	<i>description</i>
0	no cracks at all, pristine concrete
1	small cracks exclusively on the outer surface of the core (stress relaxation)
2	small, random, mostly singular cracks spread throughout the concrete
3	penetrative crack across the core diameter, the two parts still adhering
4	penetrative crack across the core diameter, actually separating the concrete
5	incoherent, disintegrated concrete

This damage rate indexing is quick (for assessment of the crack fabric with blacklight fluorescence, the core has to be impregnated anyway) and convenient while only requiring the most basic fluorescence equipment, ie. a blacklight handlamp. Of course, other methods have been documented for indexing ASR-damage [eg. 102,103,104] and may be more refined and/or accurate, but these methods are also much more elaborate and do require special instrumentation or software, not to mention specific experience or training. Probably, this impracticability is one reason why damage rate indexing hasn't found wide application in concrete damage consultancy daily practice.

2.3 Ion-selective electrode

From each core suite, one \varnothing 170mm core was dissected in 16 equally thick discs (BB244: 17) by semi-dry diamond saw cutting, for purpose of more detailed geochemical characterization (this volume). Discs were then reduced in a jaw crusher to 3-5mm, dried at 50°C to constant weight, and fine-crushed (<0.05 mm) between steel rollers. Finally, fine-crushed material was pulverized in a vibratory disc mill with agate lining.

After thorough homogenization of the pulverized sample material, each sample was digested in nitric acid and analyzed for chloride with an ion-selective electrode (ISE). The LDL was set at 0.005wt% (50ppm) in the contract with the analytical facility, however, the *instrumental* lower detection limit is far lower. Normally, when a lower detection limit is met in geochemical analysis, the elemental content is in fact to be interpreted as 'undetermined', but in this particular case the LDL is reliable. Analytical precision is quoted as near ± 0.00005 wt% (± 0.5 ppm), which low value would normally not be reliable near a true instrumental lower detection limit. The plotted ISE-chloride results provide a depth profile across the entire thickness of the bridge deck.

The ion-selective electrode is essentially the more accurate laboratory version of the well-known RCT-method (Rapid Chloride Test) that was developed by Danish Germann-Pedersen. The reliability of the RCT-method and its compatibility with the generally accepted but way more elaborate Volhardt titration method is well documented [107]. The Volhardt titration method was originally designed to measure chloride in urine and some other applications, although for concrete the sample digestion procedure was adapted. Ion-selective electrodes have been used before to determine chloride in concrete [78].

3 Results

3.1 Data presentation

Results are presented in Plate 9 for profiles BB243 through BB247. Chloride concentrations are plotted as a weight percentage on the lefthand y-axis on a logarithmic scale, so as to cover the entire data range. The damage rating index DRI is plotted on a linear scale on the right. Each profile represents a complete vertical cross-section from the top surface (disc 1; BB244: disc 0) to the bottom of the deck (disc 16). This 'profile depth' is aligned with the upper horizontal axis.

3.2 Petrographic observations

The two concretes from this investigation differ in detail. Concrete from Zaltbommel apparently contains more coarse aggregate and some more cement paste, less fine aggregate and fewer air voids. The paste also contains some fly ash, estimated at max 5wt% on cement mass. Thin section petrography indicates that deleterious ASR is the primary damage mechanism that induced the cracking. Reactive constituents include porous chert and sand- and/or siltstones. Portlandite is virtually absent around reactive grains, and occasionally, gel has extruded out along cracks into the paste. Non-porous chert may also exhibit internal gelation, most probably enhanced by cracking generated by other reactive constituents. Further macroscopic and microscopic details are described in Chapter 2 of this thesis [see also 28,29,30,108]. As mentioned in Chapter 2 of this thesis, the aggregate is characteristic for fresh-water deposited sedimentary material, with the Belgian Ardennes as the provenance area.

3.3 Cracks and crack distribution

In general, cracks appear to be concentrated in separate zones. Cracks occur most frequently in a zone near the reinforcement, both top and bottom meshes. A third zone of intensive cracking occurs near the middle of the cores, its depth somewhat variable. The confinement of cracks to distinct zones is quite obvious and not typical for ASR, rather for rebar corrosion. However, all rebars in concrete with $DRI \leq 4$ were invariably well-attached to the concrete with no trace of debonding, and had to be removed by hammering prior to further sample preparation by crushing and grinding. Upon close inspection with a stereomicroscope, none of the rebars showed signs of corrosion due to carbonation or chloride pitting, whereas their bedding planes in the concrete hardly retained any (fly) rust. Bleeding traces from chloride-mobilized reinforcement steel were absent.

The overall amount of damage seems to be greater in the Zaltbommel structure (BB246-7) where the DRI runs up to the scale maximum of 5 several times. In the Heemraadsingel viaduct (BB243-5), $DRI=5$ occurs only once (BB244A0). The cracking in the central portion of the cores from the Zaltbommel structure (BB246-7) is remarkably symmetrical, in contrast to Heemraadsingel.

3.4 Chloride content

Chloride contents range from almost 0.1wt% (BB246A1) to less than 0.005wt%, ie., under the lower detection limit. Though the highest concentrations most frequently occur near the top, they also occur near the lower end, and surprisingly, also in the central portions of the profiles. In near-mid section 10 of core BB245, the chloride concentration is almost as high as on the core top surface. The chloride content of section 9 of core BB247 is even highest of the whole core.

4 Discussion

4.1 Cracks and crack distribution

As mentioned above, the observed crack distribution is not characteristic for ASR, and more typical for reinforcement corrosion. However, corrosion products or phenomena were not observed under the microscope, and the fact that the rebars had to be removed by force from concrete with $DRI \leq 4$ indicates that the rebars still were well bonded to the rock. This latter observation is in fact supported by results from four point bending testing of beams cut from both structures [36]. Thus, reinforcement corrosion as a cause for the observed cracking is not an option.

Furthermore, solitary cracks ($DRI=2$) are randomly oriented across the entire thickness of the deck (ie., the full length of the investigated cores), implying that were caused by a non-directional mechanism, like for instance ASR. Detailed petrographic analysis indicates that indeed ASR is the primary cause for the damage in bulk concrete, however, the more severe cracking near the reinforcement may have been enhanced by other mechanisms, like eg. frost or mechanical loading during service. However, no indications have been found for either of these in petrographic analysis.

Even though precautions were taken to minimize core extraction artefacts, relaxation cracking due to release of internal stress cannot entirely be precluded. If cracking is restricted by proximate reinforcement, then the effect of stress relaxation may be much larger than in the bulk concrete where stress is not restricted by reinforcement. The lack of shear reinforcement as in these structures may be favourable for this [36]. Stress relaxation could then occur over a longer period of time, as opposed to relaxation during core extraction where stress is released momentaneous. Which mechanism (-s) can be held responsible for the somewhat unusual crack concentration around the reinforcement in these samples remains unclear, but the primary cause for the cracking is undisputedly ASR.

4.2 Correlation of DRI with chloride content

The lower detection limit of the ISE-method for chloride is set at 0.005wt% (50 ± 5 ppm). This value is frequently met in all cores from both structures, which makes it plausible that the initial background concentration of chloride is less than the lower detection limit. The fact that the aggregate material most probably represents fresh-water deposited detritus from the Belgian Ardennes, transported to the Netherlands by sedimentary processes supports the idea that the initial chloride content must be low.

Note that the chloride content is presented here for homogenized and pulverized bulk material, ie., the entire sample volume of up to $\sim 1\ell$ of concrete. Thus, locally different chloride contents may all be averaged out to one single chloride concentration for the entire disc section.

In all profiles in Plate 9, the coincidence of chloride concentrations with the DRI is striking. The plotted LDL-values make the coincidence qualitative, and not a correlation. The high chloride contents at the top of the bridge decks can surely be explained by deicing salt (sodium chloride). The locally increased chloride content on the lower side of the profiles can be interpreted as deriving from salty spraywater from passing traffic. The lower content of the lowermost section 16 in BB244 may be explained by leaching after chloride infiltration. Judging from the shape of the chloride profiles, diffusion seems to control ingress from the outer concrete surfaces inwards.

The coincidence of an elevated chloride content with DRI in the central portions of the deck, however, cannot be simply explained by diffusion. The deeper regions of the concrete are clearly beyond reach as the diffusion profile flattens out after the second or third disc section. Apparently, the chloride has entered the innermost concrete in another way, implying communication as opposed to isolation of the inside of the structure with the environment outside.

Fluid flow along cracks is called channelized, and if along grain boundaries or through micropores it is called pervasive. The debit of channelized fluid flow as compared to pervasive fluid is easily 3-6 orders of magnitude larger [109,110]. Thus, cracks provide easy pathways for fluid access and dissolved species. Fluid transport along the cracks is controlled by convection, from the crack walls into the concrete by diffusion. If the wallrock is dense, then chloride will remain confined to the direct proximity of the crack, however, if the wallrock is relatively open and accessible, then the chloride will rapidly diffuse away from the crack.

4.3 *The central portion of core BB246*

One obvious exception to the general trend where chloride concentrations correlate qualitatively with the damage rating index is the central portion of core BB246 (disc sections 6-11) in the fourth profile in Plate 9. The chloride concentration profile does not seem to correlate at all with its DRI, in contrast to adjacent core portions (disc sections 1-5 and 12-16, respectively). None of these sections nor the neighbouring sections contain steel reinforcement.

Even though cracking is most severe in the central core sections (DRI=5) and the concrete hence can be inferred to be accessible for fluids, the chloride concentration does not peak, unlike central sections in other cores. A number of potential explanations need to be checked:

1. The initial chloride background is not below the lower detection limit of the ISE-method, or
2. The cracks are very young and haven't seen enough chloride yet to build a peak, or
3. An existing chloride peak has been leveled out with its surroundings, or
4. The cracks were generated in another way not *in situ* during the service life of the structure.

These hypotheses are discussed below.

Although the cement in the Zaltbommel concrete differs somewhat from that in Heemraadsingel, it is still unlikely that its initial chloride background is higher. Had this been true, then disc section 4 in profile BB246 and disc sections 10-12 in BB247 from the same structure must have been effectively stripped of their chloride to below the lower detection limit, i.e., <0.005wt%. That doesn't seem very likely with a DRI=1-2 which comparatively has only a few cracks. Hence, the first hypothesis of a chloride background concentration >0.005wt% (i.e., higher than the DL of the ISE-method) can be ruled out.

Both macroscopic and microscopic petrography confirm the presence of ASR in individual grains of the coarse aggregate from disc sections 6-11 in BB246, and the cement paste is somewhat altered, most probably due to fluid interaction. A plausible reason for fluid interaction without introducing chloride is hard to find. The second hypothesis is contradicted by the observed fluid-alteration of the cement paste (also noticeable as the 'always dusty' nature of the drilled cores), and is hence most unlikely.

The third option doesn't accord with the observation that the core sections adjacent to the maximum damage have substantially fewer cracks and do not seem to be especially permeable. It has been verified by observations with a stereomicroscope that there are no cracks present that remained un-impregnated because they were blocked. In other words, the permeability contrast between the cracked concrete in disc sections 6-11 and the wall rock (ie., sections 1-5 and 12-16, respectively) appears to be similar to the other cores in this investigation, which would justify essential channelization of fluid flow and the occurrence of chloride peaks.

It is considered highly unlikely that laboratory bending tests would be the origin of the cracks in the central portion of BB246. The cracks are thought rather to have formed *in situ*, during service of the structure [111]. However, the eventual pre-existence of cracks prior to four-point bending testing was not verified with impregnation fluorescence on slabbed cores nor other methods. A corollary is that crack enhancement or initiation by the load experiments cannot be completely precluded. Taking all the above arguments and counter-arguments into account, the hypothesis of lab-induced cracking seems most plausible, and is perhaps the most simple and straight-forward way to explain the issue of the observed non-correlation between DRI and chloride content in the central portion of core BB246.

The good (qualitative) correlation of chloride with the damage rating index as used in this study, as opposed to the lack of correlation of chloride with laboratory-generated cracks, only reinforces the notion that chloride apparently is a good indicator for communication of the internal parts of a concrete structure through cracks with the outside environment.

5 Conclusions

The conclusions that can be drawn from this study include:

1. The most violently alkali-reactive grains are micaceous, diagenetically compacted and/or altered siltstone, sandstone, and porous chert, in that order, in accordance with previous observations [28, and Chapter 2]. Alkali-reactive grains are similar in concrete from both structures;
2. The main cause of cracking in both structures is ASR, though local coincidences with other causes and/or mechanisms cannot be totally precluded and might occur especially near the surface. Cracks tend to concentrate near reinforcement and towards the centre of the deck. Deep and penetrative cracking opens up the concrete and makes it permeable to foreign solutions potentially carrying dissolved matter;
3. The DRI alone, as applied in this study, does not specifically discriminate for ASR-caused cracking, but its accuracy as an ASR-damage indicator is notably improved when the concrete core is assessed by in-depth optical petrographical thin section analysis;
4. Coincidence of chloride content with the DRI as used here is striking. The lack of such coincidence in the central portion of sample BB246 is probably due to the cracking there being an artefact of the four-point bending testing [36]. The coincidence of chloride concentration variations with the applied DRI indicates that the internal parts of the investigated structures did communicate with the outside environment, and finally, the concrete in this study must be regarded as an open system with respect to fluid transport and accessibility.

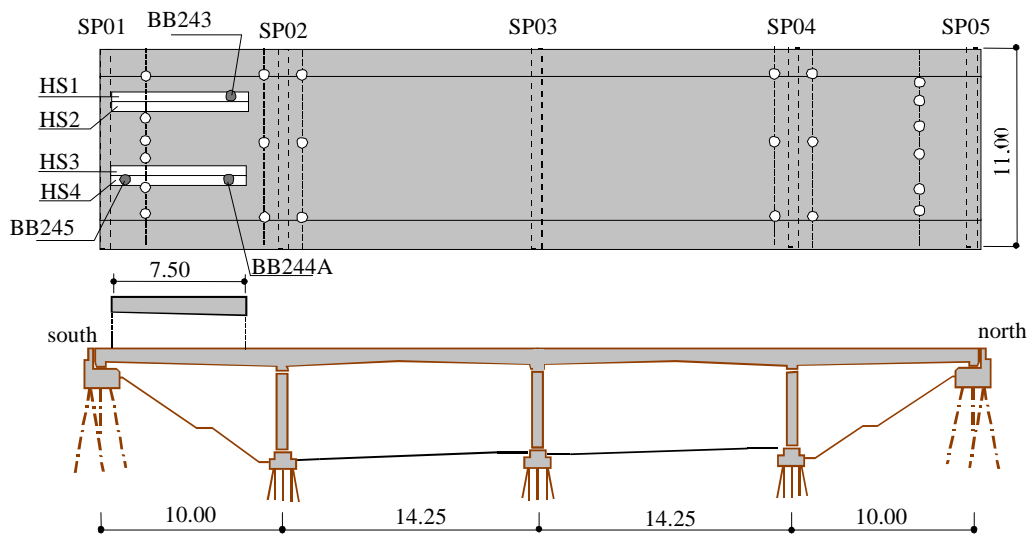


Figure 1: Core extraction locations on beams from former structure Heemraadsingel. Dimensions in metric units. Per location, 1 core $\varnothing 100\text{mm}$ and two cores $\varnothing 170\text{mm}$ were extracted. Also compare with Figures 1a,b in Chapter 2.

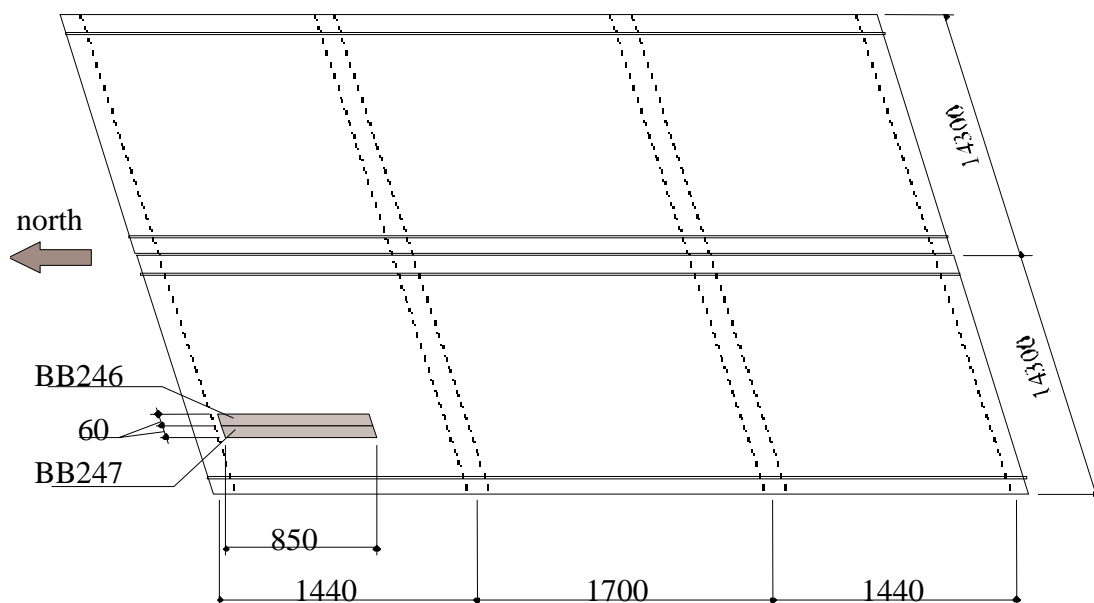


Figure 2: Core extraction locations on beams from former structure KW5 at Zaltbommel. Dimensions in metric units. Per location, 1 core $\varnothing 100\text{mm}$ and two cores $\varnothing 170\text{mm}$ were extracted. Also compare with Figures 4a,b in Chapter 2.

Chapter 4:

Origin and Mobility of Alkalies in Two Dutch ASR-concretes: Correlation with the Damage Rating Index

Adapted from:

Broekmans, MATM (2001): Origin and mobility of alkalies in two Dutch ASR-concretes I: correlation with a damage rating index. In: Stamatakis, M, Georgali, B, Fragoulis, D, and Toumbakari, EE (editors): Proceedings of the 8th Euroseminar on Microscopy Applied to Building Materials, Athens, Greece: 77-84.

1 Introduction

Early results from Chapter 2 strongly suggested that there might be a correlation between the amount of cracking and the alkali content of the bulk concrete. The observation that sand- and/or siltstone appeared to be more alkali-reactive than chert in the same samples suggested that the disadvantages of sand-/siltstone with regard to larger internal grain size and less porosity were overcome by some mechanism. It was also speculated that alkalies might be released from the aggregate material by interstitial clays beyond optical microscopic resolution.

Furthermore, in Chapter 3 it is argued that the investigated concrete profiles were open to access for fluids bearing dissolved chloride from deicing salts, and that variations in chloride content coincided with variations in the amount of damage represented as their damage rating indices DRI. Thus, it would be interesting to know how alkalies in the same concrete samples behave, how mobile they are on the same macroscopic bulk scale, and what their origin might be.

If alkali derived from aggregate material could be shown to contribute to a deleterious ASR, then that could have strong consequences for ASR-preventive regulations. Currently, regulations in general silently assume that the cement paste (eventually with admixtures and additives) is the sole provider of alkalies for ASR. Substantial alkali contribution from the aggregate is largely neglected as a serious option, even though the alkali content is sometimes measured. The inhibiting effect of blast-furnace slag on ASR is attributed to immobilization of alkali in the pore fluid¹. Thus, porous chert that relies on available external alkali to initiate ASR is denied access, and ASR is effectively suppressed.

Aggregate grains containing internal alkali could in principle be independent of external alkali provided by the cement paste via the pore fluid, so, the presence of blastfurnace slag for that reason alone would be irrelevant to them, in contrast to the case with porous chert. The occasional but not rare occurrence of gelated sand-/siltstone coarse aggregate grains in blastfurnace slag concrete cores illustrates this. Note that the internal alkali need not

¹ the actual mechanism of ASR-amelioration may be more intricate and may involve other aspects as well.

necessarily be mobile initially, but might be liberated gradually after prolonged exposure to the high-pH environment in concrete.

In an attempt to resolve the mobility and origin of the alkalis in these concrete samples, the samples from Chapter 3 have been characterized geochemically with several methods.

2 Experimental methods

2.1 Sample preparation, petrography and damage rating

Sample extraction techniques and details on petrographical methods including determination of the damage rating index DRI are described in Chapters 2 and 3 of this thesis. For the purpose of geochemical characterization, samples were crushed, pulverized and homogenized. Details on these procedures are provided in Chapter 2 of this thesis.

2.2 Geochemistry

An adequate number of (blind) duplicates and in-house standards was included with all analyses. Bulk concrete was analyzed by XRF for Na₂O, K₂O, MgO, CaO, MnO, Al₂O₃, total-Fe₂O₃, TiO₂, SiO₂, and P₂O₅ after HT-digestion in Li-tetra borate (Li₂B₄O₇). Operating conditions of the Philips PW-1480 XRF were set at 50kV and 50mA. Bulk-LOI was determined gravimetrically by weighing before and after ignition at 1000°C of a sample pre-dried at 35°C until constant weight. Raw and un-normalized main element totals are within 100.0±1.00wt%. Duplicate analyses differ only in the second decimal, SiO₂ in the first, indicating very good reproducibility.

Total-S and total-C contents were determined separately by Leco and recalculated to their respective oxides. CO₂ (from carbonated concrete and organic additives) is also included in the LOI, together with H₂O. Chloride was determined separately by ion-selective electrode ISE after digestion of bulk material in dilute nitric acid. Wet chemistry was applied to determine the Fe²⁺/Fe³⁺ ratio.

A second replicate portion of the ground bulk concrete was partly digested in *aqua regia* (concentrated 1HNO₃ : 3HCl) at ambient conditions. After filtration, the solution was evaporated and redissolved in dilute nitric acid. Thin section petrography has demonstrated [see Chapter 2] that the aggregate material is geologically mature, very rich in quartz and poor in other minerals, typically not more than a few volume percent altogether. (This has in fact been verified by geochemical analysis of digestion residue that was identical to fresh aggregate material within analytical error [61].)

The final digestion solution was then analyzed by ICP-AES for the main elements as mentioned above except Si, and the trace elements As, Ba, Co, Cr, Cu, La, Ni, Pb, Sc, Sr, V, Y, Zn, and Zr. Silica is unstable (and virtually insoluble) in *aqua regia* [77], and was therefore omitted. The aggregate material does not contain significant amounts of acid soluble minerals, as confirmed by petrographic examination of full cores and thin sections.

Lower detection limits and precision are stated according to [83] and collated in Table 1. Precision and data resolution will gradually deteriorate towards the detection limit. An extensive treatise on data evaluation is given by Shaw [112]. Some literature references do describe or mention some wet-chemical methods for some specific elements in raw materials or mortar, however, whole-rock analysis of concrete seems completely avoided [113,114]. Therefore, no standard reference materials are currently available.

3 Results

3.1 Petrographic observations

Macroscopic and microscopic details are described in Chapters 2 and 3 of this thesis. Thin section petrography confirms that deleterious ASR is the primary damage mechanism responsible for the observed cracking. Reactive constituents include porous chert, as well as sand- and/or siltstones. The latter seem more violently alkali-reactive, more frequently developing gel together with more often cracks extending into the surrounding paste. Portlandite is absent near alkali-reactive (porous) chert grains, but does in contrast occur close to reactive sandstone. Non-porous chert may also display some gelation along secondary cracks, but not pervasively throughout the grain interior. Portlandite occurs in the paste adjacent to non-porous chert grains.

The sand-/siltstone typically consists of quartz with some detrital muscovite and some accessory detrital heavy minerals. K-feldspar and plagioclase appear to be rare but may go undetected due to lack of characteristic twinning and the general fineness of these aggregate grains. Some sandstones have obviously been compacted under diagenesis, whereas others contain interstitial neogenic quartz and perhaps clay minerals, both of diagenetic origin. Grain contacts between adjacent quartz individuals in diagenetically compacted sand-/siltstones are typically serrated, and often accentuated. This latter may be due to the precipitation of clay minerals on the contact interface, beyond optical resolution, as has been described previously [95,96, and Chapter 2 of this thesis].

The confinement of cracks into zones in the concrete with a higher DRI is quite obvious to the naked eye. Cracks seem to be concentrated in the immediate proximity of the reinforcement, both at the top and the bottom of the deck. A third zone of intensive cracking occurs near the middle of the cores, at a somewhat variable depth. The overall amount of damage seems to be greater in cores BB246-7 from Zaltbommel, with the DRI reaching the scale maximum of 5 several times.

3.2 Na_2O -equivalents (Na_2O_{eq} 's)

Na_2O -equivalents are calculated as $Na_2O_{wt}\% + 0.658 \cdot K_2O_{wt}\%$. Data for the five profiles are presented in Plate 10, with Na_2O_{eq} plotted on a linear scale along the lefthand axis. Three different Na_2O_{eq} are provided:

1. Bulk material conform XRF (blue diamonds);
2. Cement paste after selective digestion conform ICP-AES (pink triangles), and
3. Aggregate material, calculated by subtracting cement paste alkali from bulk alkali (green dots).

Open markers indicate that multiple data points are superimposed upon each other. The damage rating index DRI (stippled line) is plotted on a linear scale along the righthand axis. The depth scale is aligned with the upper horizontal axis. Each depth profile represents a complete cross-section from the top at left to the bottom at right of Heemraadsingel and Zaltbommel, respectively.

Plate 11 presents the same data as above in scattergraphs of Na_2O_{eq} arranged per DRI, collated per structure (Heemraadsingel and Zaltbommel). In all cases, the data envelope indicates that the Na_2O_{eq} generally trends towards lower alkali contents up to DRI=3, then increases for DRI=4, and decreases again for DRI=5. For comparison, in Chapter 2 of this thesis the data for bulk chloride are presented in a similar way. Nota bene the different concentration scales on the left.

Collated in Plate 10, bulk $\text{Na}_2\text{O}_{\text{eq}}$ from XRF varies from 0.41wt% in disc section BB246A2 to 0.65wt% in BB247A16. Plate 10 also shows that the alkali content of the cement paste conform ICP-AES is roughly one-third of bulk concrete. Furthermore, the $\text{Na}_2\text{O}_{\text{eq}}$ -profiles for the cement paste do not run parallel to those for bulk concrete, perhaps with the sole exception of BB246 that might display some weak correlation. Also, the variation in $\text{Na}_2\text{O}_{\text{eq}}$ within one single profile is (logically) much less than for the bulk material.

$\text{Na}_2\text{O}_{\text{eq}}$ for aggregate material has been recalculated by subtracting the $\text{Na}_2\text{O}_{\text{eq}}$ for cement paste (ICP-AES-data) from the $\text{Na}_2\text{O}_{\text{eq}}$ for bulk concrete (XRF-data). The resulting $\text{Na}_2\text{O}_{\text{eq}}$ for aggregate material obviously follows the trend set by the bulk concrete. The alkali content of the bulk concrete is still dominated by the aggregate material, though the Dutch aggregate material is rather poor in alkalis compared to for example crushed aggregate used in other regions. The variation in bulk alkali-content within one profile may exceed the total alkali-content of the cement paste in that same profile.

A simple and straight-forward qualitative coincidence of all the above $\text{Na}_2\text{O}_{\text{eq}}$ with the DRI as with chloride concentrations in the very same samples as noted in Chapter 2 appears absent, as confirmed by a preliminary statistical evaluation of all the $\text{Na}_2\text{O}_{\text{eq}}$ [115].

3.3 Reverse calculation of the cement content

The alkali content of the cement paste is subordinate to that of the aggregate material. Though the original mix designs of the investigated concretes are unknown, early 1960's building practice when the investigated structures were built was to use circa $300 \pm 25\text{kg}$ cement per cubic meter of concrete. Modern Dutch cements are produced in a dry process and typically have a $\text{Na}_2\text{O}_{\text{eq}}$ of around 0.65wt% [61]. Early 1960's, Dutch cement was produced in a wet process and may hence have had an alkali content as high as 1.0wt%, or perhaps even higher.

In the investigated concretes with a measured specific mass of $2450\text{kg}\cdot\text{m}^{-3}$ [116], the alkalis in $250\text{kg}\cdot\text{m}^{-3}$ cement of 0.65wt% would contribute 0.066wt% to the bulk $\text{Na}_2\text{O}_{\text{eq}}$. A similar calculation for a less dense concrete of $2250\text{kg}\cdot\text{m}^{-3}$ containing more cement (350kg) with a higher alkali content (1.0wt%) results in a $\text{Na}_2\text{O}_{\text{eq}}$ contribution to the bulk of 0.155wt%. These values of 0.066wt% and 0.155wt% thus define wide lower and upper limits of the amount of alkali $\text{Na}_2\text{O}_{\text{eq}}$ contributed to the bulk concrete, assuming no analytical loss during partial digestion and no contamination from dissolved aggregate constituents.

Assuming a for the time of construction normal $300 \pm 25\text{kg}$ cement per cubic meter of concrete, $\text{Na}_2\text{O}_{\text{eq}}$ -contribution of the cement to the bulk concrete can be calculated to lay between 1.12wt% and 1.33wt%. This type of calculation can be reversed so as to recalculate a hypothetical cement content, assuming a $\text{Na}_2\text{O}_{\text{eq}}$ of say 1.0wt% for the cement. Thus, a hypothetical cement content can be recalculated, and should be expected to lay near $300 \pm 25\text{kg}$ cement per cubic meter of concrete, common for when the structures were built. A lower cement content would imply that some of the cement (ie. alkali) would have been depleted, a higher content would imply alkali enrichment.

Plate 11 presents hypothetical cement weight per cubic meter of concrete, as recalculated from the measured $\text{Na}_2\text{O}_{\text{eq}}$ according to ICP-AES after partial digestion in *aqua regia*, assuming a homogeneous $\text{Na}_2\text{O}_{\text{eq}}$ of 1.0wt% for the cement and a constant specific mass of $2450\text{kg}\cdot\text{m}^{-3}$. Alkali contents have first been corrected for eventually infiltrated deicing salt using the chloride content. Recalculated cement contents range from as low as

204kg·m⁻³ (BB246A1) to as high as 501kg·m⁻³ (BB244A5, BB244A16). It appears that concrete from Heemraadsingel is generally richer in cement than KW5 at Zalbommel.

4 Discussion

4.1 Trends in the alkali profiles

Metasomatism is a geochemical alteration process during which the bulk chemistry of a rock is altered. Thus, the final post-alteration composition of a rock differs significantly from its initial composition, not only mineralogically, but also geochemically. Some elements may have been newly introduced whereas other may have been removed by the passing fluids. Fluid transport and accessibility of the rock system (ie., permeability) are crucial to metasomatism [110]. Immaculate, uncracked concrete is obviously less prone to communication, fluid transport and (alkali) metasomatism than damaged concrete with a penetrative crack fabric [117]. Though the effects of metasomatism can be easily assessed by straight-forward geochemistry, the actual fluid transport properties of the crack network and initial and newly created pores require a thorough mathematical analysis [118].

The results described in Chapter 2 of this thesis strongly suggested a correlation between the Na₂O-equivalents for bulk concrete and the amount of cracks per unit surface which was used to classify damage in all of these studies. Re-assessment of the original samples from Chapter 2 in current DRI-terms reveals that ‘freshest concrete’ now classifies as DRI=1, and ‘severely attacked concrete’ as DRI=3. The original trends as observed for bulk concrete appeared straight-forward and very similar for the Heemraadsingel and Zalbommel structures studied here, as well as for two more investigated structures [Chapter 2 of this thesis]. Based upon these preliminary results, one of the main conclusions was that the Na₂O-equivalent seemed to correlate straight-forwardly with the ‘accessibility’ or, alternatively, ‘openness’ of the concrete through the (assumedly ASR-induced) crack fabric. Thus, it was inferred that a similar trend would emerge from a vertical profile comprising an entire bridge deck, providing reason for this study. This simple idea seemed initially to be confirmed by the chloride-versus-DRI profiles as discussed in Chapter 2.

There is basically only one single resource for chloride, namely sodium chloride applied as a deicing agent on the top surface of the deck. This contrasts with alkalis that are present throughout the bulk of the concrete both in paste and aggregate, and whose individual origin cannot be distinguished. Thus, in principle, the entire concrete column (ie. the whole cross-section of the original deck) could serve as a resource for alkalis, provided of course they are mobile. Alkalis from higher-up parts in the vertical concrete column could relocate to lower parts. An initially straight-forward, crack-controlled Na₂O_{eq}-versus-DRI leaching profile would then become blurred.

As indicated earlier, the variation in bulk alkali-contents in a given profile may be of the same size-order and occasionally even exceed the total alkali-content of the cement paste. This makes it highly unlikely that the cement paste alone is the sole source of available alkalis, especially as the cement paste seems largely unaffected by massive fluid transport, even in disc sections with lower bulk alkali-content than its neighbours, perhaps ‘depleted’. This suggests that alkalis could at least partially originate from the aggregate. The experimental setup of this Chapter does not allow it to be conclusive in that respect, but detailed microprobe data and element maps are provided in Chapter 5.

4.2 Reverse calculation of the cement content

In the early 1960's when the structures Heemraadsingel and KW5 at Zaltbommel were constructed, the cement content of bulk concrete was traditionally around $300 \pm 25 \text{ kg} \cdot \text{m}^{-3}$. However, the average content as recalculated for the investigated concrete samples (assuming a $\text{Na}_2\text{O}_{\text{eq}}$ of 1.0wt%) lays well over that amount. For Heemraadsingel, the average is rather on the order of $425 \pm 50 \text{ kg} \cdot \text{m}^{-3}$, and for KW5 at Zaltbommel $375 \pm 50 \text{ kg} \cdot \text{m}^{-3}$, which is definitely too high to suit Dutch building traditions, and appears contradictory with petrographic results.

There are two simple ways to explain these high average cement contents. The first is that the assumed $\text{Na}_2\text{O}_{\text{eq}}$ of 1.0wt% is too low. To obtain lower average cement contents of circa $300 \pm 25 \text{ kg} \cdot \text{m}^{-3}$ that fit better Dutch building traditions, the $\text{Na}_2\text{O}_{\text{eq}}$ has to be increased to 1.5wt% for Heemraadsingel, and to 1.35wt% for KW5 at Zaltbommel. Such alkali contents are more than twice as high as in modern cement compositions.

The second explanation is that alkalis from another constituent inadvertently could have been included in the analyses, ie. from the aggregate material during the partial digestion in *aqua regia*. However, detailed petrographic analysis demonstrated that the content in acid soluble constituents of the bulk aggregate material is very low, on the order of 2-3 percent only. Furthermore, XRF-analysis results of post-digestion residue from Heemraadsingel, KW5 at Zaltbommel and other concretes are very close to bulk aggregate material within analytical error [61], and are consistent with mineralogical data from petrographic analysis. Therefore, significant leaching from the aggregate material during partial acid digestion of bulk concrete in *aqua regia* seems unlikely.

Thus, in conclusion, it seems plausible that either the initial alkali-content of the cement was significantly higher than the 1.0wt% assumed in the calculations/graphs, or that the cement contained more alkalis from the aggregate material, not released by the analytical procedure but by processes or minerals within the concrete. Potential candidates for alkali release include sheet silicates like micas and clay minerals. Some sand-/siltstones in the aggregate material contain detrital mica, and the presence of (interstitial) clay minerals in the same aggregate grains is very likely, though they are beyond optical resolution. Both types of minerals have been documented to release alkalis under harsh conditions [see discussion in Chapter 2].

When fresh concrete is poured in the mould, the top surface is usually richer in cement and poorer in aggregate material than the bulk concrete, particularly in a water-rich mix. Thus, the cement content as recalculated from the $\text{Na}_2\text{O}_{\text{eq}}$ -ICP for paste may be expected to significantly higher than for bulk concrete, for the cement is 'undiluted by aggregate'. Here, that would be significantly higher than $300 \pm 25 \text{ kg} \cdot \text{m}^{-3}$. However, the cement content of top zones 1 (BB244A: 0) as recalculated from the alkali content is invariably considerably lower than of the bulk concrete. This coincides with a higher amount of damage (DRI) for those top zones, indicating that the concrete is better accessible to fluid infiltration and/or leaching than the bulk material at greater depth. Apparently, the paste has lost a part of its original alkalis. Thin sections study reveals that the cement paste in the severely cracked top zones is carbonated and significantly more altered and porous than the rest. The same interaction may have removed alkalis from the paste.

4.3 *Statistical analysis*

Statistical analysis of geochemical results with the software program MiniTab initially suggested moderate correlations of a few elements with the damage rating index DRI, apart from the striking coincidence with chloride [Chapter 3]. After a more thorough assessment of the data plotted in scattergraphs (Plate 12), it clearly appears that the Heemraadsingel and Zaltbommel concretes define separate sample populations by distinct differences in cement trace element composition. Whereas a single population does not have any correlation with DRI, combining two such populations results in a (moderate) pseudo-correlation, the farther apart these populations are, the higher their ‘correlation’.

Of the initial correlations found for the entire data set, none of the observed correlations persist, neither for Heemraadsingel, nor for Zaltbommel. The correlation factors for Heemraadsingel seemed higher than for Zaltbommel, but none were of an acceptable level. However, some of the cracks in core BB246 from Zaltbommel had been induced by four-point bending testing in the laboratory [Chapter 3]. Reconstructing the respective DRIs to ‘background values’ considerably affected some of the correlation factors in a positive sense, though still not to an acceptable level. Taking all the above into account, the conclusion is that there are no other element correlations with DRI, except with chloride.

4.4 *Trends in the scattergraphs, and a speculative model*

The model proposed below is speculative and solely intended to guide thoughts. It has not been verified, and could either be confirmed by further research, or be rejected. The model is presented here, merely as a provocation to invoke technical discussion on the subject, in an attempt to explain the current $\text{Na}_2\text{O}_{\text{eq}}$ ’s rather than a proof of what actually happens.

To eject a fluid phase, a matrix hosting a fluid must be able to take up tensile stress. Consider two tubes with fresh and old toothpaste (eventually with added silica), respectively. Then, the more viscous the toothpaste is, the higher the stress on the tube, and the higher tensile strength of the tube material is needed. Transcribed into concrete terms, concrete (ie., the tube) does have some tensile strength as long as it is coherent and able to take up pull, in contrast to a material broken up and parted by cracks, let alone disintegrated concrete (ie. squeezing an exploded tube brings no toothpaste on the brush).

Shortly after emplacement, the concrete is essentially free of cracks, hence DRI based on macroscopic observations equals zero. At some moment, ASR-susceptible silica starts reacting with the available alkalis, and ASR-induced internal stresses will build up gradually. If cores had been extracted from the concrete at that phase, then the release of internal stress would have led to cracks along the circumference of the core, resulting in minor damage with DRI=1. At a later stage, internal stresses will become greater than the tensile strength of the concrete, and isolated cracks will emanate from the most violently reactive grains. In impregnated cores, this amount of damage would be classified DRI=2. With increasing expansion, initially singular cracks will join, forming a penetrative and interconnected network over a larger volume, yet not partitioning concrete. Concrete with such damage classifies DRI=3.

Up to DRI=3, the concrete is coherent and able to take up tensile stress, whence bulk expansion and internal stress are basically caused by alkali-gel expansion. Some of this internal tension can be released by gel extrusion, ejecting ASR-gel to a less strained volume. Thus, alkalis could be ejected from concrete with $\text{DRI} \leq 3$ or less, and injected in concrete with $\text{DRI} > 3$. If the amount of damage increases further, concrete first loses its integrity by

partitioning along major cracks resulting in DRI=4, and finally complete disintegration to DRI=5 where the concrete merely consists of incoherent chunks.

When comparing the scattergraphs in Plate 12, a repetitive pattern seems to emerge. Starting from DRI=1 (DRI=0 does not occur in this study), the envelope of the collated Na₂O-equivalents trends towards lower values as damage increases to DRI=3. Then, in contrast to this decreasing trend, concrete with DRI=4 appears to have a higher Na₂O-equivalent, which then decreases again towards DRI=5 for concrete that has lost all of its integrity. This procession converges with the toothpaste model.

The presence of cracks enhances the accessibility (and permeability) of the concrete. More importantly, the alkali (-gel) ejected by lesser damaged concrete with DRI's up to 3 may be injected into more open media, eg. concrete with DRI of 4 since internal stresses largely have been released by the extensive cracking. Thus, the Na₂O-equivalent of concrete with DRI=4 might even become higher than that with DRI=3. Whether the Na₂O-equivalent of concrete with DRI's of 4 or 5 represents either a net enrichment or a net depletion, depends on the relative amounts of leached out initial alkali versus newly infiltrated alkali from elsewhere. This implies net alkali transport within the concrete, channelized along the crack fabric. Where cracks finally meet the surface, the solution may exit the concrete, leaving stalactites and/or trails of deposited lime that are more than merely unsightly only.

Due to the apparently localized character of the alkali-silica reaction, the concrete within one single disc section may be enriched in alkalis at one site, which is by the analytical procedures followed averaged out with a local depletion elsewhere in the same disc. This is illustrated by the inconsistent variation of chloride with the DRI in Plate 12 (compare with Plate 9), where the spread in chloride content clearly increases with increasing amount of damage, except for DRI=5 for which the spread lessens again. The presence of cracks also opens the possibility for a *secondary* alkali-silica reaction, by increasing available surface area and at the same time by providing access to the interiors of potentially ASR-susceptible, but non-porous aggregate constituents. To distinguish such 'false ASR' (ie. secondary) from true (ie. primary) ASR, detailed petrography on both sanded slabs and thin sections from the same drilled cores is essential.

4.5 *Reactive aggregate constituents*

Petrographic observations imply that sand-/siltstone is more violently alkali-reactive than chert in the same concrete, in the sense that cracks seem wider and occur more frequently, that the volume of extruded gel seems larger, and that more of the grains' interiors seems consumed by the reaction, all compliant with earlier observations [also see Chapter 2].

The very obvious differences between chert and sand-/siltstone are their mineralogical and geochemical compositions. Essentially, Dutch chert consists of (often poorly crystalline) silica with carbonate and sometimes minor pyrite, whereas sand-/siltstone may or may not contain subordinate amounts of detrital minerals, mainly muscovite, chloritized biotite, tourmaline, zircon, and opaques. Occasionally, neogenic syntactic overgrowths occur on quartz in diagenetically altered materials, while very fine-grained clay minerals beyond optical resolution may have precipitated along grain boundaries. However, K-feldspar and plagioclase seem virtually absent, thus the alkali-content of the total aggregate material is expected to be correspondingly low. This seems to be confirmed by a number of geochemical analyses performed on fresh aggregate material, typically containing >94wt% SiO₂, ranging from 88wt% up to 98wt% [61].

From the reverse calculation of the cement content exercise above, the suggestion from Chapter 2 that alkalis may be released from the aggregate material seems reconfirmed, but can not be resolved with the present geochemical results for bulk concrete. This matter will therefore be addressed in the next chapter, Chapter 5.

5 Conclusions

The conclusions that can be drawn from this study include:

1. Previous data on concrete from the same structures [Chapter 2] covered DRI's up to 3 and give in that respect an incomplete overview (since DRI's 4 and 5 were lacking);
2. Deep and penetrative cracking makes the concrete accessible to foreign solutions potentially carrying dissolved matter in or out;
3. Correlation of Na₂O-equivalents from bulk material, cement paste, and aggregate material (calculated) with DRI is obscure and not as simple and straight-forward as with chloride [see Chapter 3];
4. Scattergraphs of Na₂O-equivalents from bulk material, cement paste, and aggregate material (calculated) plotted against DRI indicate diminishing alkali contents for DRI \leq 3, somewhat higher for DRI=4, and lower again for DRI=5;
5. Hypothetically, coherent concrete with DRI \leq 3 may squeeze out alkalis due to swelling action of the gel until concrete is completely cracked and no longer able to take up tensile stress, after which the outpouring of gel ceases;
6. In the same hypothesis, alkalis leached out from concrete with DRI \leq 3 may infiltrate in to concrete with DRI $>$ 3 in which swelling of gel no longer results in expansion;
7. The precise and detailed origin of the alkalis is still unresolved, both cement paste and aggregate material may contribute. To be able to distinguish the different potential alkali resources, geochemical data with microscale resolution are necessary.

The origin of the alkalis involved in the ASR process cannot be established unequivocally from this study and hence remains somewhat unclear. There is no simple way to distinguish between alkalis originating from the cement paste or the aggregate material. Alternatively, microscale element mapping under the electron probe is relatively convenient [119]. Results from that method are presented in Chapter 5.

TABLE 1: Lower detection limits per element in bulk concrete, for different analytical methods, and instrumental precision for different element contents, after [?].

<i>element</i>	<i>instrument</i>	<i>digestion</i>	<i>unit</i>	<i>lower DL</i>	$10^2 \times DL$	$10^3 \times DL$	$10^4 \times DL$	<i>comments</i>
Na ₂ O	XRF	HT Li-pellet	wt%	0.01	0.04	0.12	4	
	ICP	aqua regia	ppm	100	500	1500	4500	as Na
K ₂ O	XRF	HT Li-pellet	wt%	0.01	0.02	0.06	2	
	ICP	aqua regia	ppm	100	200	600	1800	as K
MgO	XRF	HT Li-pellet	wt%	0.01	0.04	0.12	4	
	ICP	aqua regia	ppm	100	500	1500	4500	as Mg
CaO	XRF	HT Li-pellet	wt%	0.01	0.02	0.06	2	
	ICP	aqua regia	ppm	100	200	600	1800	as Ca
MnO	XRF	HT Li-pellet	wt%	0.01	0.02	0.06	2	
	ICP	aqua regia	ppm	2	6	18	54	as Mn
Al ₂ O ₃	XRF	HT Li-pellet	wt%	0.01	0.03	0.09	3	
	ICP	aqua regia	ppm	100	500	1500	4500	as Al
total-Fe ₂ O ₃	XRF	HT Li-pellet	wt%	0.01	0.02	0.06	2	
	ICP	aqua regia	ppm	100	400	1200	3600	as Fe
TiO ₂	XRF	HT Li-pellet	wt%	0.01	0.02	0.06	2	
	ICP	aqua regia	ppm	100	500	1500	4500	as Ti
SiO ₂	XRF	HT Li-pellet	wt%	0.01	0.03	0.09	3	
	ICP	aqua regia	ppm	–	–	–	–	omitted
P ₂ O ₅	XRF	HT Li-pellet	wt%	0.01	0.03	0.09	3	
	ICP	aqua regia	ppm	10	20	60	180	as P
LOI	gravim.	ign. at 1000°C	wt%	0.01	–	5	–	CO ₂ +H ₂ O
total-C	Leco	ign. at 1300°C	wt%	0.01	0.02	0.05	–	as CO ₂
total-S	Leco	ign. at 1300°C	wt%	0.01	0.10	0.05	–	as SO ₃
Cl ⁻	ISE	nitric acid	ppm	50	1	2	5	
FeO	titrimetric	K ₂ Cr ₂ O ₇ -sln.	wt%	0.1	5	–	–	as Fe ²⁺ /Fe ³⁺
As	ICP	aqua regia	ppm	3	30	90	270	
Ba	ICP	aqua regia	ppm	1	10	30	90	
Co	ICP	aqua regia	ppm	1	5	15	45	
Cr	ICP	aqua regia	ppm	1	5	15	45	
Cu	ICP	aqua regia	ppm	0.5	1	3	9	
La	ICP	aqua regia	ppm	0.5	2.5	7.5	23	
Ni	ICP	aqua regia	ppm	1	5	15	45	
Pb	ICP	aqua regia	ppm	2	20	60	180	
Sc	ICP	aqua regia	ppm	0.5	2.5	7.5	23	
Sr	ICP	aqua regia	ppm	0.5	5	15	45	
V	ICP	aqua regia	ppm	2	10	30	90	
Y	ICP	aqua regia	ppm	0.5	2.5	7.5	23	
Zn	ICP	aqua regia	ppm	0.5	2.5	7.5	23	
Zr	ICP	aqua regia	ppm	0.5	2.5	7.5	23	

Chapter 5

Microscale Element Distribution Around Chert and Sandstone

Adapted from:

Broekmans, MATM, Nijland, TG, and Jansen, JBH (2001): Origin and mobility of alkalis in two Dutch ASR-concretes II: microscale element distribution around sandstone and chert. Implications for the mechanism of ASR. In: Stamatakis, M, Georgali, B, Fragoulis, D, and Toumbakari, EE (editors): Proceedings of the 8th Euroseminar on Microscopy Applied to Building Materials, Athens, Greece: 85-92.

1 Introduction

The traditional model for the alkali-silica reaction presupposes that the alkalis involved originate from the cement paste. Implicitly, the alkalis have to be mobile and infiltrate potentially alkali-reactive grains, which therefore have to be porous to some degree. Porous chert complies well with these prerequisites.

Other aggregate grains, like sand-/siltstone may contain significant amounts of alkalis incorporated in common minerals like feldspars, micas, and clay minerals. Some of these minerals are detrital, others been formed during alteration and diagenesis of the sediment. The alkalis in K-feldspar and albite are more strongly bonded than in muscovite and clays, which release their alkalis rather easily, especially in a high-pH solution [120], as eg. in concrete. If these minerals do indeed release alkalis to concrete, and if their host grains contain alkali-reactive silica (whatever its definition) [also see Chapter 6], then such aggregate grains would be independent of alkalis from the cement paste to develop a deleterious alkali-silica reaction.

Even though alkali-containing minerals are commonly observed, Dutch aggregate materials in general contain only limited amounts of alkalis. Results from the analysis of bulk concrete indicate that the bulk Na₂O-equivalent of aggregate is of the order of 0.3-0.5wt.% [see Chapter 4], whereas that of cement is less than half that amount. Most of this 0.3-0.5wt.% Na₂O-equivalent is firmly consolidated in fresh K-feldspar and/or albite, the rest may be more loosely bonded in other minerals including muscovite and clays. Monomineralic grains other than quartz are rare, and may include muscovite/biotite mica, chlorite, K-feldspar and/or albite, and very rarely shell fragments.

Gravel from the river Meuse as used for concrete aggregate in the Netherlands may contain several potentially deleterious components with respect to alkali-silica reaction (ASR), like porous chert and sand-/siltstone, the latter with or without muscovite and/or clays. Both have been involved in reaction in concrete showing damage due to ASR. Because of the differences in mineralogical and geochemical composition of chert and sand-/siltstone, it seems only logical that their behavior in ASR is different. This contribution assesses this issue by element mapping at microscale.

2 Experimental methods

Polished thin sections were prepared from fluorescent dye epoxy-impregnated concrete as investigated in another study on the origin and mobility of alkalis under ASR-conditions [see Chapter 4]. The thin sections for this investigation were prepared without dye-impregnation, although locally along cracks, the concrete may contain some fluorescent epoxy-resin from the initial full-core impregnation. After petrographic characterization in polarized light with fluorescence, four areas were selected for microscale element mapping, including both intact and ASR-cracked chert and sandstone with gel present.

Electron microprobe analyses were performed at the Technical University of Delft, the Netherlands, Faculty of Civil Engineering and Applied Geosciences, Department of Applied Earth Sciences. The instrument is equipped with three detector crystals (LIF, PET, TAP), all for WDS operation. Running conditions were set at 15 kV and 20 nA. After programming the selected areas, maps of Si, Fe, Ca, Na, K and S, respectively, were produced during overnight runs of up to eleven hours per map. The elements of interest were selected primarily for their involvement in the alkali-silica reaction, and secondly for reason of optimum occupation of all three detector crystals.

3 Results

3.1 Data presentation

Results are presented in Plates 13-14 for chert and Plates 15-16 for sand-/siltstone, respectively. Each single Plate is a quilted patchwork of six images designated A-F, all of the same area, arranged K-Na-Ca for the top row, and Si-Fe-S for the bottom row. For each individual image, a relative concentration scale is printed along its right edge, black representing 0wt.% of the element, and white the highest concentration *for that particular image*. Hence, the scale is different for each of the six elements in one Plate, and for the same element between different Plates.

3.2 Figure 1/Plate 13: intact chert

Though difficult to discern without impregnation-fluorescence, the chert seems optically dense and non-porous. Verification with fluorescence illumination reveals no traces of dyed-epoxy impregnation. No signs of alkali-silica gel and/or cracking are visible, even at the highest magnification.

The distribution of K in map A and Na in map B, reveals that their background concentration is somewhat higher than that of the cement paste, especially for K. According to map C, the cement paste is the main reservoir for Ca. Perhaps infiltration of Ca occurs in a very thin ($\leq 50\mu\text{m}$) zone along the NW-SE running grain boundary of the chert. This may be due to ingress from the cement paste. However, a sedimentary origin for the Ca cannot be precluded. Single grains of K-feldspar, albite, and intermediate plagioclase are also disclosed by maps A-C.

Map D for Si shows sharp and continuous edges on all aggregate grains, indicating that no Si is migrating out of the chert grain, nor from any other grain in the field of view. This image also shows the local porosity of the cement paste and the air voids, for example immediately NW of the larger aggregate grain along the E edge of image D, and due N of the image center as well.

Map E displays a somewhat higher Fe-concentration along the margin of the chert grain, though the outermost edge again contains virtually no Fe. As Fe is immobile under high-pH conditions, ingress from the cement paste is unlikely, and infiltration of Fe into chert is almost certainly a geological feature. Optical petrography confirms the presence of Fe-hydroxides in the chert cortex. Finally, map F shows the distribution of S. Apparently, only the cement paste contains sulphur, presumably as sulphate in AFt, etc.. Sulphur did apparently not infiltrate the chert.

Summarizing the above observations, no signs of any deleterious ASR are visible, neither optical, nor in the element maps. The dense chert consists mostly of silica, but contains more K and perhaps more Na than the cement paste. There is some initial Fe present in the cortex, as well as some minor Ca. However, from the present data it cannot be resolved whether the Ca is of geological-sedimentary origin, or alternatively infiltrated when the chert got embedded in the concrete. Interaction of dense chert with its environment seems improbable, which fits with the general experience of its innocuous behavior.

There are no discernible concentration gradients in the cement paste for any of the mapped elements, on the scale of the image. These may never have been there, or they may have been levelled out by later redistribution.

3.3 *Figure 2/Plate 14: cracked chert*

The element maps of Plate 14 come from another portion of the very same chert grain as in Plate 13. Here, the chert seems to have a spongy, porous microstructure. Maps A-C clearly display two infiltration fronts for K, Na, and Ca: a primary 100-400 μ m margin along the original edge, with concentrations sharply dropping to background level, and a second one along the crack walls, considerably wider than the primary front, with lower concentrations. For Ca, the first infiltration front may be entirely or partly of geological origin. The second infiltration front evidently formed after the aggregate grain was embedded in the concrete. Maps A-C combined also disclose single grains of K-feldspar, albite and plagioclase.

The initial K-content of the chert interior as displayed by map A is clearly higher than that of the paste. The bright green specks within the infiltrated margins coincide with similar specks in map C for Ca, and can presumably be attributed to ASR-gel containing both K and Ca. The ASR-gel deposited in the crack is K-enriched compared to initial background levels of the cement paste.

Map B shows that the interior of the chert contains just a little more Na than the cement matrix, in accordance with Plate 13. The ASR-gel deposited along the wall of the WSW-ENE crack in Plate 14 is clearly enriched in Na. The brighter specks in the infiltrated portions of the chert may be due to local concentrations of alkali-rich ASR-gel.

On map C, the margin infiltrated by Ca is thinner and more sharply defined than the margins infiltrated by K and Na. The interior of the chert is essentially free of Ca, whereas the cement matrix is Ca-rich. Some grains of intermediate plagioclase clearly appear in the fine aggregate. The ASR-gel in the crack is relatively Ca-enriched, though still lower than the cement.

Map D for Si clearly reveals that the central portion of the chert has a slightly lower Si-content, illustrated by a more yellowish color with locally green specks, indicating the

presence of other elements than Si (but not Na, K, nor Ca). The Si-content of the ASR-gel in the crack is between that of the chert and the cement paste, which indicates that the gel must have been derived from the chert by dissolution and transport.

Map E illustrates the Fe-distribution. The cement paste contains some iron. The fine aggregate material also contains some Fe-richer grains, especially in the N half of map E. The interior of the grain contains considerable Fe, in contrast to Plate 13, where Fe occurs in the cortex but not in the interior. Optical petrography confirms the presence of brownish hydroxides here. Map F shows that only the cement paste contains sulphur, most likely as sulphate in AFt, et cetera. Sulphur is absent in chert and ASR-gel.

Summarizing the above observations, it appears that K, Na and Ca enter the chert, initially along its perimeter, and at a later stage when the chert has yielded to ASR, also along the crack. Si leaves the chert as an ASR-gel that can also be seen deposited on the S-wall of the crack. Though the infiltrated margins of the chert clearly show concentration gradients, these are absent in the adjacent cement paste, and do not appear on the rest of the images either. Again, this may indicate they have never existed or that they have been levelled out by later redistribution.

3.4 *Figure 3/Plate 15: intact sandstone*

Optical petrography reveals that this part of the sandstone does not have any detectable ASR-gel or cracking. Elsewhere in the same grain, ASR has induced extensive cracking and gel exudation. There are no distinguishable optical differences in mineralogical composition, internal grain texture or fabric between the alkali-reactive and innocuous parts. Interstitial porosity seems low, even without impregnated fluorescent dye (verified by fluorescence). The rock mainly consists of cemented detrital quartz grains with some interspersed detrital muscovite. Feldspars or clay minerals have not been identified individually, but the sandstone does have accentuated grain boundaries as described in Chapter 2. Average internal grain size is $\sim 100\mu\text{m}$, which makes this particular grain a fine-grained sandstone. *Nota bene*: though this sandstone is not representative of the bulk aggregate material, it is not an exceptional component either.

Map A reveals that the sandstone contains more K than the cement paste, likely incorporated in muscovite and perhaps also in interstitial clays [also see Chapter 2]. Along the S edge of the image, two K-feldspar grains appear bright red, and a fine grained siltstone bright green due to the K contained in muscovite. As for Na, the element map shows neither evidence for K migrating out of the grain, nor ingress of K into the grain.

Map B shows that the coarse aggregate grain clearly contains some Na, and considerably more than the background level in the cement paste. Albite grains in the fine aggregate material occur in the SE-corner, as well as some fine grained siltstones. The Na in the sandstone is probably incorporated in interstitial clays, or alternatively in muscovite as a minor admixture, but unlikely in albite. The element map shows no evidence for Na migrating out of or into the grain.

Map C shows that the paste material is the main Ca-reservoir. A grain of augite lights up bright green, SSW of the center of the image. The siltstone on the S edge also contains Ca in intermediate plagioclase (compare with map A). Obviously, some Ca has infiltrated the sandstone margin, while the interior of the grain is still devoid of Ca. Similar fringes are

visible in the right margin of the small siltstone fragment, suggesting that Ca may have entered along its schistosity there as well.

Map D on Si indicates that most of the fine aggregate material consists of plain quartz, with a few grains of plagioclase and K-feldspar, and the siltstone along the S edge of the map. The sandstone clearly contains minerals other than quartz, confirmed by maps A-B on K and Na. Map D also reveals the locations of air voids and porous parts near the E edge of the map, and the porous area SSW of the center. Grain boundaries are sharply defined, suggesting complete immobility of Si in this view.

Map E for Fe shows that the Fe-content of the sandstone is only slightly lower than that of the cement matrix. The augite grain of map C for Ca clearly shows here as well. The bright grain just WNW of the augite is a fragment of iron hardpan, ie. quartz cemented by Fe-hydroxides ('limonite'). The Fe in the sandstone appears to be of similar character but more finely dispersed. Boundaries between Fe-containing and Fe-free areas are sharply defined, illustrating its immobility in concrete. Finally, map F shows that sulphur S almost only occurs in the paste.

From the above observations it appears that the sandstone contains more K and Na than the cement paste, most probably in muscovite and/or clays. According to a vast literature base [eg. 95,96], interstitial clays may be present along grain boundaries, even when they can not be identified optically, and only with difficulty in an SEM. Previous petrographic work on thin sections from the same structure [see Chapter 2] argued that the 'accentuated grain boundaries' frequently met in the alkali-reactive sandstones most probably can be attributed to interstitial clays. Even though this only provides indirect evidence, the characteristics of the sandstone mapped here in fact do closely resemble those described in the literature. These include sutured contacts between adjacent quartz individuals, a compacted grain fabric and the presence of detrital mica.

Feldspar and/or albite-rich plagioclase seem to be absent from the sandstone, or at least not a common constituent. Na and K in sheet silicates like clay minerals and muscovite are loosely bonded, and are easily released under severe conditions such as high-pH, as in concrete. Neither K, nor Na seem to enter or to leave the sandstone grain margin, but it has to be noted that a change in alkali-concentration as large as that in the chert may go unnoticed, since it is completely overwhelmed by the much higher initial background concentration of the sandstone. Ca is present in the perimeter of the grain and could be of geological-sedimentary origin as well as infiltrated into the concrete. Fe and S appear to be immobile. No concentration gradients are visible in the cement paste, either because they have never existed, or they have been levelled out later.

3.5 *Figure 4/Plate 16: cracked sandstone*

The sandstone mapped in Plate 16 has a wider crack elsewhere, allowing for convenient access of fluids and solutions. Initial elemental redistributions that occur when an ASR-induced crack has just opened, may be erased by later fluid transport. In order to establish whether or not alkalis are released from sandstone, we are interested in the former. Thus, another crack that apparently just opened in an otherwise (mineralogically and structurally) indistinguishable sandstone grain from the same structure and sample but in another thin section was chosen for the element mapping.

Map A shows that in general, the sandstone is richer in K than the matrix. In a 400-500 μm wide margin parallel to the N-S running boundary of the grain, K appears to be confined to spots. In the inner portion of the grain, K also occurs between the spots, which appear smaller in size than those of the grain margin. Muscovite grains are disclosed by K occurring in 'bars', the remainder of the K most probably represents fine grained clays. The cement paste directly adjacent to the sandstone edge appears to be slightly enriched in K, in contrast to the situation described from the intact sandstone (Plate 15). The ASR-gel and the gel plug extending into the paste are enriched in K, as it is in the ESE-offshoot that has not yet propagated into the paste. K is possibly leaching from the sandstone into the paste in a diffuse way from the grain margin. K is also transported directly by extruded ASR-gel, though only in limited amounts.

Similar features are observed in map B for Na. In the margin of the grain, sodium seems more restricted to blots than in its interior, and the paste directly adjacent to the grains edge is somewhat enriched in Na, like the ASR-gel plug that here most clearly extends into the matrix. Thus, the inferences for the dissipation of potassium into the cement paste appear valid for sodium as well.

Map C for Ca shows the high Ca-content of the cement paste, versus a generally low Ca-content in the sandstone. The sandstone margin seems to be infiltrated with Ca through the pore fabric whereas its interior is essentially free of Ca. Locally within the $\sim 500\mu\text{m}$ margin, some isolated Ca-richer blotches do occur. Obviously, calcium also enters the sandstone through both the main crack and its offshoot to greater depths than the infiltrated margin, indicating that though the walls of the offshoot may not have parted visibly yet, the crack is accessible.

Map D for Si discloses the high Si-content of the sandstone and the quartz grains in the fine aggregate, and the generally lower Si-content of the cement paste. Muscovite can easily be identified by comparing with the K-map, and a K-feldspar grain is visible in the paste, just below the main crack. The Si-content of the ASR-gel in the main crack is similar to that of K-feldspar or muscovite, and a bit lower than that in the offshoot. Silicium from the sandstone has migrated into the paste along the main crack over a larger distance than the width of the gel plug itself. The ASR-gel in the offshoot is poorer in Si. Here, no Si has apparently migrated into the cement paste.

According to map E, the cement paste contains more Fe than the sandstone, where the Fe is apparently concentrated along grain boundaries, especially in the offshoot of the main crack. The presence of brown Fe-hydroxides is confirmed by optical petrography; the absence of sulphides by map F on sulphur. Fe appears to be more finely dispersed in the cement matrix. Cluster grains of alite with C_4AF occur in the SE quadrant of the image near the boundary of the sandstone. Iron is apparently immobile. Map F displays that S is mainly confined to the cement matrix as sulphate in AFt, etc. The aggregate material is free of S, as is the ASR-gel plug that extends into the cement matrix. No S/sulphate-minerals like ettringite/thaumasite are identified by optical petrography.

In conclusion, it appears that Na, K and Si migrate out of this alkali-reactive sandstone along the main crack, that Ca enters through its initial porosity in the margin and along both the main crack and its offshoot. Both Fe and S seem immobile. Na and especially K provided by the sandstone to the cement paste do seem to form a halo surrounding the aggregate grain. From current observations, it cannot be decided whether these alkalis have been collected from the cement paste and are about to enter the sandstone, or that

they have been released by the sandstone. However, given the higher initial alkali-content of the sandstone, the former option doesn't seem logical.

4 Discussion

The mechanism by which alkalis enter aggregate material is still unknown, as is to some extent the nature of the alkalis contained *ab initio* in some aggregate constituents. Plate 13 shows that the background concentration of K in uncracked chert may be up to around 1wt%, clearly higher than of the cement paste. In the same chert grain, the background concentration of Na at around 0.3wt% is of the same size-order as the cement paste. These values are in accordance with geochemical data on similar cherts from fresh aggregate [61].

Though solid silica may contain interstitial K^+ , Na^+ , and other minor elements for charge compensation of Al^{3+} and/or Fe^{3+} replacing Si^{4+} in the $(SiO_4)^{4-}$ -tetrahedra, the concentration of such charge compensators is limited to the ppm-range. Thus, though some of these elements may be contained in the silica [121], it seems probable that the K/Na occur interstitially in minor mineral constituents, like clay minerals that are known to be able to contain alkalis.

Clays have long been thought to play a role in chert formation [122,93]. Indeed, K and Al have been identified to coexist in Dutch chert [123], and in chert in general [124,125]. The interior of the dense chert in this study appears to contain more K than that of the porous chert, which could suggest that the original porosity in porous chert is obstructed by interstitial clay in the dense chert, which complies with data from Kneller [121]. Thermogravimetric analysis (TGA) on fresh chert samples from Kneller indicate a weight-loss of typically around 1.2wt% upon heating to 600°C, though the DTA-curve does not show any clear peaks in that range [see Chapter 7]. It must be noted however, that transitions from dense to open and porous chert as in the grain investigated here are quite common [93].

Infiltration of K (Na) in dense chert containing K (Na) in pore clay minerals would thus be not very likely, because either the pore channels may be physically obstructed, or because the pore fluid may be saturated in K (Na). However, the reactive nature of the silica itself is not affected in dense chert, as illustrated by the ASR-gel that often occurs along crack surfaces, the gel formation there being secondary to cracking.

The pores in the alkali-reactive sandstone are most probably also filled with clay minerals. Indeed, minor kaolinite (sericite?) occurs in sprays in compacted sandstone, together with but not associated with 'accentuated grain boundaries'. The characteristics of these latter closely resemble reported descriptions of sutured grain boundaries in diagenetically compacted quartz-rich sandstones [95]. There, it is argued that no particular reason obtains for two adjacent grains of the same mineral to develop a sutured contact, provided the contact is free of impurities.

However, imaging combining SEM, cathodoluminescence and element mapping (K+Al) demonstrates that it is most likely kaolinite that is deposited on the grain contact, producing a stylolite-like suture. In turn, this latter aspect is attributed to the catalytic effect of clay minerals and micas in increasing silica solubility by affecting the local pH of pore water at the grain edges [95,96]. Thus, detrital mica and interstitial clay minerals play a role in the dissolution (and subsequent re-precipitation) of quartz during compaction.

Earlier observations on thin sections from the Heemraadsingel structure confirmed the presence of areas with increased porosity at edges of detrital mica [see Chapter 2]. Furthermore, clay minerals and micas may swell and/or release alkalis under basic conditions [120,126,127]. Simple experiments have demonstrated that the pH is affected even with high water-solid ratios [97]. However, hard evidence for the release of alkalis from interstitial clay minerals and/or detrital mica is lacking. For the future, detailed geochemical analysis with electron micro-probe must reveal whether the edges of (detrital) mica do or do not release alkalis.

5 Conclusions

For the individual grains described, the following may be concluded:

- 1 The dense, innocuous grain of chert is initially richer in K, Fe (Si) and poorer in Ca, S than the cement paste, whereas both have low Na-contents. No migration of Na and K out of or into the chert occurred, but Ca infiltrated the chert along its grain boundary. This may be, however, a geological feature.
- 2 The porous, alkali-reactive part of the same grain of chert is infiltrated by Na, K, and Ca from the cement paste to a level that exceeds the initial background concentrations; infiltration occurred through initial porosity and through ASR-generated cracks. Si is extruded in ASR-gel along cracks.
- 3 Sandstone is initially considerably richer in K, Na (Si) and poorer in Ca, S than the cement paste, whereas Fe-contents are comparable. Both non-reactive and ASR-reactive sandstone are infiltrated by Ca along grain boundaries up to $\leq 100\mu\text{m}$ from the margin, to a concentration level clearly higher than in chert. In addition, alkali-reactive sandstone extrudes Na, K, Si into the cement paste through specific ASR-cracks, which also allow Ca to migrate inwards.
- 4 Along the alkali-reactive sandstone a halo of elevated K and possibly Na-contents is displayed by the cement paste.

From four settings, it is difficult to draw general conclusions with respect to ASR. However, they appear to indicate that porous chert depends on alkalis provided by the cement paste to develop deleterious ASR, whereas internal alkalis in sandstone may also play a role in its initiation.

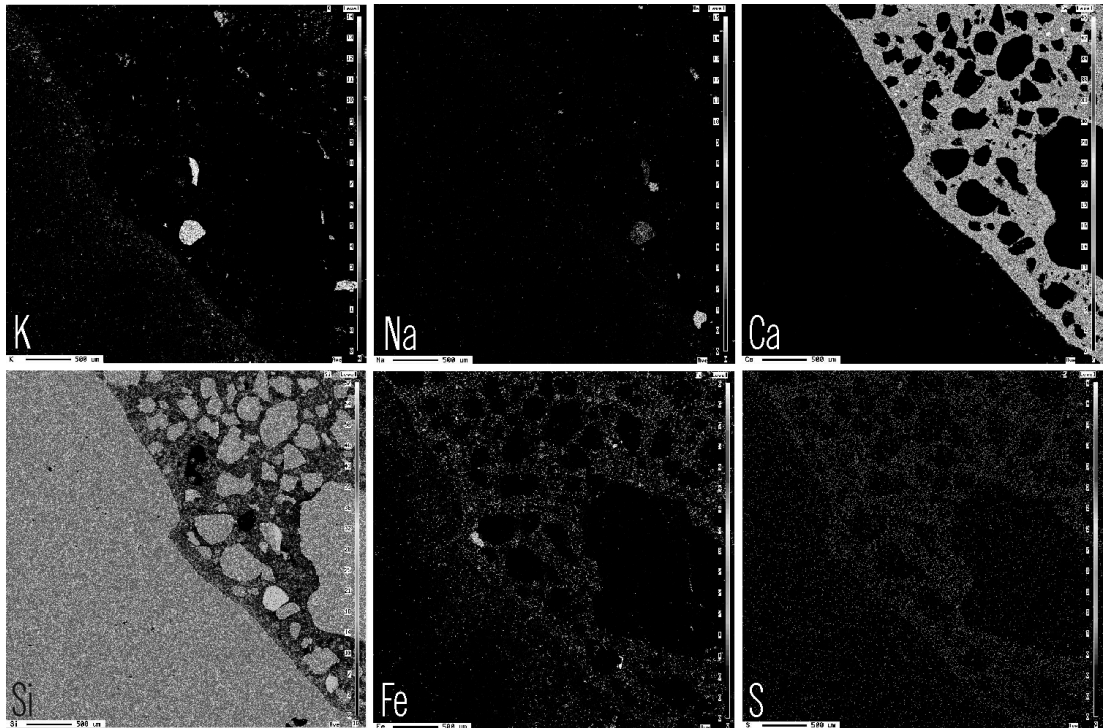


Figure 1: Element maps of intact, uncracked chert. Scale bar is 500 μ m. Full-color maps printed as Plate 13.

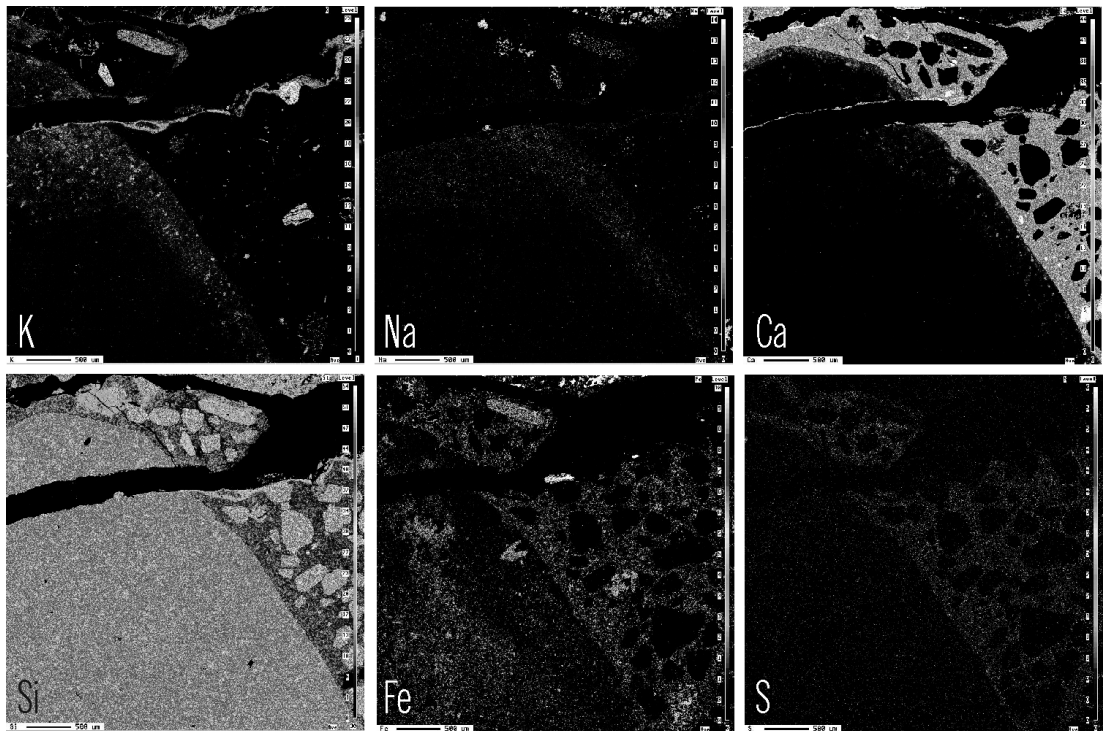


Figure 2: Element maps of the same chert grain as in Figure 1, locally cracked by ASR. Scale bar is 500 μ m. Full-color maps printed as Plate 14.

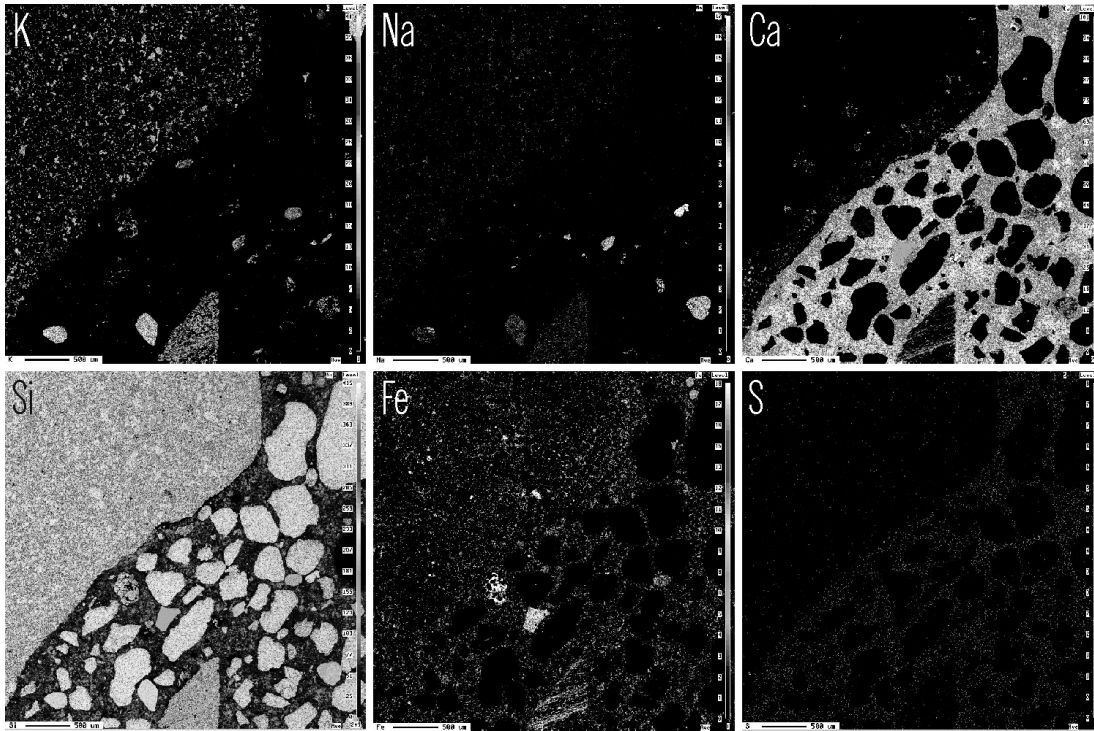


Figure 3: Element maps of intact sandstone. Scale bar is 500 μ m. Full-color maps printed as Plate 15.

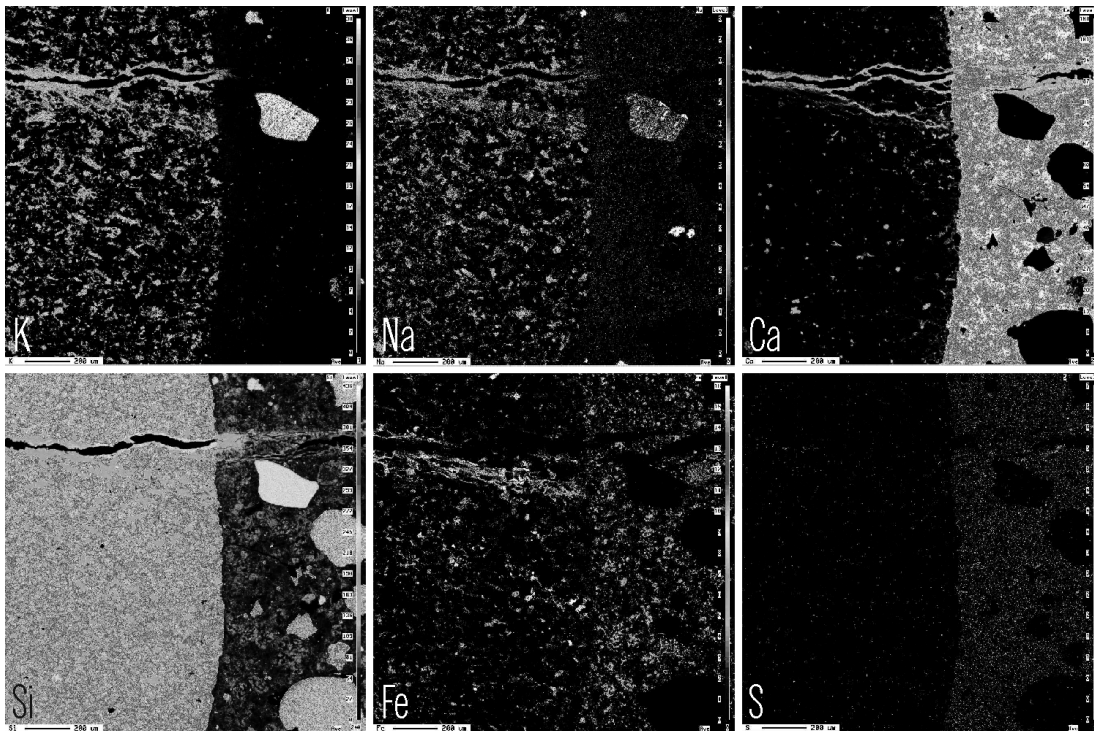


Figure 4: Element maps for a similar sandstone as in Figure 3, locally cracked by ASR. Scale bar is 200 μ m. Full-color maps printed as Plate 16.

On the Crystallinity Indices of Some Norwegian Mylonites, and Some Ohio and Dutch Cherts

This Chapter is dedicated to emeritus Bill Kneller of Sylvania/OH, in honour of his remarkable work on the characterization of Ohio cherts, and to thank him for providing me with his original samples.

1 Introduction

In Dutch ASR-concrete, chert is traditionally regarded as the main alkali-reactive constituent in aggregate material [21], even though the alkali-reactivity of eg. sand-/siltstone has been recognized [see Chapter 2]. There is no official list of alkali-reactive rock types, and aggregate material was until recently only tested for its content of porous chert. However, a revised guideline expected for publication in early 2002 commands that aggregate material be tested for porous chert and chalcedony by impregnation-fluorescence microscopy, and for other potentially alkali-reactive constituents by ultra-accelerated mortar bar testing following the latest RILEM procedures [128,129].

The provenance area of the aggregate material from the concretes investigated in this thesis is the Brabant Massif in the Belgian Ardennes of very (anchizonal) low metamorphic grade. This material is not representative for all Dutch aggregate material, as that includes Rhine sediments and off-shore, sea-dredged chert-rich material from the southern parts of the North Sea, among others. Though the geology and lithology of the Brabant Massif is quite complicated and variable, the debris mostly consists of various types of sand-/siltstone for these are most wear resistant and will survive the sedimentary transport. Chert in these aggregate materials derives from the non-metamorphic Cretaceous in the southernmost parts of the Netherlands and is at most diagenetically altered.

In Norway, alkali-reactive aggregate constituents are put on a preliminary list [130] which is to be integrated in the next update of relevant official guidelines. The metamorphic grade of aggregate materials may in principle vary from sub-greenschist to eclogite facies, but magmatic and sedimentary rocks are also utilized in concrete, all of which appear on the preliminary list of alkali-reactive rock types. Among the most violently alkali-reactive rocks are sand-/siltstone, mylonite, acid volcanic rocks, and other rock types containing quartz grains $<60\mu\text{m}$ [130]. In addition, some rock types are known to behave ambiguously, occasionally being alkali-reactive, and sometimes innocuous. Deleterious alkali-silica reactions have been identified in concrete structures in both Norway and the Netherlands, despite the very different geological background of the aggregate materials involved.

Knowing silica may possess quite a number different fundamental mineralogical and geochemical properties that affect the solubility of silica [see Chapter 7], one wonders whether silica from a chert is alkali-reactive for the same reason as silica from eg. a mylonite, just because their geological backgrounds are so different. If it is, then there is a

good reason to frame one single method for aggregate testing. If not, then perhaps the use of several testing methods, either specialized per type of aggregate material or addressing one specific fundamental property of the alkali-reactive silica in that type of material would give more accurate results, better able to distinguish between alkali-reactive and truly innocuous silica.

Taking the above into account, comparison of the properties of two different types of silica with a different geological backgrounds may reveal whether the individual reasons for their alkali-reactivity are similar or not.

2 Samples

Initially, Norwegian mylonites and Dutch cherts were chosen for the investigation for several reasons, including:

1. relevance for their respective countries of origin regarding ASR;
2. sample availability;
3. availability of documentation.

Detailed mineralogical/geochemical data on Dutch cherts and their ASR-expansion potential were unavailable [10,123] until recent, when Dutch chert and sea-dredged materials have been investigated for CUR-committee VC62 [see Introduction]. The original Ohio chert samples from the classic papers by Kneller [121,131,132] were also included in the research. Though (porous) chert and mylonite are not the only reactive constituents in the Netherlands and Norway, respectively, they both quite commonly occur as (minor) aggregate constituents.

The Dutch chert samples originate from various locations on the Netherlands' mainland but also include sea-dredged material from the North Sea. Ohio chert samples from [121,131,132] were obtained from the original author emeritus Bill Kneller, together with documentation and unpublished data.

Norwegian mylonite samples used in this research have previously been described and investigated and were provided by author Børge Wigum [54,55].

3 Analytical techniques

3.1 General

There are several fundamental mineralogical properties of crystalline silica that may increase its solubility [see Chapter 7], including structural defects as eg. dislocations, angular misfits at (sub-) grain boundaries, the occurrence of twin boundaries, the presence of foreign ions including hydrous species, polymorphism, grain or domain size, etc., all of which cause local stress and strain in the silica lattice. The degree of 'law and order' in a crystal lattice (or lack thereof) is important in determining solubility. Therefore, an ideal defect-free crystal lattice is less prone to attack eg. by dissolution in a high-pH environment [133].

To assess each single one of these mineralogical/crystallographical properties requires highly specialized techniques, not always readily available and impractical for a high throughput, if applied for aggregate testing. As a first attempt it seems more appropriate to use a method that actually addresses a combination of these properties, like the degree of crystallinity, occasionally abbreviated as DOC, or when called the crystallinity index abbreviated as CI. This concept of measuring the bulk quality of a crystal lattice is applied

to many different minerals, including eg. graphite [134] kaolinite, hydrotalcite, illite [135], and other phyllosilicates [136].

Non-geological materials include biomedical [137,138], wood [139], cellulose and starch [140], fabric materials like silk and wool [141,142], liquid crystals [143], synthetic CVD diamond substrates, perovskite superconductors and a diversity of semiconductors, on glass, synthetic spinels, titania and other ceramic materials. Among a plethora of organic materials are included polyvinyl-chloride (PVC), polyethylene (PET), polyurethane (PU), polytetrafluorethylene (PTFE, Teflon®) as well as many other polymers, and including in addition drugs, medicaments, and DNA. Depending on the nature of the sample, methods employed in assessing the crystallinity include XRD and gamma-ray diffractometry, NIR, IR, FT-IR and Raman spectroscopy, light scattering, DTA/TGA and DSC, NMR, as well as other techniques.

3.2 *Sample preparation*

Norwegian mylonites were first crushed to liberate the quartz grains and sieved to remove the fractions $<20\mu\text{m}$ and $>500\mu\text{m}$. The remaining middle fraction was then fed to a Frantz electro-magnetic separator to separate magnetic from non-magnetic minerals. The non-magnetic fraction was rinsed with double distilled water to remove the smallest adhering particles and dried at 50°C for one week.

Quartz grains were handpicked under the stereomicroscope from the resulting non-magnetic fraction, using polarized light. Only mono-mineralic grains were selected. After the handpicking, grains were again rinsed in organic solvent to remove traces of grease, rinsed in double distilled water, and dried. Acid rinsing to remove carbonates was not considered necessary. Despite all precautions, diffractograms indicate that minor contamination with feldspar did occur.

Ohio cherts were already available as powder from earlier experiments [121,131,132]. After a first run with XRD, Ohio cherts were washed in concentrated hydrochloric acid to remove carbonates and limonite. After rinsing with double-distilled water and subsequent drying, new X-ray diffractograms were made with identical operating conditions.

Dutch chert samples were first crushed with a hammer, after which the resulting grit was pulverized in a swing mill with a tungsten carbide-lined vial and ball. Before each run, the vial and ball were cleaned by short milling with calcined plain quartz. Finally, the vial and ball were wiped clean using an acetone damp, lint free cloth.

3.3 *X-ray diffractometry (XRD)*

The operating conditions of the Philips PW1800 X-ray diffractometer were set to 40kV and 50nA, using unfiltered Cu-K α radiation. By adjusting divergence and receiving slit widths and a monochromator, effectively only the Cu-K α_1 wavelength of 1.54056\AA was used.

From each sample, a diffractogram was made from $66-70^\circ 2\theta$, in $0.005^\circ 2\theta$ increments with 10s counting time per increment, a speed of $0.03^\circ 2\theta\cdot\text{min}^{-1}$. The diffractogram was used to determine the crystallinity index, defined as relative peak heights of the quintuplet (212) reflection at $67.74^\circ 2\theta$ (1.382\AA), following the method introduced by [151]. A single crystal of clear vein quartz was used as an internal standard. With its raw CI-value of 8.2, the instrumental scaling factor F was calculated to be 1.22 for this experimental set-up [83].

Another diffractogram was made from 15-45° 2 θ , in increments of 0.02° 2 θ and 10s counting time per increment, which is a scanning speed of 0.12° 2 θ ·min⁻¹. The number of counts at the strongest X-ray (101) reflection of quartz at 26.6° 2 θ (3.343Å) was recorded for its reported correlation with the CI in a previously published characterization of Japanese cherts [144].

The same diffractogram was also used to verify the eventual occurrence of moganite, which has its strongest (112) reflection at 26.7° 2 θ (3.336Å). The asymmetry of the (101) quartz peak at 26.6° 2 θ (3.343Å) was taken an indicator for the eventual presence of moganite, and the weaker reflections for (011) at 19.990° 2 θ (4.438Å), for (202) at 26.28° 2 θ (3.388Å) [145]. The resulting moganite contents must be regarded as indicative, at best as semi-quantitative. For real quantitative work, Rietveld-refinement analysis of XRD data should be applied, as recommended in [146].

3.4 *Differential thermal analysis/thermogravimetric analysis (DTA/TGA)*

For analysis by DTA/TGA, a 50±0.5mg sample material was weighed, in order to obtain an adequate response. Not all handpicked samples analyzed by XRD were assessed by DTA/TGA for lack of sample material. Temperature was increased from ambient to 500°C at 25°C·min⁻¹. The sample was kept at 500°C constant for 10 minutes to allow stabilization, after which the sample was heated further to 600°C at 0.25°C·min⁻¹.

From the peak temperature down, the cooling trajectory run was identical to the heating trajectory but in reversed order, until 250°C where the measurement was discontinued. Thermograms were recorded with 0.5s resolution, both during heating and cooling of the sample. The cooling curve is compared with the heating curve to improve the signal-to-noise ratio of minor thermal events, especially in impure or contaminated materials [147].

Determination of the quartz content is based upon the reversible α - β transition that ideally takes place at 573°C but which temperature in practice may vary a few degrees. The endothermic and exothermic effects at the transition are well-known, therefore, a thermogram from an unknown material can be compared with one from standard reference material (here clear crystalline quartz, ie. rock crystal) to determine the amount of α -quartz in the unknown sample. The result is a percentage of quartz in the material tested. If bulk material is analyzed, this percentage might represent the actual content of quartz, in a purified monomineralic sample it may serve more as a crystallinity index.

The DTA/TGA results from Kneller are semi-quantitative and do not allow quantification of the amount of quartz in the chert. Table 1 contains two columns for DTA/TGA. The left one is based upon the original data from Kneller, and every thermogram clearly contains a peak close to the α - β transition temperature of quartz. The second DTA/TGA column is based upon new data, and it shows that the α - β transition only occurs in a few samples, and that the peak is not very evident in all of the samples either.

4 Results

4.1 Data presentation

Data are compiled in TABLE 1 at the end of this chapter. Where available, original data on the same samples from different sources, have been added for comparison. For Norwegian mylonites these data include reported crystallinity indices and QXRD mineral modal data [54,58], for Ohio cherts the original DTA thermograms have been reinterpreted [121]. Data on mica and clay mineral content have been added for their potential effects on silica dissolution [see Chapters 2, 4, and 5]. Expansion data for mylonites are according to NBRI 14-day [54,58], and for Ohio cherts according to modified ASTM C227 procedures [details in 121]. Finally, some preliminary data on Dutch cherts were added [83].

4.2 X-ray diffraction

Norwegian mylonites

The crystallinity indices measured here are significantly higher than previous results [54,58] on the same samples, with two exceptions BB254 and BB259. The former contains considerable phyllosilicates (modal 28% mica + 34% chlorite; QXRD-data [54]), the latter only contains traces of mica [58]. However, a rock of the mineralogical composition as previously reported ought to have a significantly higher ignition loss, roughly double of the one found in this study.

Samples were not washed in acid to remove carbonates. Moganite could not be detected in any of the diffractograms. There appears to be no correlation with the 14-day expansion according to NBRI accelerated mortar bar testing.

Typical examples of partial X-ray diffractograms of Norwegian mylonites are illustrated in Figures 1-3 at the end of this Chapter. Note the difference in background noise between Figures 1-2 for BB251 and BB252 that both have CI 9.3. Figure 3 for BB253 has a CI 9.8, but the individual heights of the 3rd and 4th peaks in the quintuplet are different from those in Figures 1-2, as are the depths of the valleys between the peaks.

Ohio cherts

Though X-ray diffractograms were available, no crystallinity indices were reported [121]. Because an original XRD reference diffractogram for 'clear crystalline quartz' was lacking, the necessary scaling factor could not be calculated afterwards. Some of the diffractograms indicated the presence of considerable amounts of carbonate, including calcite and dolomite.

To avoid overlap with quartz peaks of interest, all samples were rinsed with hydrochloric acid, resulting in a different crystallinity index. There appears to be no systematic correlation between the carbonate content and the crystallinity index, both higher and lower indices compared to bulk chert occur. The moganite content is indicated to vary from <1wt% to <10wt%. A correlation with expansion (according to modified ASTM C227 accelerated mortar bar testing) seems absent.

Typical examples of partial X-ray diffractograms of Ohio cherts are shown in Figures 4-5 at the end of this Chapter. Figure 4 for BB280 has a CI of 2.3 whereas Figure 5 for BB279 shows a CI of 6.2. Note the difference in individual peak heights between Figures 1-3 versus Figures 4-5.

Dutch cherts

The provided data are preliminary and previously unpublished. They consist of averages calculated over several tens of analyses.

4.3 *Differential thermal analysis*

Norwegian mylonites

Data are cited from [54]. The height of the $\alpha \leftrightarrow \beta$ transition peak at 573°C (ideally) was used to quantify the quartz content in the original publication. Loss-on-ignition (LOI_{1000°C}) data for Norwegian mylonites were added to allow for comparison with the weight loss in DTA for the cherts.

The stated high content of hydrous minerals (according to QXRD-data from [54]) is, for some samples, reflected in a higher ignition-loss (ie. BB254), whereas this correlation is lacking for others (ie. BB256). Correlation with 14-day expansion according to the NBRI accelerated mortar bar test seems absent.

Ohio cherts

Original thermograms from [121] were checked for the presence of an $\alpha \leftrightarrow \beta$ transition peak, which was indeed recorded in all samples. For this study, only a limited number of Ohio chert samples was reassessed by DTA, and in contrast to the earlier data, the $\alpha \leftrightarrow \beta$ transition peak seems absent (as indicated by ‘n’) or very weak (as indicated by a question mark). The ignition loss actually resembles an ‘LOI_{600°C}’, which leaves carbonates unaffected and in fair approximation only includes hydrous minerals stable at low-grade conditions.

Nevertheless, a correlation of the ignition loss with the originally reported clay mineral content is absent. Correlations between clay mineral content and moganite content and/or crystallinity index are also absent. The expansion is reported according to ASTM C227 accelerated mortar bar testing, modified to give better data resolution.

Typical examples of DTA/TGA thermograms are illustrated in Figures 6-7 at the end of this Chapter. Figure 6 shows the entire trajectory from ambient-600°C-ambient for BB267, and Figure 7 shows the heating trajectory from 550°C-600°C. No thermal traces of any significant α - β transition are visible around the expected 573°C.

5 Discussion

5.1 *Crystallinity index*

In contrast to data considering crystallinity indices of clay minerals, that for quartz *sensu stricto* appears to be very limited. However, there are several contributions with crystallinity indices applied to aggregate materials [148,149] using XRD, or IR [150]. In an initial study called ‘a preliminary survey’ (ipse dixit [151]), crystallinity indices are given for 37 silica samples from diverse geological origins. However, a thorough literature search wasn’t able to locate a sequel to that survey.

In that preliminary survey, euhedral quartz crystals from Herkimer County in New York (dubbed ‘Herkimer diamonds’ in the trade [152]) were used for internal standard [151]. These short prismatic crystals grow in karst voids in the Little Falls Dolomite formation, near Albany, New York State. Typically, Herkimer crystals have a ‘diamond’ luster (meant relative to rock crystal in general) and are as a rule double terminated, with well defined crystal faces and knife-sharp edges. In this respect, their outer appearance is much like that

of ‘a perfect crystal’. According to the text of [151], the measured crystallinity index for Herkimer quartz was rescaled to 10 exactly. However, Table 1 in [151] states the CI of Herkimer quartz as 9.8, a synthetic quartz from an unknown resource is noted with a CI of 10.1 and one sample of natural vein quartz appears to have a CI of 10.2, higher than both the Herkimer and the synthetic quartz.

A quick survey on the internet with the search term ‘synthetic quartz’ reveals that it comes in many different grades, custom for different (often piezoelectric) applications. Synthetic quartz is hydrothermally grown in an autoclave from high purity starting materials under laboratory controlled conditions, following a patented method [eg. 153]. Of course, Herkimer quartz and vein quartz are grown under natural conditions, from impure materials and with variable conditions. Even so, minute mineral inclusions of acmite ($\text{NaFeSi}_2\text{O}_6$) and emeausite ($\text{Na}_4\text{Li}_2\text{Fe}_2\text{Si}_{12}\text{O}_{30}$) [154] and/or fluid inclusions are not uncommon in synthetic quartz.

Recent cathodoluminescence studies demonstrate that strong zoning in subhedral quartz crystals from veins is the rule rather than the exception [155,156], and similarly for quartz in mylonites [157]. Though the factors controlling the luminescent properties of different types of natural quartz are still a matter of dispute [eg. 158], there is a general consensus about the cause being impurities and substitutions in the lattice, reflecting physico-chemical variations of conditions (including fluids present) during natural crystal growth.

For naturally grown quartz crystals, size and outer perfection are the first criteria to determine its suitability for piezoelectrical purposes, after which the crystal is assessed in further detail to identify its best parts and its crystallographic orientation and handedness, by combined optical and X-ray diffraction methods. During World War II, the American war industry was in desperate need of quartz oscillator plates for transceivers and paid an enormous research effort in characterizing the suitability of natural quartz, and dedicated the entire 1945 May-June issue of *American Mineralogist* to the properties and characterization of quartz [159].

In addition to optical and XRD methods, Friedlaender applied etching with hydrofluoric acid to characterize the internal macrostructure of quartz crystals from the Swiss Alps [160,161]. The etching experiments revealed that twinning according to the Dauphiné law was very common in near 100%, and twinning to the Brazil law in up to 60% of the investigated crystals. In contrast, enantiomorphic left to right (L-D) twinning proved rare, occurring in only 0.4% of the specimens. Putting the etched surfaces under the microscope revealed that stacking faults and lattice defects are very common, even in the very finest crystals. Finally, etching revealed suture lines on the original outer surface of quartz crystals that were previously invisible, representing boundaries between twinned individuals, or between misoriented domains. Natural crystals with such a three dimensional mosaic constitution are dubbed ‘Friedlaender quartz’ [162].

For piezoelectric applications, Dauphiné twinning (alternatively called ‘electrical twinning’) is objectionable as the effect in one set of twins is cancelled out by that of the other set. Although Dauphiné twinning can be observed macroscopically as in [161,162], this type of twinning extends all the way down to electron microscopical scale. Brazil twinning also reduces the piezoelectric effect [163]. Brazil twinning is called ‘optical twinning’, which term actually applies to all other twinning modes that can be traced with optical methods [164]. Polysynthetic Brazil twinning is very common in amethyst, the purple quartz variety.

The details of amethyst coloration are still disputed but comprise a combination of electromagnetic radiation-induced charge redistribution and the presence of iron in the structure [discussion in 162, also see 165]. The presence of iron results in a reduction of the crystal symmetry of the amethyst structure, compromising piezoelectric efficiency. Polysynthetic Brazil twinning at unit cell scale of the quartz structure transforms it into the moganite structure, consisting of alternating slabs of left-handed and right-handed quartz [166]. Remarkably, the presence of iron also seems to play a role in the natural formation of moganite [167], as already obvious for amethyst.

The piezoelectric effect is directly inherent to the crystal structure of quartz and its symmetry, and quantitatively related to the degree of perfection of the crystal lattice, whence Dauphiné and Brazil twinning are objectionable. Defects and dislocations also alter the crystal structure and are hence also undesirable. Due to the nature of Dauphiné twinning, the non-planar junction between adjacent twins has a distorted β -quartz structure. The junction between bordering Brazil twins has a different structure that is still unknown in detail, but is said to contain material that is non X-ray diffracting [168]. Hence, twinning does influence the structural integrity of the quartz lattice and affects the crystallinity index in a similar manner as defects and dislocations.

If structural defects and irregularities like those mentioned in the paragraphs above require meticulous custom methods to be detected even in large quartz crystals, it must be increasingly difficult to detect them in smaller specimens. The ‘transparent rock-crystals’ used for internal standard in both [151] and [169] are not further specified. Provided the many issues that influence the crystallinity index as discussed above, that seems an omission. The lack of further characterization may also explain why some samples end up with a higher crystallinity index than the internal standard, that apparently wasn’t as ideal as thought. Thus, the current crystallinity index standard for quartz according to XRD [151] and IR [169] methods should be re-established and properly characterized.

The ideal standard would consist of powdered untwinned quartz, free of substituted elements including water and any other solid and/or fluid inclusions. Crushing and grinding of initially untwinned quartz liberates the largest inclusions, but also induces Dauphiné twinning. This mechanically caused twinning can be removed without much trouble by annealing across the α - β inversion point at 573°C and subsequent quenching [164].

Optical examination of the quartz samples in [160,161] showed that many crystals had a lamellar or concentric ‘onion ring’ constitution with slightly misoriented lamellae or rings, respectively. Crystals of such nature are usually dubbed ‘Bambauer quartz’, after the author who identified them for the first time [170]. Natural growing conditions are markedly different from Friedlaender quartz, resulting in a different crystal constitution and a different trace element composition [162: see table on p221-2]. Transitions or intergrowths from Friedlaender to Bambauer quartz within one individual crystal are known to exist. The luminescence micrographs in [155] show concentric zoning in euhedral quartz crystals, suggesting Bambauer type quartz. However, details regarding the structural constitution remain unrevealed, and optical zoning is different from luminescent zoning.

5.2 *Quartz crystallinity*

In quartz, the structure of twin boundaries, low and high angle (sub-)grain boundaries, misorientations, etc. differs considerably from that of bulk material [133,171]. The interatomic distances are generally larger and some bonds may be dangling free, defects may

occur arranged in walls. In addition, foreign ions tend to concentrate at such boundaries, effectively pinning defect and/or twin boundary migration. Twin memory has been experimentally demonstrated to occur in quartz at Dauphiné twin boundaries across the α - β transition [164,172], and similarly in anorthoclase [173]. According to early experiments, twin amnesia proved very hard to attain in quartz and quartz resonator plates.

After prolonged and repeated annealing across the α - β inversion point at 573°C and even up to 1000°C, quartz oscillator plates returned to their initial Dauphiné twin pattern, provided they had one [164]. In contrast, laboratory-induced Dauphiné twinning by applied mechanical stress or by slow cooling did not have a memory; they invariably were easy to anneal. It has been shown that seen away from mechanical stress, Dauphiné twinning memory and amnesia are related to the maximum attained temperature, the rate of cooling through the α - β transition, the presence of cracks, and sample dimensions (of the quartz oscillator plates), the latter which may perhaps be translated as grain size.

Laboratory experiments on the mylonites from this study established a moderate correlation of quartz grain size with ASR-expansion [54,55]. All samples plotted on or near a seemingly parabolic trend-line. Correlation of ASR-expansion with mineralogical composition, water absorption, and crystallinity index all seemed absent, while only a weak correlation is reported with the XRD/DTA ratio for quartz. Both XRD and DTA analyses were both performed on whole-rock samples, not on handpicked materials, compromising an accurate estimation of the bulk mineralogical composition for the interferences with the other minerals present. Chlorite is specifically mentioned to affect the quantification of quartz by XRD. Six out of twelve samples are reported to contain chlorite, in amounts varying from 3-34% [Table 2 in 55]. Oddly, XRD and DTA mineralogical data have not been verified by thin section petrography and point counting to determine mineralogical compositions, whereas an optical microscope had been used to measure quartz grain sizes.

Reliable quantification of the quartz content by either of these methods is problematic [54]. The problematic nature of XRD and DTA for quantification of quartz content in bulk material is further illustrated by the highly inconsistent ratio XRD/DTA, reported to vary from 0.48 to 4.00 [Table 3 in 55]. In other words, the relative variation of the amount of quartz as determined by either method falls between 48% and 400%. Ideally, this ratio should be unity (ie., 100%), or at least be near unity ($\pm 5\%$) for practical results. Of the twelve samples investigated, only sample 4.2 fulfills this criterion [Table 3 in 55]. Enigmatically, this sample is considered an outlier, and is together with sample 4.1 (ratio XRD/DTA 4.00) omitted from the plotted data [Figure 9 in 55]. Including this value in Figure 9 [in 55] corrodes the already as weak reported correlation further.

Performing XRD and DTA analyses on bulk material as opposed to handpicked separates affects the reliability of the crystallinity index as determined by XRD. In the work from Wigum, ‘clear single crystal euhedral quartz’ [ipse dixit 55] was used for internal standard, merely replicating the original procedure of Murata & Norman [151]. Further mineralogical details of the quartz crystal as discussed above of this standard are not reported.

5.3 *Quartz alkali-reactivity*

The above discussion illustrates that the crystallinity index of Murata & Norman [151] comprises a number of different crystal structural aspects of the quartz lattice. Which of these aspects in each sample are responsible for the deterioration of the supposedly ideal crystallinity index of 10, however, remains unclear. Combining NBRI/ASTM accelerated

mortar bar testing data with crystallinity indices doesn't result in a correlation for the investigated mylonites nor cherts. This contrasts with earlier results that show a negative correlation between silica dissolution and the crystallinity index [144,149]. However, silica dissolution is not necessarily identical to ASR deterioration, though probably similar.

The very different geological nature of chert as compared to mylonite provides more reason for a critique on this bulk parameter as a quantitative measure for determination and quantification of silica alkali-reactivity. Even though different methods were applied in expansion testing, it is quite remarkable to notice that 'highly crystalline' silica from Norwegian mylonites can be just as alkali-reactive as 'poorly crystalline' silica as in some cherts. This observation alone illustrates that the actual reason for quartz alkali-reactivity is unknown and may differ for silica of different origin.

6 Conclusions and suggestions for further research

It becomes clear from the above that a more refined and detailed characterization of both alkali-reactive and innocuous silica is essential to define their differences. Techniques and methods should assess the detailed crystal structure in terms of dislocation and defect density and distribution, including grain boundaries. Using micro-sampling and -preparation techniques, materials of interest can be extracted from thin sections for detailed characterization by XRD and other techniques.

A detailed chemical assessment is necessary to support the crystal structural data, and to understand why some features seem to have a memory in the quartz lattice. To get an indicative and qualitative impression of crystal structure and trace element composition variations of quartz *in situ* in thin sections, cathodoluminescence is a convenient technique, both in optical and/or electronic microscopy. For bulk quartz, sophisticated ICP-MS may be appropriate, whereas the same instrument equipped with laser ablation would enable *in situ* studies. For yet more detailed work at TEM scale, an analytical electron microscope equipped with FEG (field-electron gun) may be suitable. Both water content and speciation can be determined with FT-IR and/or Raman spectroscopy, eventually in thin sections.

It is important to study both fresh aggregate constituents and actually reacted aggregate grains, the latter preferably both from real life and mortar bar testing experiments. However, even more important than the data and measured numerical values themselves are their interrelations.

TABLE 1: XRD and DTA crystallinity data of some Norwegian mylonites of Wigum [54], some Ohio cherts from Kneller [121], and some Dutch cherts [83].

Norwegian mylonites [54]											
<i>sample no.</i>		<i>CI [151]</i>		<i>moganite</i>	<i>moda% hydrous</i>			<i>DTA</i>		<i>expansion</i>	
this study	Wigum	original	new	wt%	phyllo	chl	∑ other	quan.tive	LOI	NBRI ₁₄	
BB248	1,1	6.58	8.6	nd	2	0	nd	29	0.57	0.255	
BB249	1.2	7.72	8.5	nd	2	0	nd	29	0.65	0.297	
BB250	1.3a	7.45	9.0	nd	1	0	nd	33	0.46	0.236	
BB251	1.3b	7.65	9.3	nd	2	0	nd	26	0.59	0.226	
BB252	3.1	7.87	9.3	nd	8	8	nd	29	1.50	0.170	
BB253	3.2	8.26	9.8	nd	0	24	nd	29	0.53	0.080	
BB254	3.3	9.54	9.4	nd	28	34	nd	40	3.06	0.250	
BB255	4,1	6.13	8.9	nd	1	20	12	6	1.94	0.230	
BB256	5,1	8.25	8.8	nd	4	15	22	23	0.40	0.170	
BB257	1.4	7.94	8.9	nd	3	0	2	16	0.67	0.098	
BB258	PH275/95	9.3	10.0	nd	0	0	nd	–	0.22	0.040	
BB259	PH276/95	10.8	10.2	nd	0	0	nd	–	0.25	0.080	
BB260	–	–	10.0	nd	–	0	nd	–	2.26	–	
Ohio cherts [121]											
this study	Kneller	new	acid	wt%	phyllo	chl	clay	qual.tive	LOI	ASTM _{C227}	
BB261	1L	3.8	3.3	<1	nd	nd	2.9	y –	–	0.036	
BB262	2HD1	1.8	1.9	<1	nd	nd	1.9	y n	1.09	0.031	
BB263	2MD2	1.9	2.6	<1	nd	nd	2.1	y –	–	0.066	
BB264	2HD2	2.1	2.2	<1	nd	nd	1.8	y n	1.14	0.093	
BB265	3L	4.9	4.9	<1	nd	nd	3.0	y –	–	0.035	
BB267	4AL	3.6	3.2	<1	nd	nd	3.1	y n	1.05	0.084	
BB268	4BM	2.4	1.8	<1	nd	nd	0.9	y –	–	0.105	
BB269	5HD	3.8	3.6	<5	nd	nd	5.1	y ?	0.65	0.069	
BB270	5HG	4.4	4.1	<1	nd	nd	3.2	y –	–	0.132	
BB271	6L	3.7	4.0	<1	nd	nd	4.4	y –	–	0.061	
BB272	6M	3.5	3.7	<1	nd	nd	4.4	y –	–	0.112	
BB273	6H	6.2	5.8	<10	nd	nd	3.2	y ?*	1.32	0.048	
BB274	7L	4.5	3.5	<1	nd	nd	2.9	y –	–	0.035	
BB275	7M	3.5	3.4	<1	nd	nd	4.0	y ?	1.55	0.054	
BB276	7H	5.4	4.6	<5	nd	nd	4.6	y ?	1.49	0.047	
BB277	8L	6.1	7.3	<10	nd	nd	3.7	y –	–	0.036	
BB278	8M	5.7	5.8	<5	nd	nd	1.9	y y	0.42	0.043	
BB279	8H	6.3	6.2	<5	nd	nd	1.9	y y	1.80	0.038	
BB280	9HD	2.6	2.3	<10	nd	nd	5.6	y –	–	0.088	
BB281	10M	4.6	4.0	<5	nd	nd	3.6	y –	–	0.061	
BB282	10H	3.5	3.5	<1	nd	nd	2.9	y –	–	0.057	
Dutch cherts [83]											
this study		avg	spread	wt%	phyllo	amph	clay	qual.tive	LOI	expansion	
porous chert (land)		1.5	<1-6.4	up to 10	0	0	0	–	–	–	
dense chert (land)		1.5	<1-3.3	up to 10	0	0	0	–	–	–	
cortex (land)		3.0	<1-7.1	up to 10	0	0	0	–	–	–	
porous chert (sea)		1.3	<1-3.2	–	0	0	0	–	–	–	
dense chert (sea)		1.1	<1-2.6	up to 10	0	0	0	–	–	–	
cortex (sea)		1.8	<1-3.1	up to 10	0	0	0	–	–	–	
sand-/siltstone (land)		9.2	8.2-10	–	0	0	0	–	–	–	
vein quartz (land)		9.0	4.0-10	–	0	0	0	–	–	–	

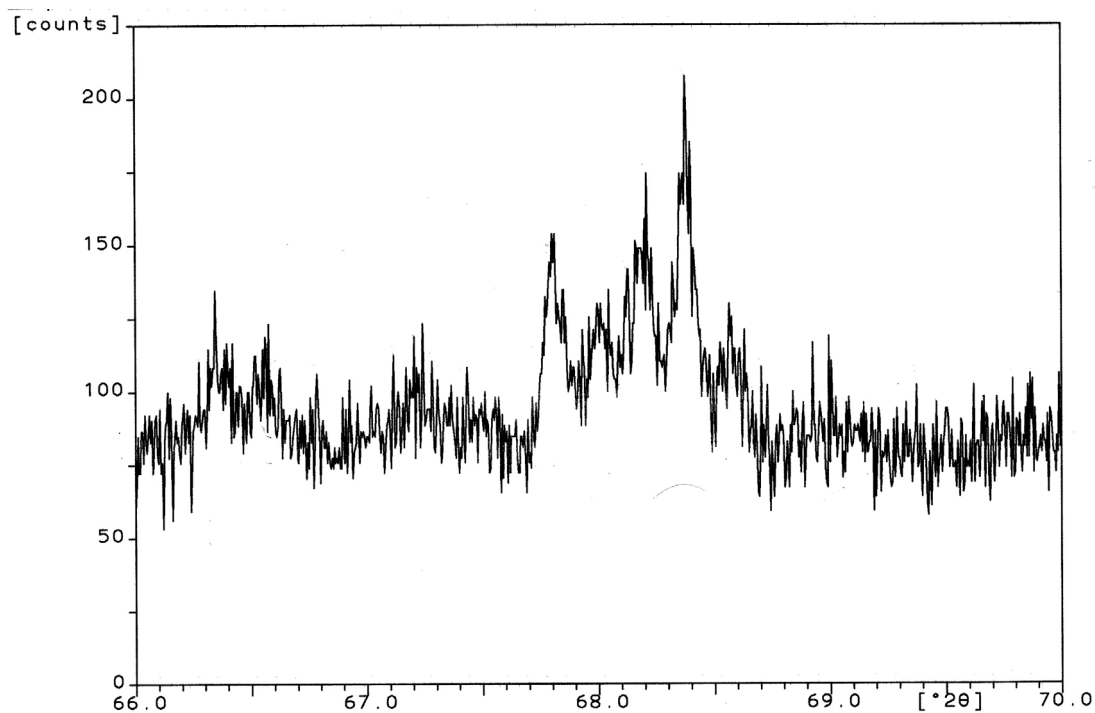


Figure 1: X-ray diffractogram of handpicked quartz from BB251, with CI=9.3.

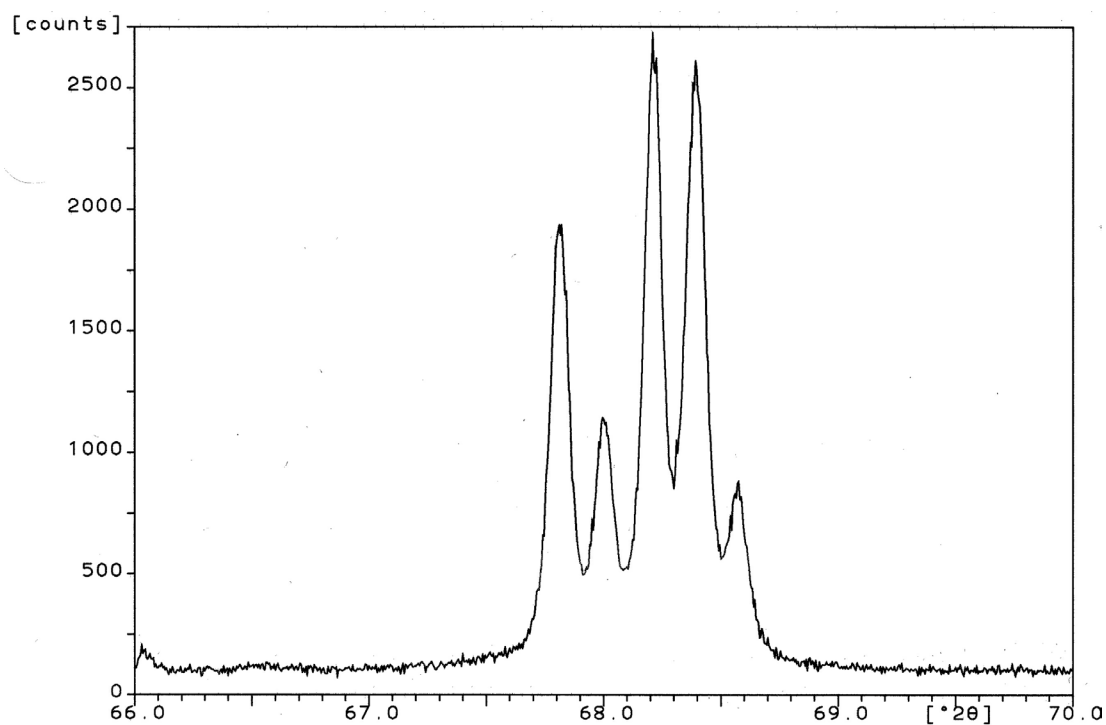


Figure 2: X-ray diffractogram of handpicked quartz from BB252, also with CI=9.3. Note the difference in background noise with Figure 1.

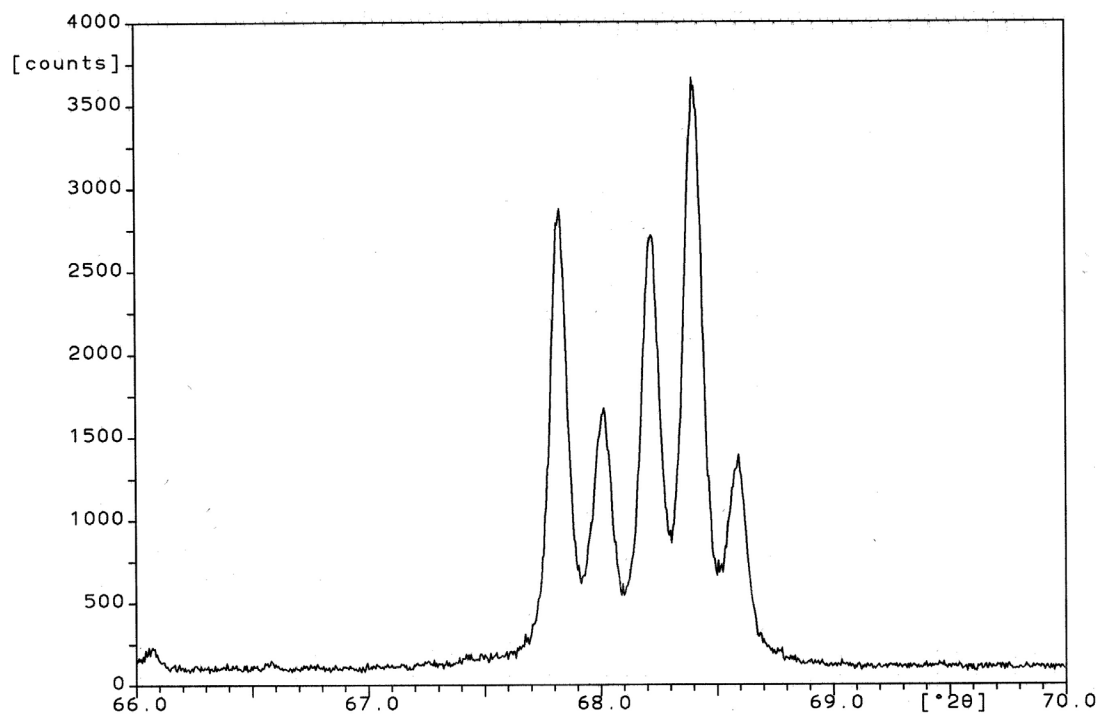


Figure 3: X-ray diffractogram from handpicked quartz from BB253, with CI=9.8. Note the difference in individual peak heights compared to Figure 2.

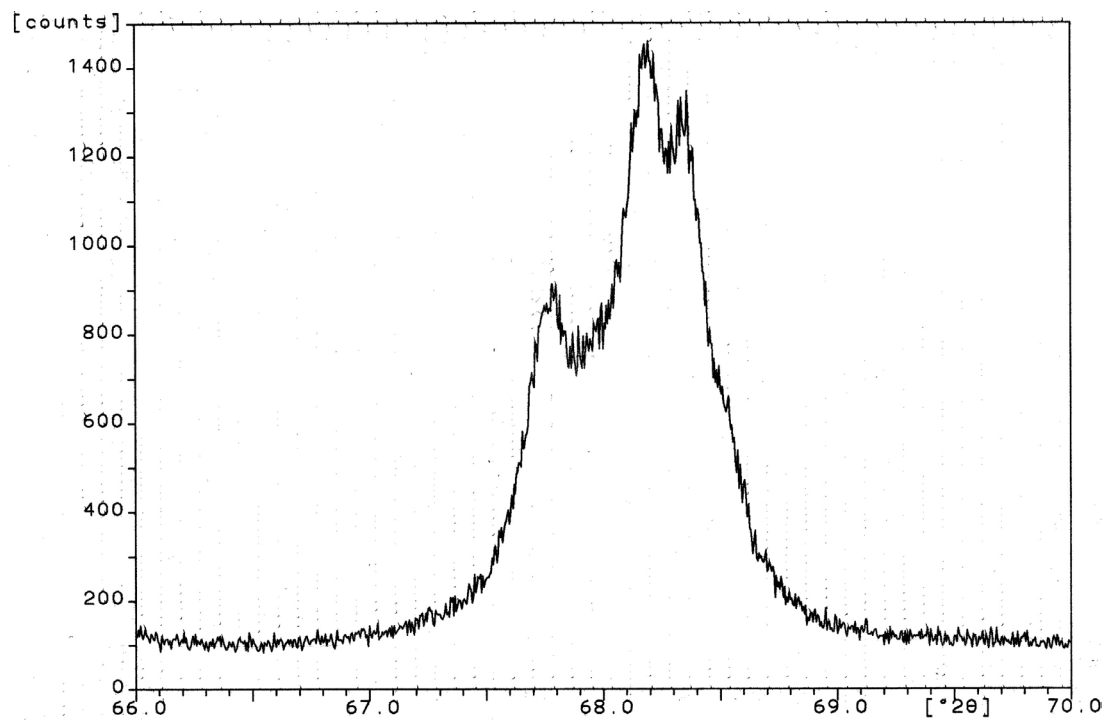


Figure 4: X-ray diffractogram from Ohio chert BB280, with CI=2.3.
Note the difference in individual peak heights compared to Figures 1-3.

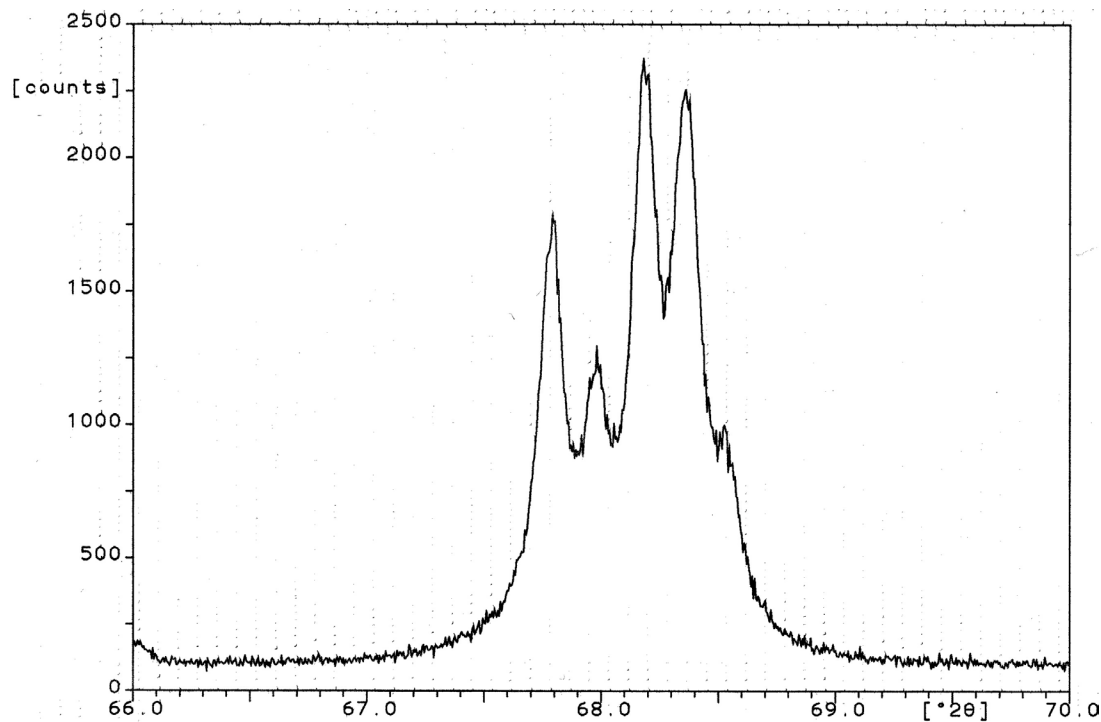


Figure 5: X-ray diffractogram from Ohio chert BB279, with CI=6.2.
Note the difference in individual peak heights compared to Figure 4.

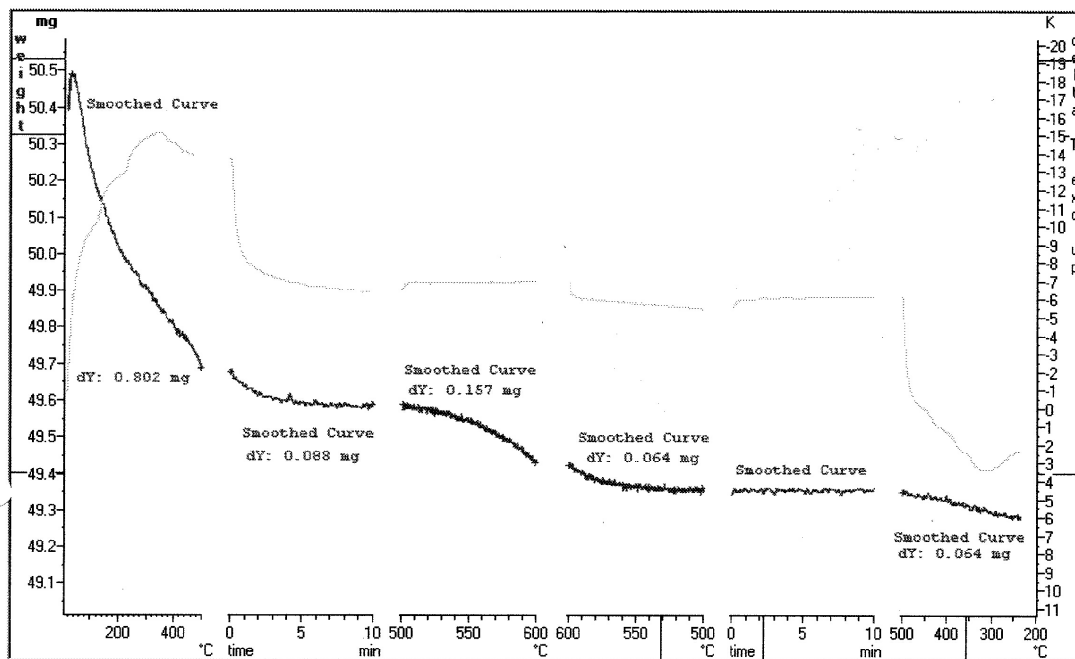


Figure 6: Thermogram of BB267, showing the entire DTA/TGA trajectory. Further explanation in Chapter 6.

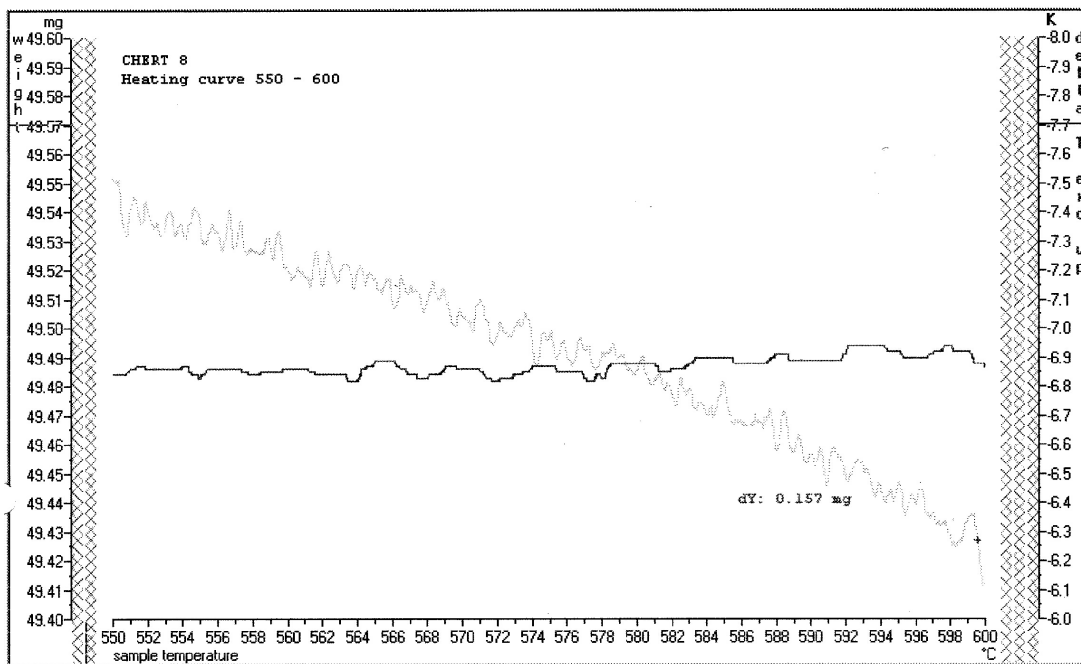


Figure 7: Partial thermogram of BB267, showing the heating trajectory 550°C-600°C. No α - β transition visible around 573°C.

Silica Dissolution Related to the Alkali-Silica Reaction: A Review

Adapted from:

Broekmans, MATM (1999): Classification of the alkali-silica reaction in geochemical terms of silica dissolution. In: Pietersen, HS, Larbi, JA, and Janssen, HFA (editors): Proceedings of the 7th Euroseminar on Microscopy Applied on Building Materials, Delft: 155-170.

1 Introduction

Three constituents are essential to the alkali-silica reaction: alkalies and silica as reagents and moisture both as a reagent and a transport medium. The alkalies are supplied by the cement paste or can under certain circumstances be derived from the aggregate material (this volume), and the water is mostly provided by 'exposure conditions', i.e. meteoric or otherwise. Considered in their pure substance, these constituents behave consistently when reacting to form a silica gel, regardless of their origin. The mechanism of silica dissolution is not so much controlled by alkalies, but rather by dissolved OH-ions breaking silica bonds which then recombine with alkali-ions present. Of course, differences in concrete composition and local micro-environment *sensu lato* do affect the alkali-reaction (i.e. silica dissolution) conditions.

The reaction of finely dispersed microsilica is generally not regarded as an alkali-silica reaction since it is not deleterious. The silica present in aggregate can be of very different nature, affecting its degree of alkali-reactivity or inertia. Many publications have been dedicated to the relationship between the nature and reactivity of aggregate [eg. 174,175,69]. It is therefore interesting to sum up possible fundamental reasons that affect the dissolution of silica from a combined mineralogical and/or geochemical point of view.

Already in 1955, Iler published the first edition of "The colloid chemistry of silica and silicates" [176], a standard work that over the years has become famous. It provides an excellent introduction to the chemistry of silica dissolution, however, since its first publication much research has been conducted. The recent review volume edited by Heaney et al. [177] contains an exhaustive compilation of contributions dealing with silica and its behavior under various geological conditions. Silica dissolution under weathering conditions is reviewed in [178].

2 Silica in the geological environment

2.1 Silica polymorphs and varieties

Some 12% of the volume of the entire earth's crust is made of the 'pure' oxide SiO₂, representing a weight of $\sim 3.2 \cdot 10^{21}$ kilogram. In total, some nine silica polymorphs are known to exist, each of the composition SiO₂ and each with its own unique crystal structure. Best known are: α -quartz, β -quartz, tridymite, cristobalite on the high-T side, and

coesite and stishovite on the high-P side. A P,T-diagram illustrating the stability regions of diverse silica polymorphs is given in Figure 1 at the end of this Chapter.

Lechatelierite is an amorphous silica glass from fused sand found in fulgurites, and keatite is crystalline but has as yet only been synthesized in the laboratory. The silica polymorph moganite has not (yet?) been officially acknowledged by the CNMMN/IMA, though evidence that moganite is a valid polymorph *sensu stricto* is gathering. A monograph on silica polymorphs, varieties and their natural appearances was written by Rykart [162].

Most of the silica in the earth's crust occurs as the α -polymorph quartz (see Figure 2), due to its large stability region in the P,T-field [168]. The high-temperature polymorph β -quartz does not occur at the surface as the transformation is instantaneous. The α - β transformation is displacive and involves adjustment of bond angles; no bonds are broken. Compare Figure 3 with Figure 2 to see that the di-trigonal α -quartz c-axes change into hexagonal c-axes in high-temperature β -quartz.

Other higher temperature and pressure polymorphs are in principle unstable in the α -quartz P,T-region, but may persist due to sluggish reconstructive recrystallization, during which existing Si-O bonds are broken and new bonds are made to allow atoms to move to appropriate positions in the more stable polymorph. This is illustrated in Figure 4 which shows the great differences between the structures of α -quartz, tridymite and cristobalite. Heating α -quartz under ambient pressure results in a direct transformation to cristobalite, skipping the transformation to tridymite which is stable before cristobalite. However, reconstructing the initial α -quartz structure first into tridymite and then into cristobalite requires much more energy than going directly to cristobalite.

In addition to the high-grade polymorphs stable only under elevated conditions, a number of low-grade modifications are also known, including the polymorph moganite as mentioned above of which the crystal structure is illustrated in Figure 5. An extensive review on the crystal structures and other properties of micro- and non-crystalline silica polymorphs can be found in [179].

2.2 Silica dissolution controls

General

Parameters controlling quartz dissolution have been well studied by many researchers. Recent reviews are given in [178,91], and new contributions are frequently published in international journals. The key point in the alkali-silica reaction is the hydrous dissolution of silica in the presence of dissolved Na and/or K at high pH>13, commonly obtaining in OPC concrete. The properties and qualities of the silica and its environment may affect its solubility under the given conditions. These will be discussed below in separate paragraphs.

Equilibrium dissolution

The dissolution reaction of silica can be represented by the equation:



However, the true nature of the silica in dissolution is not simply $\text{H}_4\text{SiO}_4 \text{ (aq)}$, which notation is merely used for convenience, but rather depends on solution properties like pH, time, et cetera [176,180]). Due to dimerization and polymerization of the dissolved silica

upon ageing, the ratio $\text{SiO}_2:\text{H}_2\text{O}$ trends towards less than 1:2. However, if hydrogen bonded waters are counted, the balance goes the other way.

Reaction equation 1 is in principle an equilibrium reaction with a constant K written as:

$$K = \frac{a_{\text{H}_4\text{SiO}_4}}{a_{\text{SiO}_2} \cdot a_{\text{H}_2\text{O}}^2} \quad (2)$$

The principal shape of this equilibrium equation holds for all silica polymorphs, though the solubility of silica is different for different polymorphs. A general rule of thumb is, the lower the activity (or alternatively ΔG_f°) of the silica, the lower the solubility. This means that though the shape of equation 2 for quartz stays the same for other silica polymorphs, the respective a -values do change [178]. It also means that a plotted graph of such equations for each polymorph will essentially have the same shape, but will be shifted parallel to the abscissa.

From thermodynamic data as experimentally confirmed by laboratory experiments, it appears that quartz is the least soluble polymorph, glassy silica the most soluble, whilst other are intermediate [181]. Apart from the differences attributed to a different bulk crystal structure, a higher lattice integrity with fewer defects also affects silica solubility. Thus, the concentration of the dissolved species strongly depends on the whole nature of the solid silica with which the solution is in equilibrium.

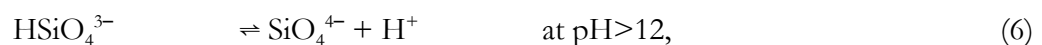
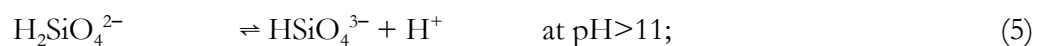
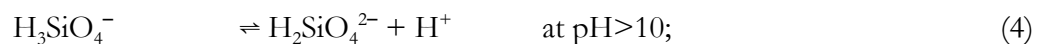
Effects of solution pH

Silica is an amphoteric material, which means that it dissolves at extreme pH values in strongly acidic or strongly alkaline conditions, and less around neutral pH. At high pH in a basic environment, dissolved silica as H_4SiO_4 behaves like a weak acid. The molecule is suspended between complexing water molecules as illustrated in Figure 6.

From pH9 and upwards, silica dissolves according to the equation:



The predominant species in solution is no longer H_4SiO_4 (aq), but the deprotonized variant of that. At yet higher pH values, deprotonization takes progress according to the cascaded sequence:



all with equilibrium constants similar to the model of equation 2. This sequence of equations 1 and 3-6 actually represents a cascade of reactions that subsequently occur when pure silica dissolves in pure water at $\text{pH} > 12$. If the final concentration of dissolved silica is high enough, then silica will polymerize to $\text{H}_6\text{Si}_4\text{O}_7^{2-}$. This is merely an effect of ageing and not so much of pH. Thus, the speciation of silica in a *freshly prepared* solution mostly depends on pH.

Effect of foreign species in the solution

Natural (silica) solutions are almost always contaminated by other dissolved species. Some dissolved ions interact with the surrounding water molecules to form a complex, whereas others interact similarly with dissolved silica species (H_4SiO_4 , H_3SiO_4^- , et cetera) in the solution. The latter interaction then lowers the activity (read: concentration) of the reacting dissolved silica species, shifting the equilibrium defined by equation 1. As dictated by reaction equation 1, more silica then dissolves to fulfil equilibrium equation 2. The total amount of dissolved silica determines the total solubility, regardless of speciation under the given circumstances. If the interaction of the dissolved non-silica species lowers the activity of water, the balance goes the other way and the solubility of silica is suppressed.

Above pH9, the dominant solution species of silica is H_3SiO_4^- . Other dissolved species can be arranged according to their affinity to react with H_3SiO_4^- , e.g. like $\text{H}^+ > \text{Fe}^{3+} > \text{Mg}^{2+} > \text{Ca}^{2+} > \text{Na}^+$ [178]. These ions capture H_3SiO_4^- away, and hence the same molar amount of H_4SiO_4 will then deprotonate according to equation 3 -see above-, and finally some solid silica will dissolve according to equation 1 to replenish the generated H_4SiO_4 -depletion. The net balance is that more silica has gone into solution. Fluoride F^- interacts strongly with dissolved silica, bouncing the attached OH^- effectively and forming SiF_6^{2-} -complexes. Organic compounds have also been reported [182] to have a similar effect on silica dissolution under ambient or weathering conditions, though the effect was negligible for oxalate [183].

Dissolved (earth) alkali ions tend to affect the water molecules in their vicinity, with the result that the hydrogen bonds with dissolved silica become stronger, increasing the total solubility. This increase is in principle *not* related to solution pH, but only to the concentration of the (-earth- alkaline) electrolyte. Though this effect of (earth) alkalis is greatest at elevated temperatures, it is still considerable at ambient conditions with a six-fold increase in solubility [178].

As an alternative to effects on the solute or the solvent, dissolved species may adsorb to the solid silica surface and inhibit dissolution. The iso-electric point of silica is near pH2 at which the silica surface has a zero charge. In a more acid environment, the surface becomes positively charged attracting negative species in the solution, and at more basic conditions the surface is negatively charged (see Figure 7). Thus, at the high pH so typical for concrete, the silica surface is electrically negative and hence attracts positively charged species from the solution which then become adsorbed. Apart from the above, many more mechanisms for adsorption of soluble species onto a mineral surface exist [184].

Some adsorbed species may influence silica dissolution by effectively shielding the surface from the solute or electrolyte according to [180,185], whereas other species rather promote dissolution [182]. All the species present in an electrolyte may or may not adsorb on the silica surface depending on environmental conditions, making it hard to contribute an eventual in- or decrease of the solubility to a single dissolved species.

Effect of foreign species in the solid silica

Quartz is one of the purest mineral species in nature; yet it may contain some amount of foreign ions. The crystal structure of pure quartz is very rigid and doesn't easily accommodate ions of deviating size, whence replacement is limited to minor amounts and specific locations. Most common replacants for Si^{4+} are Al^{3+} and Fe^{3+} , leaving uncompensated charges in the structure. To maintain electrical balance, small monovalent cations like H^+ , Li^+ , Na^+ and/or K^+ enter the quartz structure in interstitial spaces and not

at original Si-locations [186]. As the Al^{3+} and/or Fe^{3+} ions are strongly bonded in the quartz structure they are immobile, whereas the interstitial charge compensating ions are rather mobile and can be exchanged for other species by electrochemical treatment [187].

Effect of hydrous species in the solid silica

One other major way to replace silicium in quartz is by four H^+ replacing one Si^{4+} [186]. The four H^+ -s are all bonded to their own O^{2-} , thus in fact making up four hydroxyls. This entire arrangement is called a silanol group. In larger structural flaws, more water molecules may get H-bonded to the silanol groups, making patches of more or less bonded water. Silanol groups occur e.g. in dislocation defects, in previous cracks healed under elevated conditions as demonstrated experimentally by Bakker [188], and in neogenic quartz in compacted sandstone as demonstrated from geological practice [189].

Crack growth may be enhanced by water molecules entering the quartz structure through the crack as it grows. This is illustrated in Figure 8. A water molecule interacts with the oxygen in the strained Si-O-Si bond at the crack tip, and is split to form two OH-groups, causing the crack to grow [92].

Heavily deformed quartz has a high density of dislocations requiring charge compensation. Depending on the fluid and dissolved species present, monovalent cations may then easily enter the quartz structure. All kinds of impurities do have an enhancing effect upon the solubility of quartz [91,186]. Water has an outspoken effect since silanol groups near the surface provide the very best opportunity for dissolution to start. Quartz containing water indeed has a proven increased solubility [91].

Effects of polymorphism

Quartz is by far the most ubiquitous silica polymorph in the earths' crust. Nevertheless, some other polymorphs may perhaps be important in specific environments and bear importance for concrete materials science. It is therefore interesting to take a closer look at them.

The polymorphs coesite and stishovite which are stable at high pressure, and β -quartz which is stable above 573°C all immediately transform to ordinary α -quartz when conditions change to ambient (also see Figures 1-4). With respect to the alkali-silica reaction, these polymorphs are hence less relevant for civil engineering and are omitted from this review.

The polymorphs tridymite and cristobalite, normally only stable at elevated temperatures over 870°C , do also crystallize under authigenic, near-to-ambient conditions in opal-CT. The recrystallization of amorphous opal-A under diagenetic circumstances appears to involve intermediate phases that have a tridymite- or cristobalite-derived crystal structure [93], usually explained by its strong resemblance to the 3D-network structure of silica glass. All structures of these minerals essentially represent a spatial framework of arranged SiO_4 -tetrahedra. Depending on their character (reconstructive versus displacive), phase transformations may be easy or sluggish.

There are some other varieties of SiO_2 that are of particular interest with respect to the alkali-silica reaction, including chert, flint, and chalcedony [174,69]. Applying the appropriate nomenclature to fine grained silica varieties is still a matter of debate [190], as are their respective crystal structures [179]. It is argued that only moganite is a polymorph *sensu stricto*, and that agate, chert, flint, chalcedony, et cetera are rather to be regarded as

rock names instead. The rather new silica polymorph moganite [191] has to the best knowledge of the author up to date, never been mentioned as participant in a deleterious alkali-silica reaction. The crystal structure of moganite can be described as derived from quartz by polysynthetic twinning to the Brazil-law at unit cell scale [168]. This structure has been used to explain the structure of chalcedony as composed of alternating quartz and moganite domains in all three dimensions, with variable domain size.

All the silica varieties mentioned above are to some degree thermodynamically unstable, and hence more prone to dissolution and/or alkali reactivity than quartz. If the solubility rate of quartz in pH-neutral water at 25°C is set at unity, then cristobalite dissolves 2.05 times as fast, tridymite 2.71 times [91], and moganite at pH3.5 even 7.4 times [192]. The relative volumes of quartz versus moganite and the degree of misfit between their respective domains are very likely to influence the dissolution of such silica in (alkaline) solutions, perhaps also explaining the observed inconsistency regarding the dissolution of chalcedony [93].

Though the speciation of dissolved silica depends on pH, the *concentration* of the dissolved species thus also strongly depends on the nature of the solid silica the solution is in equilibrium with. All this implies that though the model of equilibrium equation 2 will not change, the effective concentration of dissolved silica *will* change, depending on the polymorph and its degree of crystallinity (elsewhere this volume).

Effect of the quality of the crystal lattice

The exact definition of a grain boundary differs with the boundary type. In general terms, a grain boundary is defined as a “two-dimensional lattice defect that introduces a misorientation with no long-range stress field.” In this respect, a high-angle misorientation is in fact a plane between two individual grains, in contrast to a low-angle misorientation that is to be regarded as a defect in one single crystal [171]. Thus, a grain boundary formally represents a planar array of dislocations.

Within a dislocation, and in a small volume embedding the dislocation, the crystal lattice is distorted and deviates significantly from the proper quartz structure. Interatomic bonds may be dangling loose and incompatible foreign ions tend to concentrate at dislocations and their direct vicinity since lattice stress can be released easier. As a result, aggressive media have an easier job breaking the stressed bonds in and next to structural defects than elsewhere. Thus, the solubility of a solid at dislocation arrays including grain boundaries is increased relative to immaculate material. A corollary to this is that quartz solubility would in fact reflect the quality of its crystal lattice.

The above provides the basis for the supposedly increased alkali-solubility of deformed quartz as compared to defect-free quartz [see eg. 175]. Experimental mortar bar expansion testing on heavily deformed rocks (ie. Norwegian mylonites) confirmed these are indeed aggressively alkali-reactive [54], though unexpectedly two samples tested behaved innocuously [58]. However, these two samples do not differ in any particular way from the alkali-reactive mylonites in the same project, according to detailed petrographical and geochemical analysis. Apparently, there is more to the alkali-reactivity of deformed quartz in mylonite than merely undulous extinction and a strongly oriented grain fabric.

Twin planes also represent a discontinuity in a crystal lattice, albeit for a totally different reason. In quartz, Dauphiné-twinning is most common, followed by Brazil-twinning, and a number of other twinning modes [164,161]. The lattices of both twin individuals are

differently oriented by some symmetry operation, like eg. a rotation or a mirror plane, or a combination. Where these lattices meet, their relative misorientation results in a distortion of the interface structure. Thus, the interface between α -quartz twin individuals does not have an α -quartz structure proper, and the interatomic bonds in the interface are stressed. In Dauphiné-twinned quartz, the structure of the twin plane becomes a distorted β -quartz structure; for other twinning modes, the resulting interface structure is otherwise [168]. The thermodynamic stability of the quartz *sensu lato* at a twin interface is reduced relative to bulk material, which is why twin interfaces in principle are more prone to attack in aggressive environments, including high pH.

Macroscale Dauphiné-twinning in natural quartz is most common. However, identifying its occurrence in quartz plates and thin sections is difficult and requires etching because this type of twinning has no optical effect in itself [164,161]. Dauphiné-twinning extends to microscale and is there also most common. It can be identified easily in (high-resolution) TEM [193]. High-temperature experiments in TEM have disclosed that Dauphiné-twins disappear when the quartz is heated to above the α - β transition temperature at 573°C, conform expectation. However, when the sample is cooled to go through the transition in the reverse way, the original Dauphiné-twin pattern reappears. Repetitive thermal cycling resulted in only minor changes [172]. In fact, early heating experiments on quartz oscillator plates in the 1940's already gave very similar results macroscopically [164]. There, it was also found that even heating well over the transition temperature up to 1000°C did not eliminate an initial, natural Dauphiné-twin pattern. Mechanically synthesized Dauphiné-twins, however, did *not* reappear after an identical heat treatment.

It has been speculated that this memory-effect might be attributed to foreign ions present at the location of the twin interfaces that effectively pin the twin boundary and cause it to reappear at its original position. The slight deviations from the quartz structure at the twin contact interface may harbor foreign ions. Dry heating only slowly moves these ions, which then is why the original twin pattern keeps coming back and why changes are only minor. On an entirely different size scale in geological bulk rock deformation, interspersed small mineral grains are known to effectively pin pre-existing quartz grain boundaries, especially mica grains [171].

The deformation inflicted on the quartz lattice by crushing and grinding of rocks to aggregate produces highly disordered micro-volumes on the surface of the crushed grains, which may have a glassy, virtually non-crystalline structure, so-called Beilby layers after the first author who discovered them on the surface of polished metals [194], until a depth of a few hundred Ångstrom. Beilby layers have been identified in a variety of materials, including oxides (ie. gem materials), and were originally thought to be caused by polish-induced flow of the top surface. However, the original theory of how Beilby layers are produced has been demised in the 1980's [195].

Beilby layers are known to affect surface reactivity of silica with respect to its toxicity in respiratory issues; acid etching of silica powder removes the Beilby layer and as a result, the silica powder is far less reactive [196]. Simply ageing the surface in a wet environment has a similar effect. The surface of freshly crushed aggregate can therefore be expected to be more reactive in a similar way.

Effect of silica particle size

The internal grain size of aggregate granules is of major importance since that parameter is directly but inversely related to the surface area of the silica available for alkali attack.

Modeling equations for the effects of particle size are based on free energy of the surface for a particle of given size, the molar volume of the involved silica species, and the particle geometry [for further details see 178].

Porosity and/or microporosity in chert enhances the accessibility of individual grains for fresh (pore) solutions to get in and for reaction products to get out, but the effect is secondary and not fundamental. However, this situation is different for opal, which consists of tightly packed micro-spherules of hydrated silica. The interstices between the opal spherules provide channels that enable so to say 3D fluid access, allowing dissolution to take place throughout the entire grain, instead of only along cracks/channels, or along the circumference.

It appears that the solubility of silica 1) increases when the radius decreases for a convex surface (ie. spherically curved), and 2) decreases with decreasing radius for a concave surface (ie. hollow). The first argument is the reason for quartz spherules with a radius smaller than $\sim 0.1\mu\text{m}$ to have a markedly increased solubility compared to massive bulk material [178]. This grain size is well beyond optical microscopic resolution in thin sections under transmitted illumination [197]. The second argument asserts that tiny discontinuities or micro-cracks are healed by precipitation of quartz at their extremities [92; also see 178]. Similarly, irregular microvoids tend to become rounded or completely filled depending on initial size, effectively reducing microporosity.

Catalytic effects of coexisting minerals

In recent decades, more and more articles have been published concerning the potential catalytic action of one mineral upon the precipitation or dissolution of another. Biotite has been documented to promote the formation of sillimanite at elevated conditions [198], and of hydrogarnet at lower grade conditions [99]. Phyllosilicates, clay minerals, and zeolites have proven catalytic properties on the most diverse chemical processes [199,200], and it has even been postulated that clay minerals would have been closely involved in the origin of life [201].

Some minerals are well known to affect the pH of pore solutions. An elegantly simple study published in 1983 clearly demonstrated that finegrained muscovite suspended in water affected the final pH of the suspension to a different degree than biotite did under identical conditions [97]. Depending on mineral composition and detailed crystal structure (dioctahedral versus trioctahedral), phyllosilicates may either act as a H^+ -donor or -acceptor, ie. as an acid or a base, influencing pH. Additionally, alkalies are rather easily accessible from the sides of phyllosilicate flakes, and may be leached from there into the pore water.

The phenomena of phyllosilicates affecting quartz solubility have previously been described for muscovite in sandstone. Upon compaction of once deposited sand into sandstone under diagenetic conditions, single flakes of muscovite appear to penetrate sideways deeply into quartz grains without even bending or kinking. The quartz grains are of proven (cathode-luminescence) detrital origin and are definitely not neogenic precipitates. Elsewhere in the same samples, quartz dissolution appears to be enhanced between adjacent quartz individuals, apparently in the presence of clay minerals even beyond electron-microscopical resolution. Optically, such grain boundaries typically appear to have 'enhanced visibility'. The dissolution phenomena are attributed to the combined catalytic action of mica and clay phyllosilicates [95,96].

Klopprogge documented the catalytic properties in the synthesis of organic compounds for clayey phyllosilicates [202; also see 199]. Depending on their (dioctahedral or trioctahedral) composition and structure, they may either act as supplier or receptor of H^+ . This way, clay minerals efficiently affect the pH of the pore fluid in the reacting system which then has consequences for quartz dissolution.

3 Comparison with silica in the concrete environment

3.1 Geological vs. ambient conditions

Geological crustal conditions range from ambient up to roughly 1.5GPa and 1200°C, whereas ambient conditions as in common concrete structures may range up to ~30MPa at temperatures ranging from around -20°C to +30°C in a temperate climate, although extreme values may be higher. Such ambient conditions would in nature perhaps be called ‘authigenic’ if prograde (towards higher-grade conditions) and ‘weathering’ if retrograde (towards conditions of lower grade), respectively. Under such ambient conditions, some minerals will dissolve and re-precipitate in another assemblage, as compared to the initial assemblage stable under the initial, elevated crustal conditions. Dissolved chemical species are transported by fluid water, resulting in the local depletion of some chemical species and enrichment elsewhere. Corollary to this is that porosity and permeability of the final product rock are affected as well.

3.2 Silica dissolution

Silica gel composition

The true chemical composition of silica gel from laboratory, natural, or concrete systems cannot be represented by H_4SiO_4 , though such is sometimes done for simplicity. As argued above, the solubility of silica amongst others may be influenced by other species in solution, each with its specific affinity to the silica present. The more outspoken the affinity of a given species, the more firmly that species attaches itself to the silica present, dissolved or solid [178].

True compositions of alkali-silica gel usually include significant amounts of Na^+ , K^+ , and Ca^{2+} ions, whereas microscopic observations on the mineralogy of the alkali-silica reaction and its products suggests that Al^{3+} , SO_4^{2-} , CO_3^{2-} , and possibly also Mg^{2+} and $Fe^{2+/3+}$ play a consistent role [119]. The alkali-silica product gel may also under advanced ASR-circumstances also be mobile along cracks and finally be extruded from the concrete into the outer world. Depending on the degree of affinity and degree of attachment to dissolved silica, the firmly attached, high gel-affinity element species will also behave in a mobile fashion whereas the other rather reside in the residual material that stays behind [74]. This neatly converges with own observations, as reported elsewhere [see Chapter 4].

Silica particle size and aggregate porosity

A note of key-importance is that the initial porosity of a particular aggregate grain is *not* a reason for its alkali reactivity in itself, but merely enhances chemical communication with the outside world. Nor is the greater reaction surface of a fine-grained siltstone the fundamental reason for its greater alkali-reactivity when compared to a coarser sandstone of otherwise similar composition.

By geological definition, siltstones have a grain size ranging down to 2µm while cherts have an average grain size of 8-10µm [93]. Optical resolution in thin sections does usually not go beyond 3-5µm, and theoretically not below ~1µm [197]. Silica solubility only increases

significantly at grain sizes below $\sim 0.1\mu\text{m}$ [178], a size considerably beyond optical resolution in concrete petrographical practice. The mathematical relationship between grain diameter and surface area *sensu stricto* is quadratic, i.e. reducing the diameter (or radius) of a mineral grain by a factor of two increases surface area by a factor four².

Within the size range of siltstones that are in microscopical practice much coarser than $0.1\mu\text{m}$, grain size is therefore *not a fundamental mineral property or quality* for the increased silica dissolution. Dissolution of silica coarser than $0.1\mu\text{m}$ has a straight forward connection to the available surface area in a simple linear relationship if side effects are omitted. This linear relationship becomes a quadratic one when ‘available surface area’ is replaced by ‘grain diameter’.

The logarithmic plot of NBRI-expansion vs. quartz mean grain size provided for Norwegian mylonites by Wigum [55] is in some way suggestive of such a quadratic relationship. However, the fundamental reason for the increased solubility of ‘mylonite silica’ is governed by other mineralogical properties (provided it is the same property for all mylonites). Though the above discussion on silica dissolution at $<0.1\mu\text{m}$ vs. dissolution $>0.1\mu\text{m}$ may seem a matter of terminological formicophilia only, both issues are controlled by entirely different parameters. In other words, grain size and/or aggregate porosity in the size range $\gg 0.1\mu\text{m}$ only enhances the initially present alkali-reactivity of silica, and is not a fundamental reason *sensu stricto*. This holds in principle for other fine grained silica varieties.

Closely related to the above discussion on silica granularity and dissolution is how to define individual grains and conversely grain boundaries. A grain boundary can be exactly defined as a certain degree of angular misfit between the crystal lattices of two individuals, usually a two dimensional array of dislocations in the crystal lattice, but in some occasions also a twin plane, or other planar arrangements like deformation lamellae [171]. Quartzose rocks with high dislocation density (e.g. mylonites) may indeed be aggressively alkali-reactive though exceptions exist. Comparing such exceptions with reactive species may shed light upon the fundamental reason for their alkali-reactivity.

Chemical impurities and foreign ions including water and silanol groups tend to associate with dislocations, vacancies and structural irregularities in the quartz lattice, providing prominent ‘handles’ for attack by chemical and/or physical forces [203]. Planar arrays of discontinuities may furnish excellent channels for material transport. The issue of lattice defects and grain boundaries has recently been addressed to some extent by Wigum [55]. He recognizes the impact of the problem in proper characterization of aggregate materials. He developed a new counting method for the case of mylonites, but if and/or to what extent the method works for other rock types has currently not been tested.

Identification and characterization of silica

According to literature and experience, quartz is by far the predominant silica polymorph in most (reactive) aggregate materials. What also emerges from such literature is that in many cases the reactive silica is hardly more than *identified* by petrography, and only rarely *characterized* by mineralogical, geochemical and/or related methods [eg. 204].

² NB: the relationship between grain diameter and total surface area *per unit volume* is on the other hand linear, i.e. half the grain diameter results in ‘only’ a doubling of surface area.

Whereas quartz is easy to identify by petrographical microscopy, other polymorphs or varieties may be more difficult, especially when they are fine grained. As discussed above, the different silica polymorphs do have different solubilities. According to recent personal communication [83], proper identification of silica polymorphism and crystallinity are of key importance to understanding of ASR-susceptibility of aggregate.

Heaney & Post [146] found after thorough analysis of over one hundred and fifty samples that moganite is much more common than originally assumed after its first discovery [191] and it occurs in virtually all types of fine grained rock silica varieties. Recent research on the thermodynamic properties of moganite revealed that it is metastable with respect to quartz [205], and laboratory experiments showed that moganite has a >7 times higher solubility at pH3.5 than quartz [192]. Moganite appears to be identical with the lutecite of Michel-Lévy & Munier-Chalmas from Parisian sandstones [206].

Moganite has the crystal structure of a quartz that is polysynthetically twinned after the Brazil law at unit cell scale [168]. Henceforth, other silica varieties like chalcedony and others can be modeled as an interlaced stacking of quartz and moganite substructures. The optical similarity of fine grained silica species makes it arduous to identify these by optical microscopy, which may be one reason for moganite having been overlooked. Another reason may be that the fine grained moganite-quartz blends can only be quantified even with XRD after Rietveld-refinement [146].

To mention another example, quartz in Norwegian felsic mylonites has been reported by Jensen [50] and Wigum [54] to be especially alkali-reactive. Though a reasonable correlation of expansion vs. total quartz area has been demonstrated [55], the fundamental reason for the increased silica solubility has not been revealed. There are several possibilities for an increased solubility, including a high dislocation density in the crystal structure due to the extensive deformation, hence subgraining, grain size reduction, and deformation lamellae, all affecting the degree of crystallinity [55]. However, blastomylonites that have recrystallized after the main mylonitic deformation are roughly equally reactive as reported in the newly finished NORMIN2000 project [58], yet they have a strongly reduced dislocation density. Recently, two Norwegian mylonites of similar felsic composition were found [207] to behave as inertly as their undeformed precursors in the NBRI-procedure.

In addition, hydrous species in quartz are known to increase its solubility, and wet quartz is reportedly mechanically weaker than dry quartz [186]. Hydrous species occur in all kinds of quartz, grown under varying but of course hydrous conditions, including neogenic quartz in sandstones and highly deformed quartz in mylonites which as stated are among the most alkali-reactive types of aggregate [69,58]. Therefore, proper characterization of silica species in potentially and actually alkali-reactive aggregate must also include these aspects.

Catalytic actions of coexisting minerals

The presence of some non-silica minerals has been tied to the occurrence of ASR in several cases, eg. phlogopite [100], dawsonite [208,119], and basalt rock [209,210]. Recently, the possible enhancing effect of muscovite mica on ASR in diagenetically compacted sandstones has been mentioned [28,29,30]. Bell-shaped areas of increased porosity at the edges of muscovite grains are described from alkali-reactive sandstone of Dutch origin. The grain boundaries in these sandstones also have a remarkably high optical contrast in thin section. However, interstitial porosity is negligible according to fluorescence microscopy [see Chapter 2], and eventually present interstitial minerals are beyond optical resolution.

These observations accurately match descriptions in geological sedimentary-diagenetic literature [95,96].

Catalytic or otherwise interaction of redactional character among minerals has not often been established in natural systems, and certainly not in the case of ASR and other causes of concrete deterioration. Such interaction can for instance be a matter of incongruent dissolution preferentially releasing alkalis [eg. 211], or a truly catalytic action [97; see also 212]. Though the nature of catalytic interaction is unknown (at least into detail), it seems to be a relevant issue since many of the minerals in the cement paste do have a crystal structure similar to clay minerals, or parts in that structure with a catalytic potential similar to clays [199].

Recently, it was noticed that portlandite occurred intimately intergrown with and within frayed biotite flakes in Dutch concrete [101], strongly suggesting a pH-dependent relationship present in concrete, at least during the precipitation of portlandite [99].

4 Conclusions

There are a great number of aspects and properties about the material silica that may or may not affect its dissolution under ASR conditions. Some are quite obvious and relatively easy to assess, others are more difficult to characterize as they require specific analytical instrumentation and/or skills. Detailed and thorough analysis of alkali-reactive silicas from different origins with a range of techniques and methods will be needed to understand why some silica is alkali-reactive and why others are not, what their differences are, in order to be able to develop simple and quick testing procedures.

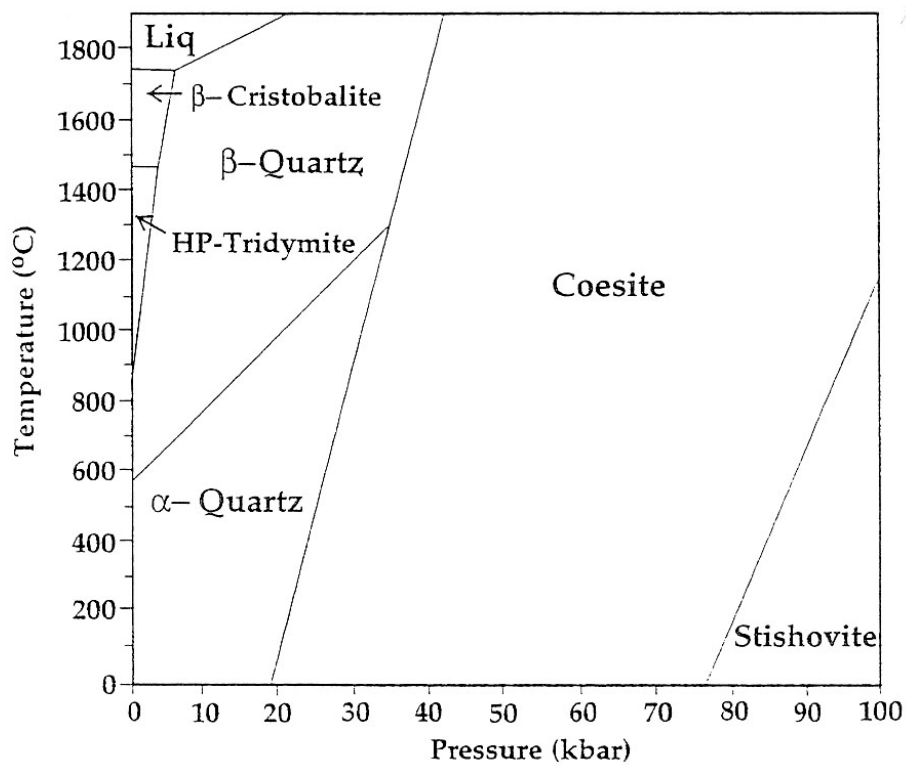


Figure 1: P,T-diagram of the stability of silica polymorphs. From [177].

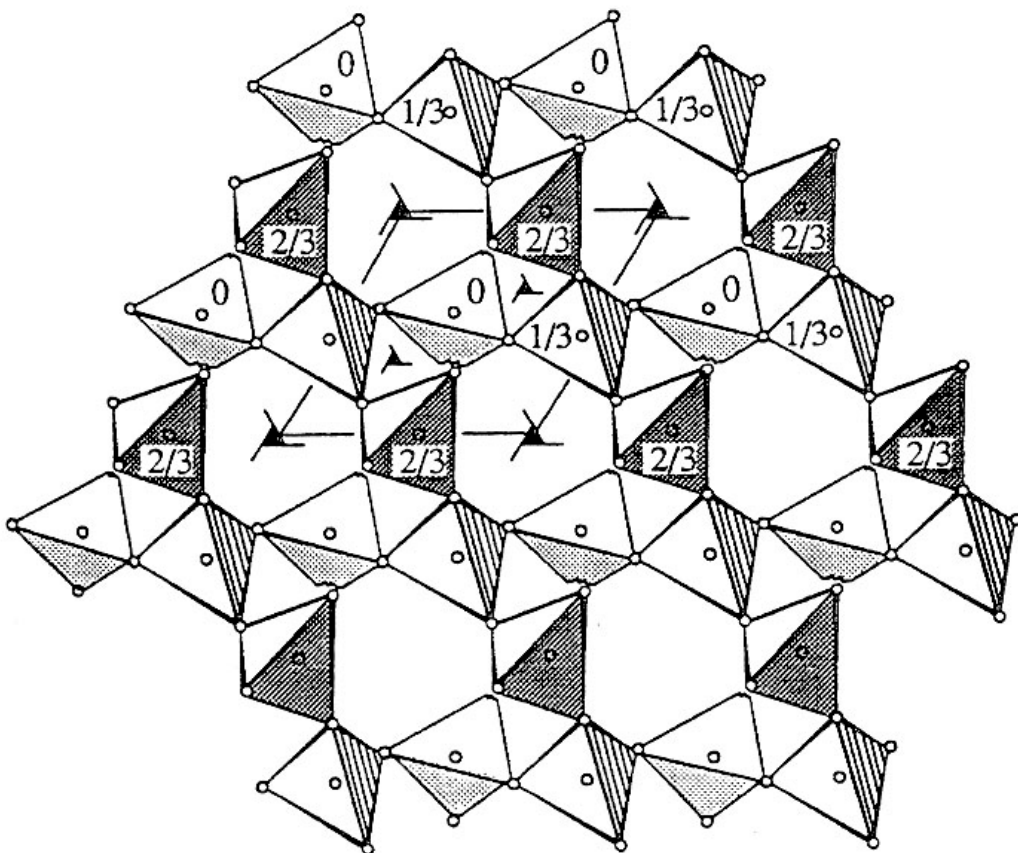


Figure 2: The crystal structure of low-temperature α -quartz. Note the presence of the di-trigonal axes. From [177].

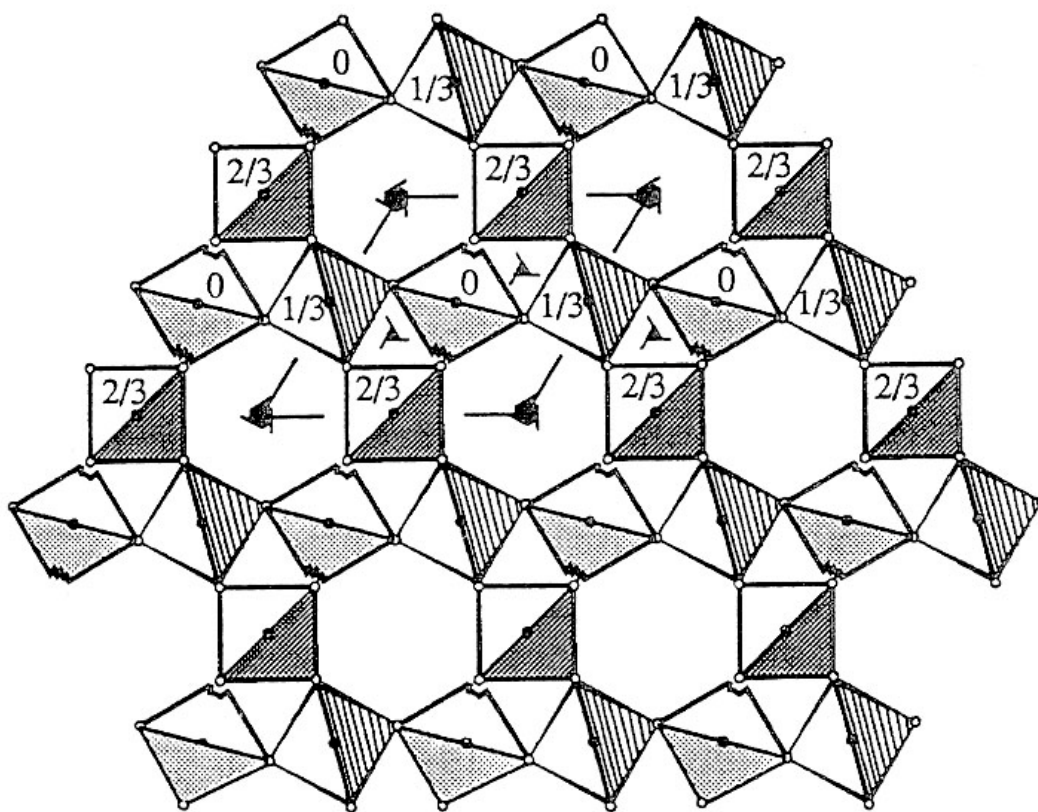


Figure 3: The crystal structure of high-temperature β -quartz. Note the rotation of the SiO_4 -tetrahedra relative to α -quartz (compare with Figure 2). The α - β transformation is thus displacive. From [177].

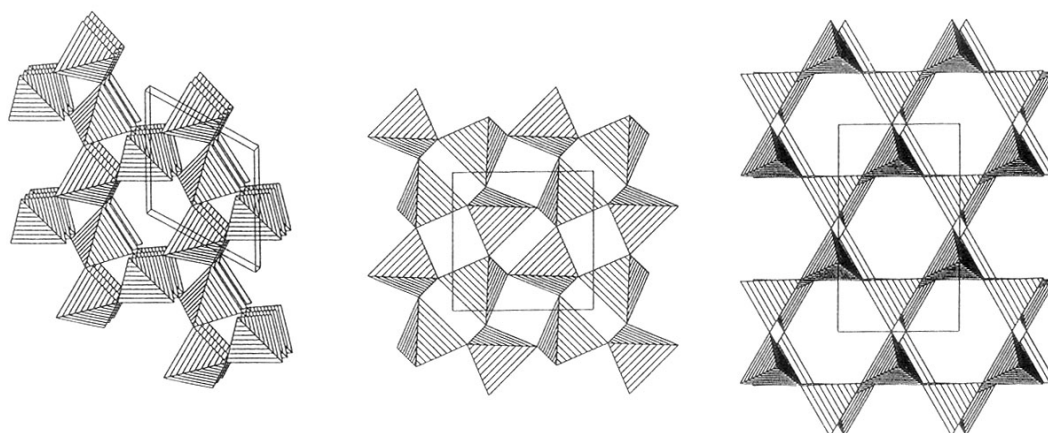


Figure 4: Crystal structures of α -quartz (left), tridymite (middle), and cristobalite (right). Successive phase transformations between these polymorphs are reconstructive, requiring much energy, and these are therefore sluggish. From [177].

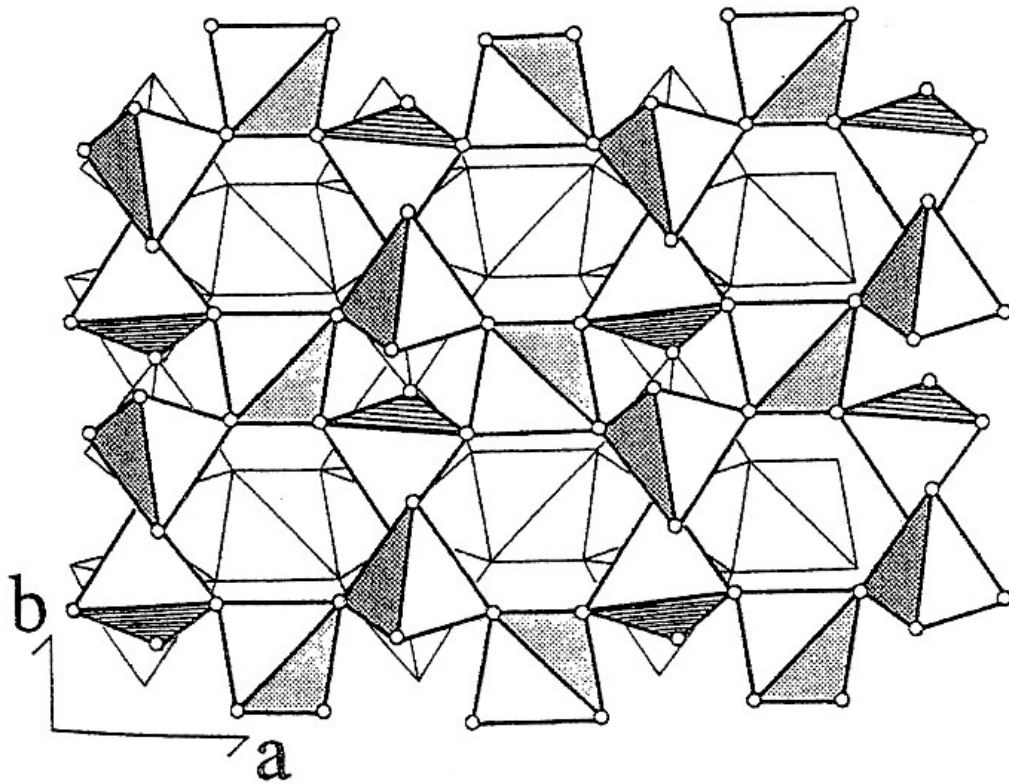


Figure 5: The crystal structure of moganite (compare with Figure 2). Note that it essentially consists of two slices of α -quartz, translated along the a-axis. From [177].

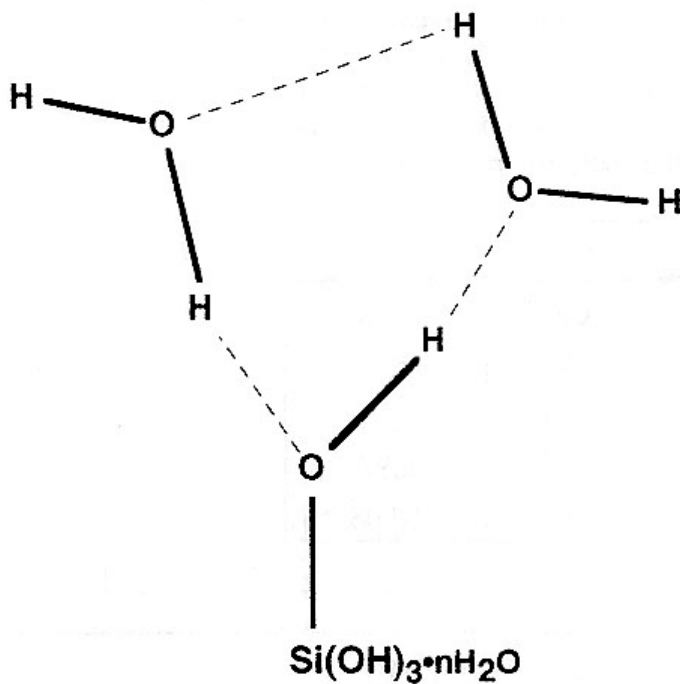


Figure 6: Dissolved H_4SiO_4 , suspended between complexing water molecules. Stippled lines are H-bonds. From [177].

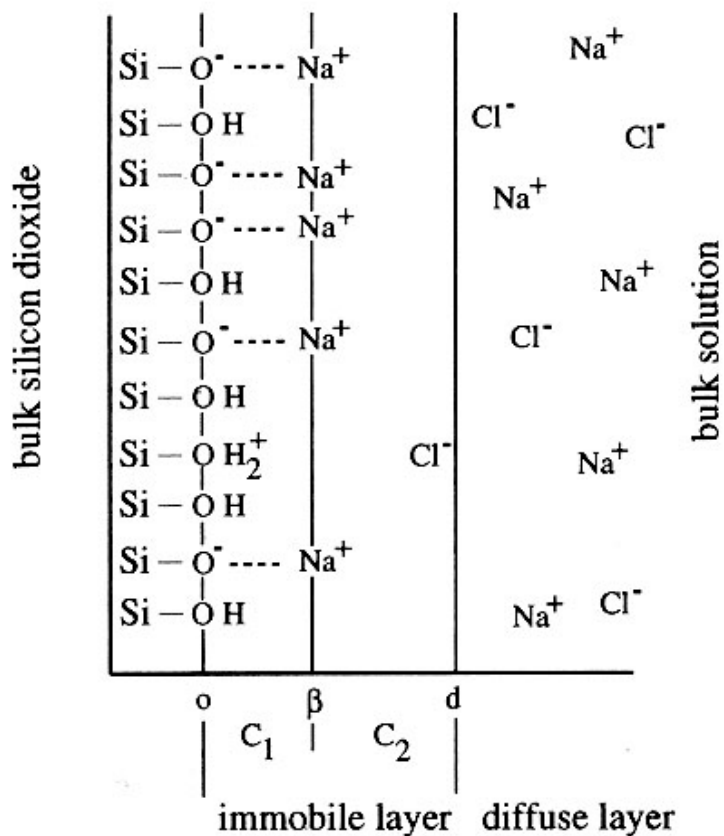


Figure 7: Surface adsorption on silica (at left) of dissolved foreign species. From [177].

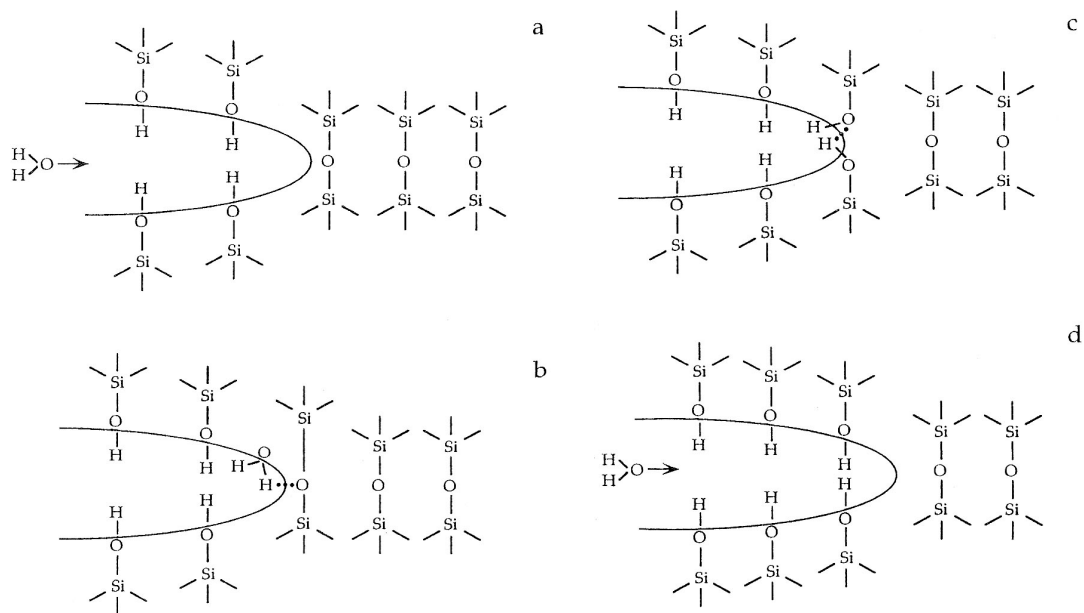


Figure 8: Crack growth is enhanced by water, interacting with the strained Si-O-Si bond at the crack tip, causing the crack to grow. From [177].

Summary

Chapters 2 through 5 of this thesis deal with petrographic analysis of concrete from four structures (Heemraadsingel, Wolput, Vlijmen-Oost, and KW5 at Zaltbommel), and geochemical aspects of two of these (Heemraadsingel and KW5 at Zaltbommel). The research characterizes in fact as gradually zooming in to greater detail, from bulk concrete sampled spread over the structure (Chapter 2), via bulk concrete in 16-section cores from 3+2 locations on the two structures presented as chloride- and alkali-profiles, to detailed element mapping on both intact and alkali-reactive chert and intact and alkali-reactive sandstone. Petrographic analysis is as essential in interpreting geochemical results as in selecting suitable analytical (digestion) methods and instrumentation.

One of the conclusions from petrographic analysis is that some but not all sand-/siltstone grains are alkali-reactive, consistently those with 'accentuated grain boundaries'. These grains typically have stylolites that were formed by pressure solution and their texture is characteristic of compaction, both under geological conditions. Both processes involve dissolution and (re-) precipitation of quartz. Neogenic quartz precipitates under low grade conditions, syntactically on detrital cores that were formed under high grade conditions. Which of these two quartz types actually reacts is unknown and would be most worthwhile to investigate, for example with cathodoluminescence.

Cathodoluminescence on thin sections makes it rather easy to distinguish high-grade detrital from neogenic low-grade quartz as their luminescence is markedly different. Optical cathodoluminescence provides not only information on brightness but also color, whereas cathodoluminescence in the electron microscope provides greater spatial resolution. In addition, an electron microscope can be operated in several other ways, each providing additional information. Many more rock types than sand-/siltstone may contain two or more generations of quartz, each formed during a different phase in the history, mylonite only being one of such rock types.

The sand-/siltstone grains appear to be more violently reactive than chert, whereas they do have a lower internal porosity and greater grain size which actually should make them *less* reactive. Similar sand-/siltstone grains have been reported to form silica gel in concrete made with blast-furnace slag cement. It seems that some property or constituent of the sand-/siltstone overcomes the 'disadvantages' of porosity and grain size. Here, it is suggested that interstitial clay minerals (most probably these 'accentuate' interior grain boundaries) may release alkalis, not necessary to dissolve silica which is rather controlled by OH⁻ splitting Si-O bonds, but mobilizing the silica gel once formed.

Clay minerals also behave catalytic and are able to significantly change local porewater pH, enhancing silica dissolution under geological conditions, independent of alkali-release. Which of these plays a role in the investigated samples is unclear, and could perhaps be

resolved by electron microscopy into very minute detail. Particularly together with cathodoluminescence as mentioned above, electron microscopy will be a very advantageous technique to investigate ASR silica-dissolution sites within individual aggregate grains.

Other sand-/siltstone grains with different features appear non-reactive. In contrast to this, *all* sand-/siltstone is regarded as potentially alkali-reactive in Norway, without further specification. On the other hand, there are no petrographic criteria available to distinguish between reactive and non-reactive types of sandstone, neither in the Netherlands, nor in Norway. Originally, the Dutch national recommendation 'CUR-Aanbeveling 38' only mentioned chert as an alkali-reactive constituent. The soon forthcoming recommendation however, provides methods and criteria also for chalcedony and opal, and refers to RILEM TC106 procedures to identify potentially alkali-reactive constituents other than chert, chalcedony and opal.

Mortar-bar testing is still a somewhat empirical approach. Even ultra-accelerated mortar bar testing takes considerably longer time than petrographic analysis which can be extremely important in construction. In addition, the expansion measured in the experiment is some derivative of the expansion in real life, and there is always some chance of a false outcome, though minimal. The larger the construction project, the more important this becomes.

If the fundamental mineral properties responsible for alkali-reactivity would be known for different types of silica from different geological backgrounds, then these could be quantified by specific methods, which can eventually be customized to answer construction engineers' demands. For that, we need to understand which properties and/or qualities control dissolution for different types of silica.

The crystallinity index for quartz as introduced in 1976 has found some application in aggregate research and characterization. However, it appears that the crystallinity index lumps many different kinds of lattice defects and irregularities into one index, suggesting the possibility to compare quartz types from different origins. Chapter 6 provides data from different types of silica, and though crystallinity indices range from <1 through >10 , there appears to be no uniform straight-forward correlation with mortar bar expansion results over the entire crystallinity index range.

This strongly suggests that different types of silica with different geological backgrounds may have different reasons for increased solubility under ASR conditions. Chapter 7 reviews controls for silica dissolution under geological circumstances from an ASR point of view. The common (ie. non-exotic) character of the mineral properties potentially controlling quartz (silica) dissolution suggests that they are likely to play a role in the alkali-silica reaction as well.

Taken all the above together, there appears to be an obvious demand for in-depth characterization of silica in terms of dissolution, preferably both on fresh material and *in situ* on deteriorated concrete from real life. Initial academic techniques applied to uncover the properties and parameters of interest will have to be replaced by standardized methods, customized and specified to the requirements of concrete users and engineers.

Chapter 9

Acknowledgments

There's only one author of this thesis, but there are many contributors, direct and indirect, perhaps sometimes even without them being aware. I will hereby take the opportunity to thank all those who have helped me from when I was a kid until present.

First and foremost, I have to thank my parents Anton Broekmans and Helena Broekmans-Kuypers, and my late grandfather Marinus Broekmans. Sitting on my parents bed after having watched a tv-show, aged 5, it was you dad, who 'ignited' my interest for geology by explaining that you thought volcanism came from "deep, very, very deep", and that it was "hot, very, very hot, but I don't know how hot". Mom, your never-off, always-on encouragements to pursue my studies did help me over some high up-ramps. Grandad, thanks for all the little rock treasures you collected for me from your driveway.

From my highschool period (1975-1983), I have to thank Bart Peletier for all the precious hours we spent in physics and chemistry lab classes experimenting with lasers, 40kV Rumkorff coils, concentrated acid blends, kitchen explosives, etc. The more dangerous the experiment, the more shock, lightning, or boom there was to it!

From the period when I studied geology at Utrecht University (1984-1992), I'd like to thank Jeroen 'Knoeihok' Morshuis, Erik-Jan Kornman, Dick Liefink, Andries Krijgsman, and many others I can't possibly begin to mention, for companionship, time spent out and about in the field, and innumerable hours of genuine (frat) fun and (brat) laughter.

From the period when I was employed as the technical manager of Nebest BV (1992-1997), I wish to thank Wim Brink for bringing up the idea of pursuing this PhD, and to my (now former) colleagues. Special thanks to the 'six-pack' Carla Bremer and Jérôme Krakeel, Wim Segers and Mel Hesselman, and Eddy Folten and Mirjam van de Ven for many hours of intranslatable Dutch 'gezelligheid'!

Research always starts with an idea, and I wish to express my gratitude to Ben Jansen for putting the ideas for this research in my mind, for helping streamline them, for 'performing' a great deal of the analyses rather than merely executing them, and for indispensable support in critical data-assessment. Ben, you are a great source of inspiration and an invaluable resource of facts and feats.

Ideas are then followed by extracting samples. If it hadn't been for the efforts of Wim de Bruijn, Niek Kaptijn, and Jaap Bakker from Rijkswaterstaat Tilburg who arrested the Heemraadsingel and KW5 at Zaltbommel beams for sampling after four-point bending experimenting, and for Wim Segers from Wijk-en-Aalburg and Joop den Uijl from the Delft Technical University who both took care of the actual drilling and sending, I wouldn't even have been here.

Børge Wigum from ERGO/Iceland is thanked for providing me with the original mylonite samples from his PhD-research and his original data, giving me a reference framework and saving me a lot of time. In the same line, I wish to thank all members of FARIN for introducing me to Norwegian ASR: Per Hagelia, Marit Haugen, Viggo Jensen, Hans-Christian Gran, Jan-Viggo Holm, Bård Pedersen, Per-Christian Vedeler, and Arnhild Ulvik. All your contributions have been very valuable!

The Ohio chert samples were donated by emeritus Bill Kneller from Toledo University, currently of Sylvania/OH, United States of America. During a residential visit that lasted two full days, Bill told me “Everything I always wanted to know about ASR, but was afraid of to ask.”, and based upon his experiences back in the 1960's, he encouraged me to go on. Bill, your work is simply amazing in both detail and extension, and will not be forgotten. The very least I could do is to dedicate Chapter 6 entirely to you.

Petrography ain't easy, especially when you care about both detail and overview. Peter Laugesen from Dansk Beton Teknik A/S is not only a concrete microscopist ‘par excellence’ whom as a scientist may ‘agree to disagree’, but he is also a true friend. Peter, thanks for your numerous contributions and frank comments!

Organizing and arranging all data wasn't an easy job, putting it all down on paper proved even more difficult. I am much indebted to Timo Nijland with whom I had many in-depth technical discussions on all aspects of ASR, in particular the peculiarities of geochemical analyses, and how to evaluate data quality and reliability. In addition, Timo xeroxed many Dutch and other references for me even before me asking. Many, many thanks! To his current colleague Joe Larbi I will say one thing only he'll understand: “Thanks, mom!”.

Since 1997, I have been employed at the Geological Survey of Norway (NGU). Many people contributed one way or another to help me understand the intricacies of sample preparation, notably Børre Davidsen and Andreas Grimstvedt, as did Geert-Jan de Haas from the nearby Geological Institution of the Norwegian University of Science and Technology (NTNU). Tom Jacobsen and Bengt Johansen provided tremendous help with crushing and grinding concrete and mylonite samples, Brit Inger Vongraven with the magnetic separation of crushed mylonites, and NTNU-undergraduate Nadine Hülbig who meticulously handpicked the mylonite quartz grains.

The analytical expenses were partially sponsored by a research grant through Niek Kaptijn from the Dutch Ministry of Transport, Directorate-General of Public Works and Water Management, for which I am most grateful. The remainder was sponsored by NGU, and Peer-Richard Neeb, Morten Smelror, Helge Hugdahl, Nigel Cook, and the late Brian Sturt all contributed in their own way.

Last but not least I am grateful to the editorial committee who reviewed the quite preliminary draft version. In alphabetical order: Sidney Diamond, Patrick Grattan-Bellew, Peter Laugesen, Timo Nijland, and Donald Ramsay, and my paranymphs Roland Vogels and Paul Stolzenburg who helped with the preparations for my thesis-defense.

To all those I haven't mentioned above: you have *not* been forgotten and you *did* contribute by being there for me when at times I felt between a piece of concrete and a hard place. :)

Chapter 10

References

- 1 Stanton, TE (1940): Expansion of concrete through reaction between cement and aggregate. *Proceedings of the American Society for Civil Engineering* (66): 1781-1811.
- 2 Pearson, JC, and Laughlin, GF (1923): An investigation case of dangerous aggregate. *Proceedings of the American Concrete Institute* (19): 142-54.
- 3 Powers, TC, and Steinour, HH (1955a): An interpretation of some published researches on the alkali-aggregate reaction. Part 1 - the chemical reactions and mechanism of expansion. *Journal of the American Concrete Institute* (26): 497-516.
- 4 Powers, TC, and Steinour, HH (1955b): An interpretation of some published researches on the alkali-aggregate reaction. Part 2 - a hypothesis concerning safe and unsafe reactions with reactive silica in concrete. *Journal of the American Concrete Institute* (26): 785-811.
- 5 Bhatti, MSY (1985): Mechanism of pozzolanic reactions and control of alkali-aggregate expansion. *Cement, Concrete & Aggregates CCAGDP* (7): 69-77.
- 6 Diamond, S (1991): Alkali aggregate reactions in concrete: an annotated bibliography, 1939-1991. Strategic Highway Research Program Report (SHRP/C/UWP-92/601): pp 470.
- 7 Bosschaert, RAJ (1957): Alkali-reacties van de toeslag in beton. *Cement* (9): 494-500.
- 8 Bosschaert, RAJ (1958): »Alkali-reacties van de toeslag in beton.«. Danish abstract in: *Beton-Teknik* (2): 122-3.
- 9 Rosema, AA (1956): Slechte uitvoering van beton. *Bouw* (11): 806-9.
- 10 Van de Fliert, C, Ten Hove, JF, and Schrap, LW (1962): Alkali-aggregaat reactie in beton. *Cement* (14/1): 20-8.
- 11 Bakker, RFM (1980): On the cause of increased resistance of concrete made from blast furnace cement to the alkali-silica reaction and to sulphate corrosion. PhD-thesis University of Aachen, Faculty of Mining and Metallurgy: pp 144.
- 12 De Ceukelaire, L (1988): Alkali-silicareactie nu ook in België? *Cement* (40/10): 21-5.
- 13 Soers, E, and Meyskens, M (1989): Petrographical research on alkali-aggregate reactions in concrete structures in Belgium. In: Okada, K, Nishibayashi, S, and Kawamura, M (editors): *Proceedings of the 8th International Conference on Alkali-aggregate Reaction in Concrete*, Kyoto: 463-8.
- 14 Van Gemert, D (1989): Alkali-aggregate reaction in Belgium: concrete highway and office building. In: Okada, K, Nishibayashi, S, and Kawamura, M (editors): *Proceedings of the 8th International Conference on Alkali-aggregate Reaction in*

- Concrete, Kyoto: 43-9.
- 15 Hudec, PP, and Larbi, JA (1989): Chemical treatments and additives to minimize alkali reactivity. In: Okada, K, Nishibayashi, S, and Kawamura, M (editors): Proceedings of the 8th International Conference on Alkali-aggregate Reaction in Concrete, Kyoto: 193-8.
 - 16 Hudec, PP, and Larbi, JA (1989): Rapid methods of predicting alkali reactivity. In: Okada, K, Nishibayashi, S, and Kawamura, M (editors): Proceedings of the 8th International Conference on Alkali-aggregate Reaction in Concrete, Kyoto: 313-9.
 - 17 Hudec, PP, and Larbi, JA (1989): A study of alkali-aggregate reaction in concrete: measurement and prevention. Part I: measurement - development of a rapid AR test method. *Cement & Concrete Research* (19): 193-8.
 - 18 Larbi, JA, and Hudec, PP (1990): A study of alkali-aggregate reaction in concrete: measurement and prevention. Part II: AR in saturated hot and cold NaCl solutions. *Cement & Concrete Research* (20): 73-8.
 - 19 Soers, E, and Meyskens, M (1990): Alkali-aggregaat reactie. *Uitbreiding kwaliteitscontrole noodzakelijk*. *Cement* (42/11): 20-7.
 - 20 Heijnen, WMM, and Van der Vliet, J (1991): Alkali-silicareactie ook in Nederland. *Cement* (43/7-8): 6-11.
 - 21 Heijnen, WMM (1992): Alkali-aggregate reactions in the Netherlands. In: Poole, AB (editor): Proceedings of the 9th International Conference on Alkali-Aggregate Reaction in Concrete (1): 432-9.
 - 22 Heijnen, WMM, Larbi, JA, and Siemes, AJH (1996): Alkali-silica reaction in the Netherlands. In: Shayan, A (editor): Proceedings of the 10th International Conference on Alkali-aggregate Reaction in Concrete (1): 109-16.
 - 23 Bakker, RFM, Heijnen, WMM, Soen, HHM, and De Vries, J (1994): Maatregelen om de alkali-silicareactie in beton te voorkomen. *Cement* (46/6): 57-61.
 - 24 CUR-Aanbeveling 38 (1994): Maatregelen om schade aan beton door de alkali-silicareactie (ASR) te voorkomen. *Civiltechnisch Centrum Uitvoering Research en Regelgeving*, Gouda: pp 8.
 - 25 De Paepe, R (1991): Omzendbrief nr. 225/910131: Alkali-silicareacties in beton. *Ministerie van de Vlaamse Gemeenschap, Department Leefmilieu en Infrastructuur*: pp 12.
 - 26 Anonymous (1994): Dienstorder LI 94/80. *Ministerie van de Vlaamse Gemeenschap, Department Leefmilieu en Infrastructuur*: pp 8.
 - 27 Broekmans, MATM (1996): Pilotstudy drie ASR-onderhevige viaducten in rijksweg A59. *Nebest-report C1264* (24): pp 126.
 - 28 Broekmans, MATM, and Jansen, JBH (1997): ASR in impure sandstone: mineralogy and chemistry. In: Sveinsdóttir, EL (editor): Proceedings of the 6th Euroseminar on Microscopy Applied to Building Materials, Reykjavik, Iceland: 161-76.
 - 29 Broekmans, MATM, and Jansen, JBH (1998): Silica dissolution in impure sandstone: application to concrete. In: Vriend, SP, and Zijlstra, JJP (editors): Proceedings of the Conference on Geochemical Engineering: Current Applications and Future Trends. *Journal of Geochemical Exploration, Special Volume* (62): 311-8.

- 30 Broekmans, MATM, and Jansen, JBH (1998): Possibility of enhanced silica dissolution in concrete as in diagenetically altered sandstone. *NGU-Bulletin* (433): 42-3.
- 31 Borsje, H, Spoon, AC, Walthaus, W, and Bubberman, RAL (1992): Onderzoek naar de conditie van kunstwerk 44G-117 "Heemraadsingel" in de Rijksweg 59 (Maasroute). Bijlage 8: Petrografisch onderzoek TNO. Excerpt Nebest-report PN813 (1): pp 11.
- 32 Bubberman, RAL, and Broekmans, MATM (1994): Petrografisch onderzoek aan viaduct 'Wolput', A59, hm 124,78. Nebest-report C1264 (3): pp 87.
- 33 De Bruin, WA (1994): personal communication.
- 34 TNO-Rapport (1996): Basisonderzoek van een betonconstructie waarin schade door ASR wordt vermoed. TNO-report 96-BT-R1012/00: pp 59.
- 35 TNO-Rapport (1997): Voortgezet ASR-basisonderzoek voor viaducten waarin schade door ASR is opgetreden; project A59; viaducten Heemraadsingel, Wolput en Vlijmen-Oost. Nader constructief onderzoek. TNO-report 97-CON-R0359: pp 85.
- 36 Den Uijl, JA, Kaptijn, N, and Walraven, JC (2000): Shear resistance of flat slab bridges affected by ASR. In: Bérubé, MA, Fournier, B, and Durand, B (editors): *Proceedings of the 11th International Conference on Alkali-Aggregate Reaction in Concrete*: 1129-38.
- 37 Siemes, T, and Gulikers, J (2000): Monitoring of reinforced concrete structures affected by alkali-silica reaction. In: Bérubé, MA, Fournier, B, and Durand, B (editors): *Proceedings of the 11th International Conference on Alkali-Aggregate Reaction in Concrete*: 1205-14.
- 38 Siemes, T, and Visser, J (2000): Low tensile strength in older concrete structures with alkali-silica reaction. In: Bérubé, MA, Fournier, B, and Durand, B (editors): *Proceedings of the 11th International Conference on Alkali-Aggregate Reaction in Concrete*: 1029-38.
- 39 ISE (1992): Structural effects of alkali-silica reaction. The Institution of Structural Engineers, SETO, London: pp 45.
- 40 Siemes, AJM, and Bakker, JD (2000): Evaluation of the Institution of Structural Engineers' procedure on concrete structures with alkali-silica reaction in the Netherlands. In: Bérubé, MA, Fournier, B, and Durand, B (editors): *Proceedings of the 11th International Conference on Alkali-Aggregate Reaction in Concrete*: 1195-204.
- 41 Nijland, TG, and Jansen, JBH (2000): Overzicht van nieuwe kennis en Nederlandse ervaring met betrekking tot alkali-silica reactive sedert CUR-Aanbeveling 38 (1994). TNO-report 2000-BT-MK-R0317: pp 46.
- 42 Musæus, HB (1962): Alkali-kiselsyre-reaksjoner i betong. Unpublished Masters thesis, Geological Institute, Technical University of Trondheim: pp ??.
- 43 Idorn, GM (1967): Durability of concrete structures in Denmark: a study of field behavior and microscopic features. PhD-thesis, Technical University of Denmark, Copenhagen: pp 208.

- 44 Kjennerud, A (1978): Alkaligrusreaksjoner påvist i Norge. Skadene vanligere enn antatt? *Plan & Bygg* (1): pp 3.
- 45 Anonymous (1981): Alkali-kiselreaksjoner i betong i svømmebasseng. Skader og utbedringsmåter. Norges byggforskningsinstitutt, Byggforskserien, Byggedetaljer E527.260: pp 2.
- 46 Haugen, M (1986): Mulige alkalikiselreaksjoner i betong, med enkelte norske tilslagsmaterialer. Unpublished MSc thesis engineering geology. Norsk Teknisk Høyskole, Trondheim: pp 84.
- 47 Svendsen, VN, and Torblaa, EJ (1989): Alkalireaksjoner i norske betongdammer. Norges Vassdrags- og Energiverk (V20): pp 32.
- 48 Gautefall, O (1990): Status for dammer av betong i Norge. SINTEF STF65 Report (A90072): pp ??.
- 49 Wigum, BJ (1990): Alkalireaksjoner i betong med tilslag fra Trondheimsområdet og Gauldalen. Master of Engineering thesis, Technical University of Trondheim: pp 88+appendices.
- 50 Jensen, V (1993): Alkali aggregate reaction in southern Norway. Doctor Technicae-thesis Technical University of Trondheim: pp 262.
- 51 Jensen, V, and Haugen, M (1996): Alkalireaksjoner i nord-Norge. Rapport nr 1: felt-og laboratoriumundersøkelser. SINTEF Report STF22 (A96805): pp 35+appendices.
- 52 Jensen, V, and Haugen, M (1996): Alkalireaksjoner i nord-Norge. Rapport nr 2: Løsmasse-forekomster og petrografiske analyser. SINTEF Report STF22 (A96806): pp 37+appendices.
- 53 Jensen, V, and Haugen, M (1996): Alkalireaksjoner i nord-Norge. Rapport nr 3: In-situ malinger av fukt og dilatasjon. SINTEF Report STF22 (A96807): pp 46+appendices.
- 54 Wigum, BJ (1995): Alkali-aggregate reactions in concrete: properties, classification and testing of Norwegian cataclastic rocks. Doctor Ingeniør-thesis, University of Trondheim: pp 227.
- 55 Wigum, BJ (1995): Examination of microstructural features of Norwegian cataclastic rocks and their use for predicting alkali-reactivity in concrete. *Engineering Geology* (40): 195-214.
- 56 Normin2000 (1996): Alkalireaksjoner i betong. Forprosjektrapport, Norges Forskningsråd, Trondheim: pp 86.
- 57 Norsk Betongforening (1996): Bestandig betong med alkalireaktivt tilslag. NB Publikasjon (21): 5+27.
- 58 Normin2000 (1999): Alkalireaksjoner i betong. Hovedprosjektrapport, Norges Forskningsråd, Trondheim: pp 166 + bildeatlas: pp 14.
- 59 Broekmans, MATM, and Wigum, BJ (1999): Alkali-aggregate reaction research in Norway: current status and future quo. In: Pietersen, HS, Larbi, JA, and Janssen, HHA (editors): *Proceedings of the 7th Euroseminar on Microscopy Applied on Building Materials*, Delft: 241-4.

- 60 Broekmans, MATM, and Wigum, BJ (2001): Farin research in Norway: current quo vadis and future status. In: Stamatakis, M, Georgali, B, Fragoulis, D, and Toumbakari, EE (editors): Proceedings of the 8th Euroseminar on Microscopy Applied to Building Materials, Athens, Greece: 101-3.
- 61 Broekmans, MATM, and Jansen, JBH (1996): Unpublished results. Research for PBTS-grant NM95064. Confidential Nebest-reports (permission for publication pending).
- 62 Wigum, BJ (1997-2002): personal communication.
- 63 ISE (1992): Structural effects of alkali-silica reaction. The Institution of Structural Engineers, SETO, London: pp 45.
- 64 CUR (1995): Pre-advies constructieve aspecten van alkali-silicareactie in betonconstructies. TNO-report 95-BT-R1128/001, Delft: pp 26.
- 65 Wubs, AJ (1997): Voortgezet ASR-basisonderzoek van viaducten waarin schade door ASR is opgetreden; project A59, viaducten Heemraadsingel, Wolput en Vlijmen-Oost. TNO-report 96-BT-R1492/00: pp 85.
- 66 DenUijl, JA (2000): Restdraagvermogen na ASR-aantasting. Delft University of Technology, Faculty of Civil Engineering, Report (25.5.99-4): pp 69.
- 67 Heijnen, WiMM, Larbi, JA, and Siemes, AJH (1996): Alkali-silica reaction in the Netherlands. In: Shayan, A (editor): Proceedings of the 10th International Conference on Alkali-aggregate Reaction in Concrete (1): 109-16.
- 68 Hobbs, DW (1988): Alkali-silica reaction in concrete. Thomas Telford, London: pp 183.
- 69 French, WJ (1992): The characterization of potentially reactive aggregates. In: Poole, AB (editor): Proceedings of the 9th International Conference on Alkali-aggregate Reaction in Concrete 1992 (1): 338-46.
- 70 Bakker, JD (1999): ASR in 20 bridges in and over motorway 59 in The Netherlands. In: Forde, MC (editor): Proceedings of the 8th International Conference on Structural Faults and Repair, London (cd-rom): pp 8.
- 71 Visser, JHM, and Siemes, T (1998): Vooronderzoek naar de treksterkte van viaduct KW5 nabij Zaltbommel. TNO-report 97-BT-R1655/VRJ: pp 24.
- 72 Prøvningsmetode TI-B 5 (1987): Strukturanalyse af beton i forbindelse med kvalitetskontrol. Byggeteknik, Teknologisk Institut.
- 73 Laugesen, P (1995-2001): personal communication.
- 74 Taylor, HFW (1997): Cement chemistry. 2nd edition, Thomas Telford, London: pp 459.
- 75 Cremer, M, and Schlocker, J (1976): Lithium borate decomposition of rocks, minerals, and ores. American Mineralogist (61): 318-21.
- 76 Kristmann, M (1977): Portland cement clinker: mineralogical and chemical investigations. Part I: microscopy, X-ray fluorescence and X-ray diffraction. Cement & Concrete Research (7): 649-58.
- 77 Varma, A (1991): Handbook of inductively coupled plasma atomic emission spectroscopy. CRC Press, Boca Raton: pp 380.

- 78 Atkins, CP, Scantlebury, JD, Nedwell, PJ, and Blatch, SP (1996): Monitoring chloride concentrations in hardened cement pastes using ion selective electrodes. *Cement & Concrete Research* (26): 319-24.
- 79 Broekmans, MATM (2001): A simple and straight-forward damage rating index and its correlation with infiltrated chloride. In: Papadopoulos et alii (editors): *Proceedings of the 8th Euroseminar on Microscopy Applied to Building Materials*, Athens, Greece: pp 8.
- 80 Jacobsen, S, Marchand, J, and Hornain, H (1995): SEM observations of the microstructure of frost deteriorated and self-healed concretes. *Cement & Concrete Research* (25): 1781-90.
- 81 Kühnel, RA (1995): Problems of quantification of fabrics. In: Elsen, J (editor): *Proceedings of the 5th Euroseminar on Microscopy Applied to Building Materials*: 58-67.
- 82 Aplin, AC (1992): The composition of authigenic clay minerals in recent sediments. In: Manning, DAC, Hall, PL, and Hughes, CR (editors): *The Mineralogical Society Series* (4): 81-106.
- 83 Jansen, JBH (1995-2001): personal communication.
- 84 Kjellsen, KO, Jennings, HM, and Lagerblad, B (1996): Evidence of hollow shells in the microstructure of cement paste. *Cement & Concrete Research* (26): 593-600.
- 85 Hadley, DW, Dolch, WL, and Diamond, S (2000): On the occurrence of hollow-shell hydration grains in hydrated cement paste. *Cement & Concrete Research* (30): 1-6.
- 86 Casey, WH, and Bunker, B (1990): Leaching of mineral and glass surfaces during dissolution. In: Hochella jr, MF, and White, AF (editors): *Mineral-water interface geochemistry*. *Reviews in Mineralogy* (23): 397-426.
- 87 ASTM D75-87 (1988): Standard practice for sampling aggregates. *Annual book of ASTM Standards*. American Society for Testing Materials, Section 4, Construction. Volume 04.08 Soil and rock, building stones; geotextiles: 62-5.
- 88 Howarth, RJ (1998): Improved estimators of uncertainty in proportions, point-counting, and pass-fail test results. *American Journal of Science* (298): 594-607.
- 89 Broekmans, MATM (1999): Classification of the alkali-silica reaction in geochemical terms of silica dissolution. In: Pietersen, HS, Larbi, JA, and Janssen, HHA (editors): *Proceedings of the 7th Euroseminar on Microscopy Applied on Building Materials*, Delft: 155-70.
- 90 Marshall, WL, and Warakomski, JM (1980): Amorphous silica solubilities—II. Effect of aqueous salt solutions at 25°C. *Geochimica et Cosmochimica Acta* (44): 915-24.
- 91 Dove, PM, and Rimstidt, JD (1994): Silica-water interactions. In: Heaney, PJ, Prewitt, CT, and Gibbs, GV (editors): *Silica*. *Reviews in Mineralogy* (29): 259-308.
- 92 Brantley, SL (1992): The effect of fluid chemistry on quartz microcrack lifetimes. *Earth and Planetary Science Letters* (113): 145-56.
- 93 Knauth, LP (1994): Petrogenesis of chert. In: Heaney, PJ, Prewitt, CT, en Gibbs, GV (editors): *Silica*. *Physical behavior, geochemistry and materials applications*. *Reviews in Mineralogy* (29): 233-58.

- 94 Jensen, V (1997-2001): personal communication.
- 95 Bjørkum, PA (1996): How important is pressure in causing dissolution of quartz in sandstones? *Journal of Sedimentary Research* (66): 147-54.
- 96 Oelkers, EH, Bjørkum, PA, and Murphy, WM (1996): A petrographic and computational investigation of quartz cementation and porosity reduction in North Sea sandstones. *American Journal of Science* (296): 420-52.
- 97 Boles, JR, and Johnson, KS (1983): Influence of mica surfaces on pore-water pH. *Chemical Geology* (43): 303-17.
- 98 Claeys, PF, and Mount, JF (1991): Diagenetic origin of carbonate, sulfide and oxide inclusions in biotites of the Great Valley Group (Cretaceous), Sacramento Valley, California. *Journal of Sedimentary Research* (61): 719-31.
- 99 Nijland, TG, Verschure, RH, and Maijer, C (1994): Catalytic effect of biotite: formation of hydrogarnet lenses. *Comptes Rendues de l'Academie des Sciences Paris* (318-II): 501-6.
- 100 Grattan-Bellew, PE, and Beaudoin, JJ (1980): Effect of phlogopite mica on alkali-aggregate expansion in concrete. *Cement & Concrete Research* (10): 789-97.
- 101 Nijland, TG (1997): personal communication.
- 102 Grattan-Bellew, PE, and Danay, A (1992): Comparison of laboratory and field evaluation of AAR in large dams. *Proceedings of the International Conference on Concrete AAR in Hydroelectric Plants and Dams, CEA, Fredericton, Canada*: pp 23.
- 103 Rivard, P (1998): Quantification de l'endommagement du béton atteint de réaction alcali-silice par analyse d'images. *Masters thesis, Université de Sherbrooke, Canada*: pp 166.
- 104 Rivard, P, Fournier, B, and Ballivy, G (2000): Quantitative assessment of concrete damage due to alkali-silica reaction (ASR) by petrographic analysis. In: Bérubé, MA, Fournier, B, and Durand, B (editors): *Proceedings of the 11th International Conference on Alkali-Aggregate Reaction in Concrete*: 889-907.
- 105 Anonymous (2000): Key Word Index to Volume 30. *Cement & Concrete Research* (30): 2025-8.
- 106 Prøvningsmetode TI-B 5 (1987): *Strukturanalyse af beton i forbindelse med kvalitetskontrol. Byggeteknik, Teknologisk Institut, København*: pp ??.
- 107 Anonymous (1998): Summary of 14 correlations between RCT and laboratory measurements for chloride content. *Germann Instruments A/S, Emdrupvej 102, DK-2400 Copenhagen, Denmark*.
- 108 Broekmans, MATM (2000): Source and mobility of alkalis in two Dutch ASR-concretes. *Geological Survey of Norway, NGU Report (2000.0139)*: pp 43.
- 109 Valley, JW (1986): Stable isotope geochemistry of metamorphic rocks. In: Valley, JW, Taylor, HP, and O'Neil, JR (editors): *Stable isotopes in high temperature geological processes. Reviews in Mineralogy* (16): 445-90.
- 110 Lichtner, PC, Steefel, CI, and Oelkers, EH (1996; editors): *Reactive transport in porous media. Reviews in Mineralogy* (34): pp 438.

- 111 Den Uijl, JA (1999-2001): personal communication.
- 112 Shaw, DM (1969): Evaluation of data. In: Wedepohl, KH (editor): Handbook of geochemistry. Springer Verlag, Berlin (1): 324-75.
- 113 Figg, JW, and Bowden, SR (1971): The analysis of concretes. Building Research Establishment, Her Majesty's Stationery Office: pp 68+folding plate.
- 114 Figg, JW (1989; editor): Analysis of hardened concrete - a guide to tests, procedures and interpretation of results. A report of a joint working party of the Concrete Society and Society of Chemical Industry. The Concrete Society, London, Technical Report (32): pp 117.
- 115 Vogels, RJMJ (1995-2001): personal communication.
- 116 Siemes, AJM, and Borsje, H (1996): Basisonderzoek van een betonconstructie waarin schade door ASR wordt vermoed. TNO-Rapport 96-BT-R1012/00: pp 59.
- 117 Broekmans, MATM (1993): Metasomatose: een type betonschade. Land+Water (33/7-8): 47-9.
- 118 Bernabé, Y (1995): The transport properties of networks of cracks and pores. Journal of Geophysical Research (100): 4231-41.
- 119 Thaulow, N, Jakobsen, UH, and Clark, B (1996): Composition of alkali silica gel and ettringite in concrete railroad ties: SEM-EDX and X-ray diffraction analyses. Cement & Concrete Research (26): 309-18.
- 120 Choquette, M, Bérubé, MA, and Locat, J (1991): Behavior of common rock-forming minerals in a strongly basic NaOH solution. Canadian Mineralogist (29): 163-73.
- 121 Kneller, WA, Kriege, HF, Saxer, EL, Wilband, JT, and Rohrbacher, TJ (1968): The properties and recognition of deleterious cherts which occur in aggregate used by Ohio concrete producers. Aggregate Research Group, Geology and Civil Engineering Departments, University of Toledo, Ohio, Final Report (1014): pp 201 + appendices.
- 122 Keene, JB, and Kastner, M (1974): Clays and formation of deep-sea chert. Nature (249): 754-5.
- 123 Buurman, P, and Van der Plas, L (1971): The genesis of Belgian and Dutch flints and cherts. Geologie & Mijnbouw (50): 9-28.
- 124 Murray, RW (1994): Chemical criteria to identify the depositional environment of chert: general principles and application. Sedimentary Geology (90): 213-32.
- 125 Stout, W, and Schoenlaub, RA (1945): The occurrence of flint in Ohio. Ohio Division of Geological Survey, Bulletin (45): pp 110.
- 126 Diamond, S, White, JL, and Dolch, WL (1964): Transformation of clay minerals by calcium hydroxide attack. In: Ingerson, E (editor): Proceedings of the 12th National Conference on Clays and Clay Minerals, Pergamon Press, New York: 359-79.
- 127 Bérubé, MA, Choquette, M, and Locat, J (1990): Effects of lime on common soil and rock forming minerals. Applied Clay Science (5): 145-63.
- 128 RILEM TC 106-AAR (2000): A-TC 106-2 - Detection of potential alkali-reactivity of aggregate/regates - the ultra-accelerated mortar bar test. Materials & Structures (33): 283-9.

- 129 RILEM TC 106-AAR (2000): B-TC 106-3 - Detection of potential alkali-reactivity of aggregates - method for aggregate combinations using concrete prisms. *Materials and Structures* (33): 290-3.
- 130 Wigum, BJ (2000): "Normin2000" - A Norwegian AAR research program. In: Bérubé, MA, Fournier, B, and Durand, B (editors): *Proceedings of the 11th International Conference on Alkali-Aggregate Reaction in Concrete*: 523-31.
- 131 Kneller, WA (1967): Aggregate solubility related to chert petrographic textures and electron surface morphologies. In: Angino, EE, and Hardy, RG (editors): *Proceedings of the 3rd Forum on Geology of Industrial Minerals*. State Geological Survey of Kansas, Special Distribution (34): 110-9.
- 132 Wilband, JT, and Kneller, WA (1967): Relationships between α -quartz cell parameters and some physio-chemical properties of chert aggregates. *Proceedings of a Symposium on Industrial Minerals Exploration and development*. Forum on Geology of Industrial Minerals, University of Kansas: 111-9.
- 133 Salje, EKH (2000): Mesoscopic twin patterns in ferroelastic and co-elastic minerals. In: Redfern, SAT, and Carpenter, MA (editors): *Transformation processes in minerals*. *Reviews in Mineralogy and Geochemistry* (39): 65-84.
- 134 Pasteris, JD (1999): Causes of the uniformly high crystallinity of graphite in large epigenetic deposits. *Journal of Metamorphic Geology* (17): 779-87.
- 135 Jaboyedoff, M, Bussy, F, Kubler, B, and Thelin, P (2001): Illite 'crystallinity' revisited. *Clays & Clay Minerals* (49): 156-67.
- 136 Arkai, P, Balogh, K, and Frey, M (1997): The effects of tectonic strain on crystallinity, apparent mean crystallite size and lattice strain of phyllosilicates in low-temperature metamorphic rocks. A case study from the Glarus overthrust, Switzerland. *Schweizerische Mineralogische und Petrographische Mitteilungen* (77): 27-40.
- 137 Qu, S, Fan, H, Chen, J, Feng, J, Fu, R, Wei, D, and Zhang, X (2001): Effect of the crystallinity of calcium phosphate ceramics on osteoblast proliferation in vitro. *Journal of Materials Science Letters* (20): 331-2.
- 138 Zyman, Z, Ivanov, I, Rochmistrov, D, Glushko, V, Tkachenko, N, and Kijko, S (2001): Sintering peculiarities for hydroxyapatite with different degrees of crystallinity. *Journal of Biomedical Materials Research* (54): 256-63.
- 139 Yixing, L, Jun, S, Zhenbo, L (2001): The effect of crystallinity index on vibration properties of picea wood. *Journal of the Northeast Forestry University* (29/2): 4-6.
- 140 Hulleman, SHD, Kalisvaart, MG, and Vliegthart, JFG (1999): Origins of B-type crystallinity in glycerol-plasticised, compression-moulded potato starches. *Carbohydrate Polymers* (39): 351-60.
- 141 Yanagi, Y, Kondo, Y, and Hirabayashi, K (2000): Deterioration of silk fabrics and their crystallinity. *Textile Research Journal* (70): 871-5.
- 142 Cao, J, and Billows, CA (1999): Crystallinity determination of native and stretched wool by X-ray diffraction. *Polymer international* (48): 1027-33.
- 143 Thisayukta, J, Nakayama, Y, and Watanabe, J (2001): Effect of chemical structure on the liquid crystallinity of banana-shaped molecules. *Liquid Crystals* (27): 1129-35.

- 144 Morino, K (1989): Alkali-aggregate reactivity of cherty rock. In: Okada, K, Nishibayashi, S, and Kawamura, M (editors): Proceedings of the 8th International Conference on Alkali-aggregate Reaction in Concrete (1): 501-6.
- 145 Mieke, G, and Graetsch, H (1992): Crystal structure of moganite: a new structure type for silica. *European Journal of Mineralogy* (4): 693-706.
- 146 Heaney, PJ, and Post, JE (1992): The widespread distribution of a novel silica polymorph in microcrystalline quartz varieties. *Science* (255): 441-3.
- 147 Deutsch, Y, Sandler, A, and Nathan, Y (1989): The high-low inversion of quartz. *Thermochimica Acta* (148): 467-72.
- 148 Stroger, P (1993): Study of cherts in fine and coarse aggregates in Ireland. *Concrete* (27/3): 26-9.
- 149 Wakizaka, Y (2000): Alkali-silica reactivity of Japanese rocks. *Engineering Geology* (56): 211-21.
- 150 Berra, M, Mangialardi, T, and Paolini, AE (1999): A new approach for assessing the potential alkali expansivity of slowly reactive siliceous aggregates in concrete. *Advances in Cement Research* (11): 139-47.
- 151 Murata, KJ, and Norman II, MB (1976): An index of crystallinity for quartz. *American Journal of Science* (276): 1120-30.
- 152 <http://www.berkimerdiamond.com>
- 153 Laudise, RA (1962): Hydrothermal synthesis of single crystals. In: Cotton, FA (editor): *Progress in Inorganic Chemistry* (3), Wiley Interscience: 1-47.
- 154 <http://www.ndk-j.co.jp/english/pr/sg/js/esq0008.pdf>
- 155 Penniston-Dorland, SC (2001): Illumination of quartz vein textures in a porphyry copper ore deposit using scanned cathodoluminescence: Grasberg igneous complex, Irian Jaya, Indonesia. *American Mineralogist* (86): 652-66.
- 156 Henderson, IHC (1994): Fluid pressure variations in contrasting types of faulting, Pyrenees, France. A fluid inclusion and cathodoluminescence study. Unpublished PhD-thesis University of Leeds, Scotland: pp210 + appendices.
- 157 Hervig, RL, and Peacock, SM (1989): Implications of trace element zoning in deformed quartz from the Santa Catalina mylonite zone. *Journal of Geology* (89): 343-50.
- 158 Demars, C, Pagel, M, Deloule, E, and Blanc, P (1996): Cathodoluminescence of quartz from sandstones: interpretation of the UV range by determination of trace element distributions and fluid-inclusion P-T-X properties in authigenic quartz. *American Mineralogist* (81): 891-901.
- 159 Frondel, C (1945): History of the quartz oscillator-plate industry, 1941-1944. *American Mineralogist* (30): 205-13.
- 160 Friedlaender, C, and Locher, F (1945): Vorläufige Untersuchungsergebnisse über die Eignung alpiner Quarze für piezoelektrische Zwecke. *Vierteljahrsschrift der Naturforschenden Gesellschaft in Zürich* (90/2): 125-35.
- 161 Friedlaender, C (1951): Untersuchung über die Eignung alpiner Quarze für piezoelektrische Zwecke. *Beiträge zur Geologie der Schweiz, Geotechnische Serie*,

- Lieferung (29): pp 98.
- 162 Rykart, R (1995): Quarz-Monographie. 2nd edition. Ott Verlag, Thun: pp 462.
- 163 Lukesh, JS (1945): The effect of imperfections on the usability of quartz for oscillator-plates. *American Mineralogist* (30): 291-5.
- 164 Frondel, C (1945): Secondary Dauphiné twinning in quartz. *American Mineralogist* (30): 447-61.
- 165 Nassau, K (1983): *The physics and chemistry of color: the fifteen causes of color*. John Wiley & Sons, New York: pp 454.
- 166 Hyde, B, and McLaren, A (1996): The crystal chemistry of moganite and amethyst. *Australian Journal of Chemistry* (49): 861-6.
- 167 Heaney, PJ, and Vicenzi, EP (1994): A geochemical investigation of the silica polymorph moganite. *Transactions of the Spring Meeting of the AGU, Abstracts. EOS* (75): 356.
- 168 Heaney, PJ (1994): Structure and chemistry of the low-pressure silica polymorphs. In: Heaney, PJ, Prewitt, CT, and Gibbs, GV (editors): *Silica: physical behavior, geochemistry and materials applications*. *Reviews in Mineralogy* (29): 1-40.
- 169 Shoval, S, Ginott, Y, and Nathan, Y (1991): A new method for measuring the crystallinity index of quartz by infrared spectroscopy. *Mineralogical Magazine* (55): 579-82.
- 170 Bambauer, HU, Brunner, GO, and Laves, F (1961): Beobachtungen über Lamellenbau an Bergkristallen. *Zeitschrift für Kristallografie* (116): 173-81.
- 171 Poirier, JP (1985): *Creep of crystals: high-temperature deformation processes in metals ceramics and minerals*. Cambridge University Press, Cambridge: pp 260.
- 172 Heaney, PJ, and Veblen, DR (1991): Observation and kinetic analysis of a memory effect at the α - β quartz transition. *American Mineralogist* (76): 1459-66.
- 173 Hayward, SA, and Salje, EKH (2000): Twin memory and twin amnesia in anorthoclase. *Mineralogical Magazine* (64): 195-200.
- 174 Fookes, PG (1980): An introduction to the influence of natural aggregates on the performance and durability of concrete. *Quarterly Journal of Engineering Geology* (13): 207-29.
- 175 Dolar-Mantuani, L (1983): *Handbook of concrete aggregates - a petrographic and technological evaluation*. Noyes Publications, New York: pp ??.
- 176 Iler, RK (1955): *The colloid chemistry of silica and silicates*. 1st edition. Cornell University Press, Ithaca, New York: pp 324.
- 177 Heaney, PJ, Prewitt, CT, and Gibbs, GV (1994; editors): *Silica: physical behavior, geochemistry and materials applications*. *Reviews in Mineralogy* (29): pp 606.
- 178 Dove, PM (1995): Kinetic and thermodynamic controls on silica reactivity in weathering environments. In: White, AF, and Brantley, SL (editors): *Chemical weathering rates of silicate minerals*. *Reviews in Mineralogy* (31): 235-90.
- 179 Graetsch, H (1994): Structural characteristics of opaline and microcrystalline silica minerals. In: Heaney, PJ, Prewitt, CT, and Gibbs, GV (editors): *Silica: physical*

- behavior, geochemistry and materials applications. *Reviews in Mineralogy* (29): 209-32.
- 180 Liefink, DJ (1997): The preparation and characterization of silica from acid treatment of olivine. PhD-thesis University of Utrecht, Faculty of Chemistry: pp 177.
- 181 Robie, RA, Hemingway, BS, and Fischer, R (1978): Thermodynamic properties of minerals and related substances at 298.15K and 1bar (10^5 Pascals) and at higher pressures and higher temperatures. *United States Geological Survey Bulletin* (1452): pp 456.
- 182 Bennett, PC (1991): Quartz dissolution in organic-rich aqueous systems. *Geochimica et Cosmochimica Acta* (55): 1781-97.
- 183 Poulson, SR, Drever, JI, and Stillings, SL (1997): Aqueous Si-oxalate complexing, oxalate adsorption onto quartz, and the effect of oxalate upon quartz dissolution kinetics. *Chemical Geology* (140): 1-7.
- 184 Hochella jr, MF, and White, AF (1990; editors): Mineral-water interface geochemistry. *Reviews in Mineralogy* (23): pp 603.
- 185 Liefink, DJ (1995-2001): personal communication.
- 186 Kronenberg, AK (1994): Hydrogen speciation and chemical weakening of quartz. In: Heaney, PJ, Prewitt, CT, and Gibbs, GV (editors): *Silica: physical behavior, geochemistry and materials applications*. *Reviews in Mineralogy* (29): 123-76.
- 187 Kats, A (1962): Hydrogen in alpha-quartz, parts 1 & 2. *Philips Research Reports* (17): 133-95; 201-79.
- 188 Bakker, RJ (1992): On modifications of fluid inclusions in quartz. PhD-thesis University of Utrecht, *Geologica Ultraiectina* (94): pp 189.
- 189 Kronenberg, AK, and Wolf, GH (1990): Fourier transform infrared spectroscopy determinations of intragranular water content in quartz-bearing rocks: implications for hydrolytic weakening in the laboratory and within the earth. *Tectonophysics* (172): 255-71.
- 190 Flörke, OW, Graetsch, H, Martin, B, Röller, K, and Wirth, R (1991): Nomenclature of micro- and non-crystalline silica minerals, based on structure and microstructure. *Neues Jahrbuch für Mineralogie, Abhandlungen* (163): 19-42.
- 191 Flörke, OW, Jones, JB, and Schmincke, HU (1976): A new microcrystalline silica from Gran Canaria. *Zeitschrift für Kristallographie* (143): 156-65.
- 192 Gíslason, SR, Heaney, PJ, Oelkers, EH, and Schott, J (1997): Kinetic and thermodynamic properties of moganite, a novel silica polymorph. *Geochimica et Cosmochimica Acta* (61): 1193-204.
- 193 Heaney, PJ, and Veblen, DR (1991): Observations of the α - β phase transition in quartz: a review of imaging and diffraction studies and some new results. *American Mineralogist* (76): 1018-32.
- 194 Beilby, GT (1912): *Aggregation and flow of solids*. MacMillan & Co, London: pp ??.
- 195 Crowcroft, PJ (1981): Demise of the Beilby-Bowden theory of polishing. *Journal of Gemology* (17/7): 459-65.

- 196 Goldschmidt, DF (1994): Health effects of silica dust exposure. In: Heaney, PJ, Prewitt, CT, and Gibbs, GV (editors): *Silica. Physical behavior, geochemistry and materials applications. Reviews in Mineralogy* (29): 545-606.
- 197 StJohn, DA, Poole, AB, and Sims, I (1998): *Concrete petrography*. 1st edition, Arnold Publishers, London: pp 474.
- 198 Foster, CT (1991): The role of biotite as a catalyst in reaction mechanisms that form sillimanite. *Canadian Mineralogist* (29): 943-63.
- 199 Vogels, RJMJ (1996): Non-hydrothermally synthesized trioctahedral smectites. Preparation, characterisation and catalytic properties of synthetic clay minerals. PhD-thesis University of Utrecht, Faculty of Chemistry: pp 191.
- 200 Titulaer, M (1993): Porous structure and particle size of silica and hydrotalcite catalyst precursors. PhD-thesis University of Utrecht, *Geologica Ultraiectina* (99): pp 268.
- 201 Cairns-Smith, AG, and Hartman, H (1986): *Clay minerals and the origin of life*. Cambridge University Press, Cambridge: pp 193.
- 202 Klopogge, JT (1992): Pillared clays. Preparation and characterization of clay minerals and aluminum-based pillaring agents. PhD-thesis University of Utrecht, *Geologica Ultraiectina* (91): pp 349.
- 203 Bloss, FD (1994): *Crystallography and crystal chemistry*. 2nd edition, Mineralogical Society of America: pp 545.
- 204 Rayment, PL (1992): The relationship between flint microstructure and alkali-silica reactivity. In: Poole, AB (editor): *Proceedings of the 9th International Conference on Alkali-Aggregate Reaction in Concrete* (2): 843-50.
- 205 Petrovic, I, Heaney, PJ, and Navrotsky, A (1996): Thermochemistry of the new silica polymorph moganite. *Physics & Chemistry of Minerals* (23): 119-26.
- 206 Michel-Lévy, MM, and Munier-Chalmas (1892): Mémoire sur diverses formes affectées par le réseau élémentaire du quartz. *Bulletin de Société Française de Minéralogie* (15): 159-90.
- 207 Hagelia, P (1997-2001): personal communication.
- 208 Gillot, JE, and Rogers, CA (1994): Alkali-aggregate reaction and internal release of alkalis. *Magazine of Concrete Research* (46): 99-112.
- 209 StJohn, DA, and Goguel, RL (1992): Pore solution/aggregate enhancement of alkalis in hardened concrete. In: Poole, AB (editor): *Proceedings of the 9th International Conference on Alkali-Aggregate Reaction in Concrete* (2): 894-901.
- 210 Goguel, R (1995): Alkali release by volcanic aggregates in concrete. *Cement & Concrete Research* (25): 841-52.
- 211 Pokrovski, VA, and Helgeson, HC (1991): Unified description of incongruent reactions and mineral solubilities as a function of bulk composition and solution pH in hydrothermal systems. *Canadian Mineralogist* (29): 909-42.
- 212 Aplin, AC (1992): The composition of authigenic clay minerals in recent sediments. In: Manning, DAC, Hall, PL, and Hughes, CR (editors): *Geochemistry of clay-pore fluid interactions. The Mineralogical Society Series* (4): 81-106.

Chapter 11

Curriculum Vitae

Marinus Antonius Thomas Maria Broekmans (Maarten) was born on Thursday May 16, 1963, in Rotterdam, the Netherlands. In 1983, Maarten graduated at the athenaeum the Katholiek Geldersch Lyceum in Arnhem, the Netherlands. After one year of military service, he commenced his study in Geology at the University of Utrecht in 1984. In May 1992, he graduated with the *judicium* 'with pleasure' at the Faculty for Earth Sciences, majoring in Mineralogy and with a second major in Experimental Petrology.

From November 1992 through January 1997, Maarten was employed as the technical manager of Nebest BV Engineering Consultancy in Groot-Ammers, the Netherlands. From February 1997 until present, Maarten has been employed at the Geological Survey of Norway, as a building materials scientist. Since 1993, he has also been involved in several Dutch national research committees for the CUR organization, initially related to electrochemical realkalization and chloride-extraction of concrete to prevent corrosion of the steel reinforcement, and after that related to the alkali-silica reaction. He is also co-founder of the national Forum for Alkali-Reactions In Norway, FARIN.

After this PhD, Maarten will continue to work in his (permanent) position at NGU.

Maarten A.T.M. Broekmans, MSc, PhD
Geological Survey of Norway
Department of Mineral Resources
N-7491 TRONDHEIM
Norway
www.ngu.no

phone: +47 7390 4000
facsimile: +47 7392 1620
cellular: +47 4132 5132
e-mail: maarten.broekmans@ngu.no

Appendix

Color Plates

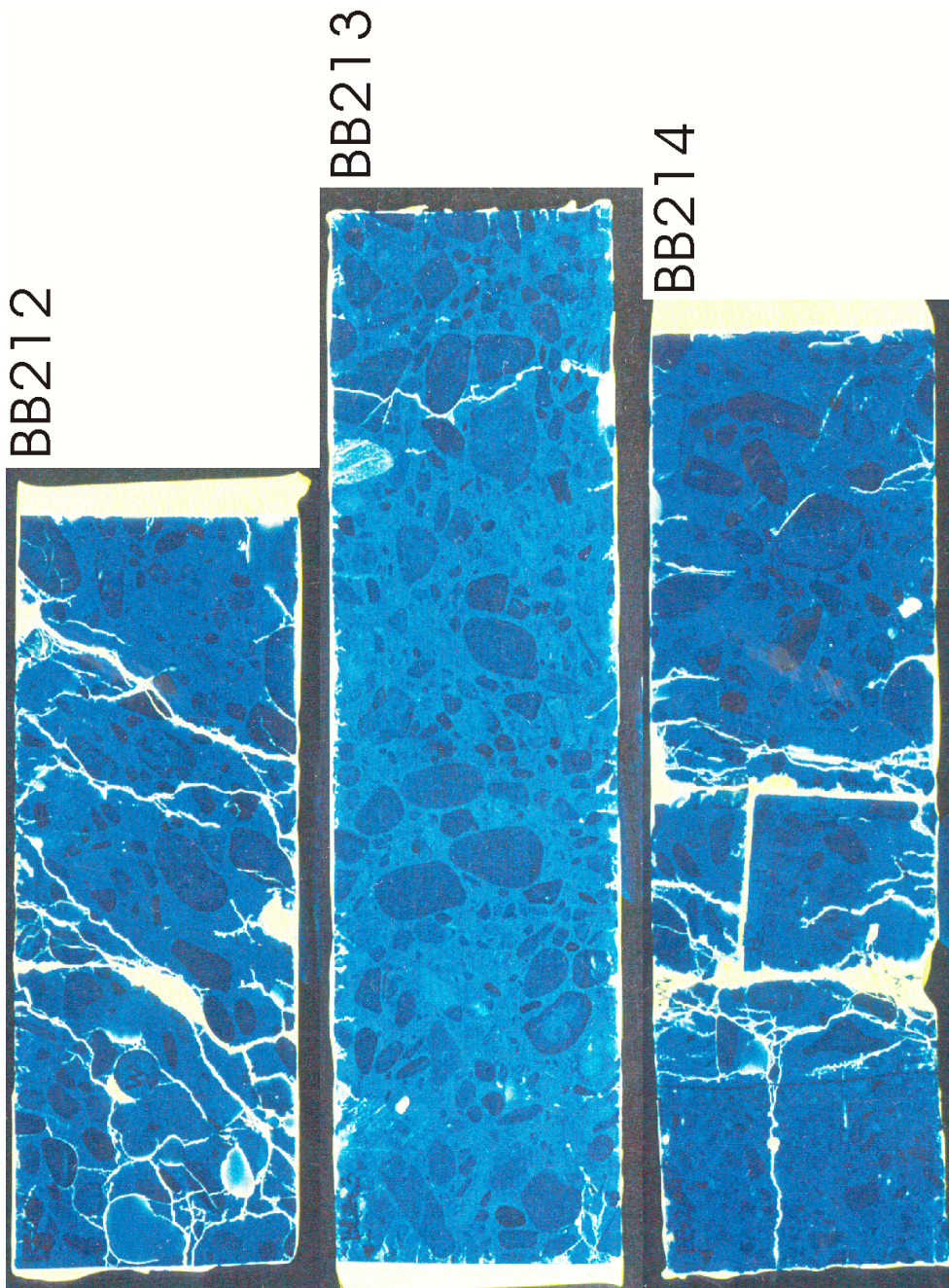


Plate 1: Heemraadsingel cores under fluorescent illumination. Original diameter $\varnothing 100\text{mm}$. The wide N-S crack right above the steel L-profile in BB214 originally contained two parallel $\varnothing 24\text{mm}$ rebars with disintegrated concrete in between. Original top surface to left of this text.

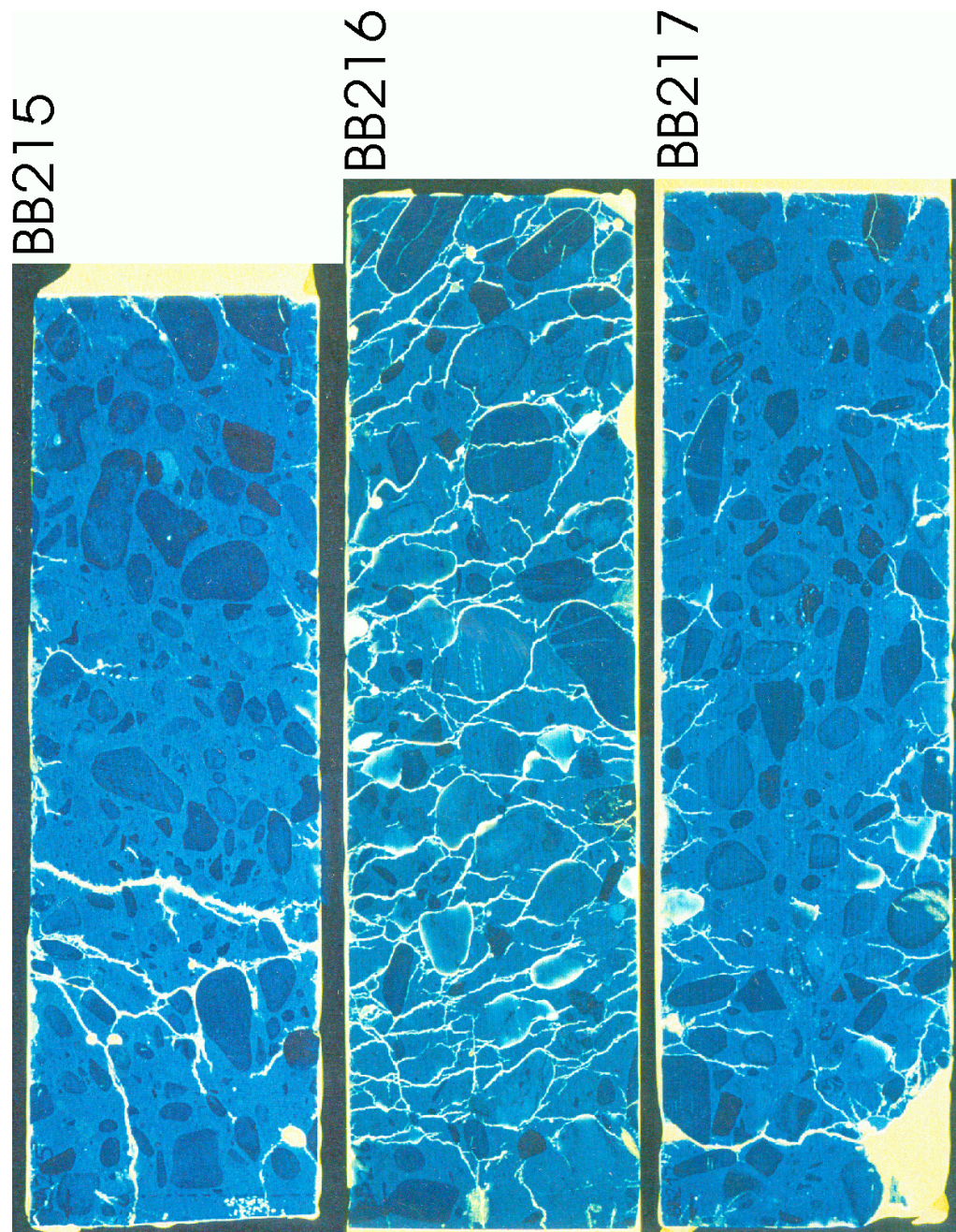


Plate 2: Full cores from structure Wolput under fluorescent illumination. Original diameter \varnothing 100mm. Note the stress-release cracks along the circumference of BB217. Original top surface to the left of this text.

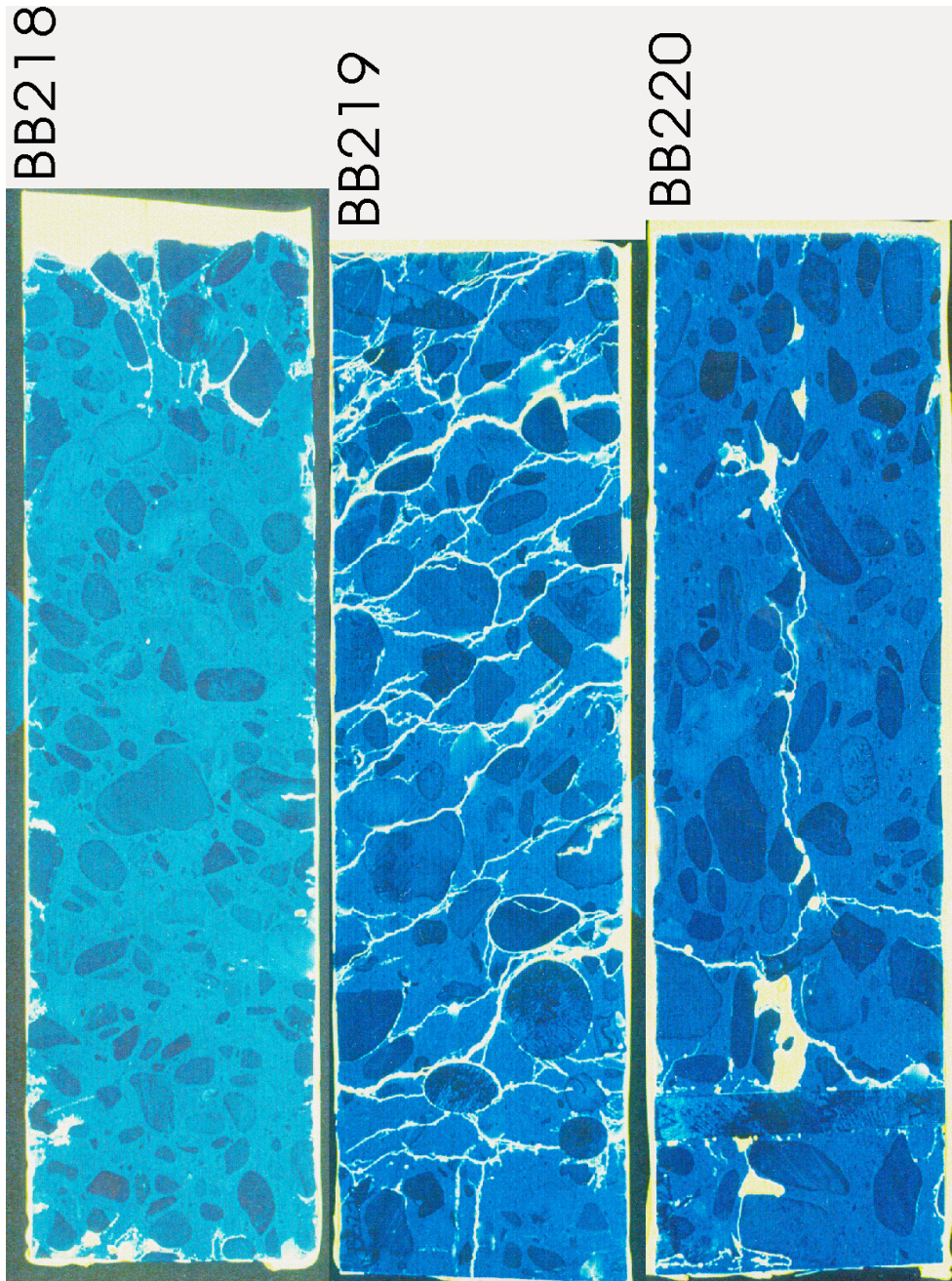
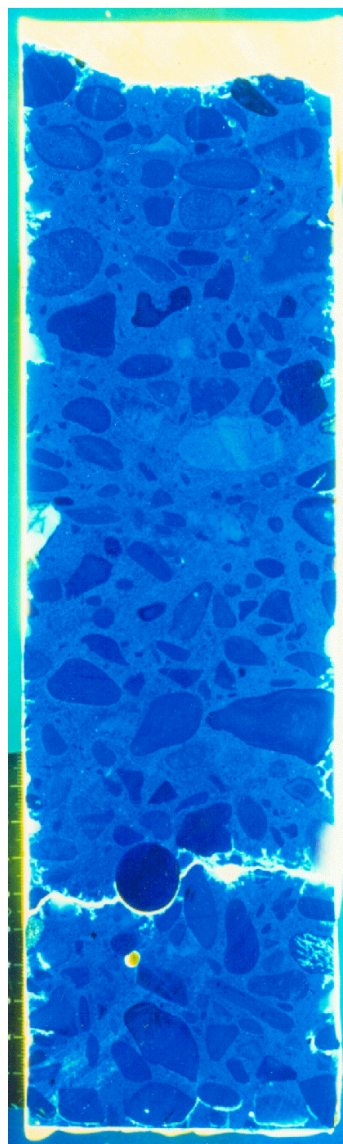
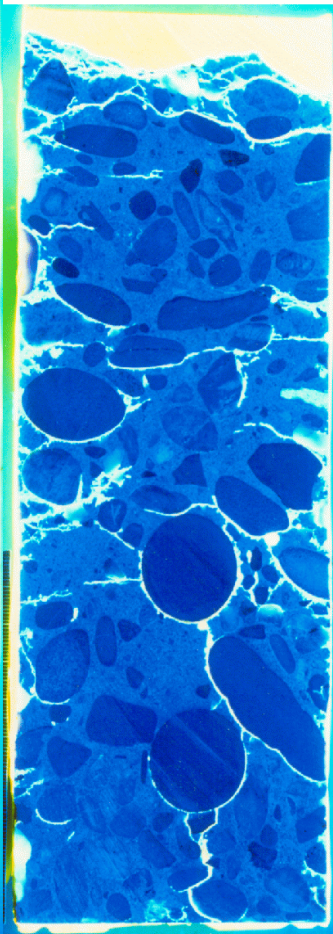


Plate 3: Full cores from structure Vlijmen-Oost under fluorescent illumination. Original diameter $\varnothing 100\text{mm}$. The lengthwise 'crack' in BB220 is not a crack but rather a seam between two concrete batches. Original top surface to the left of this text.

BB240



BB241



BB242

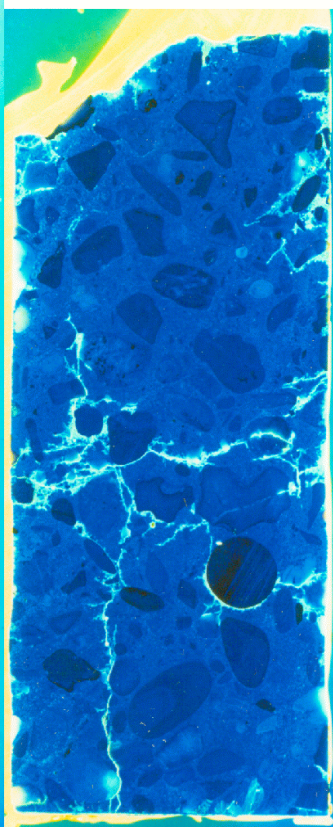
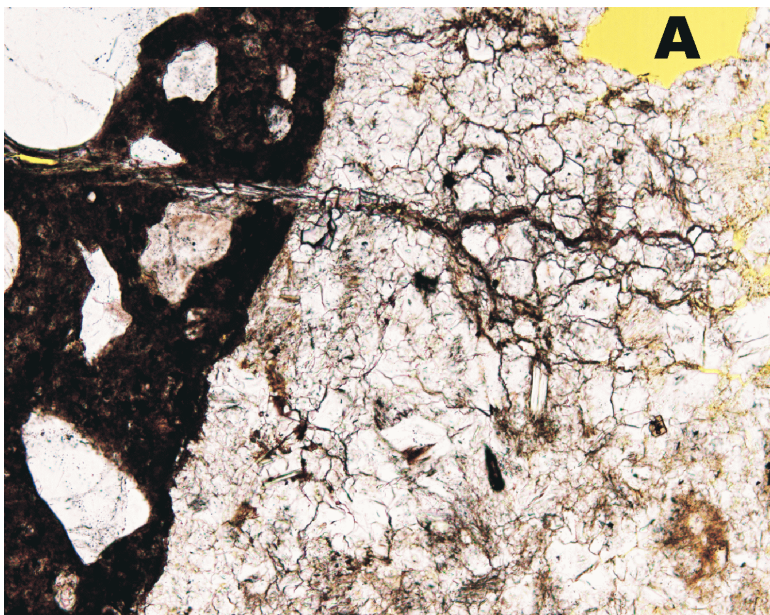
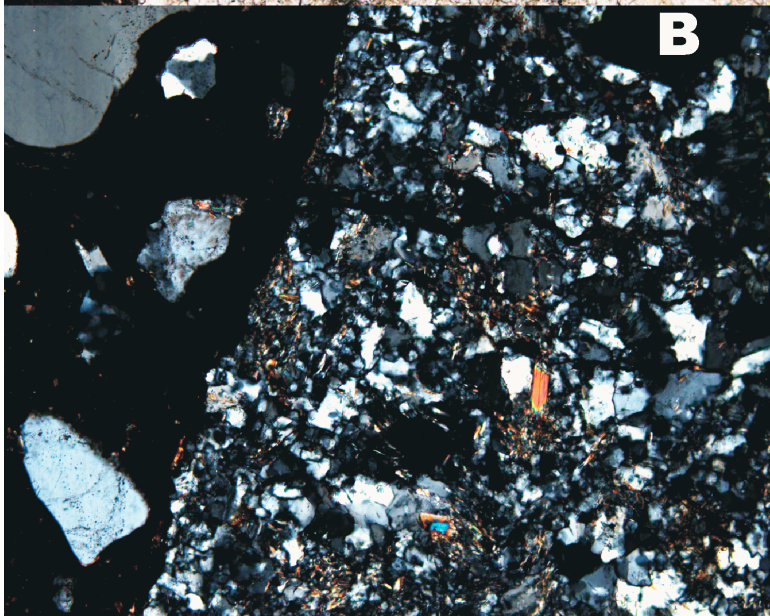


Plate 4: Full cores from structure Zaltbommel under fluorescent illumination. Original diameter \varnothing 100mm. Original top surface to the left of this text.

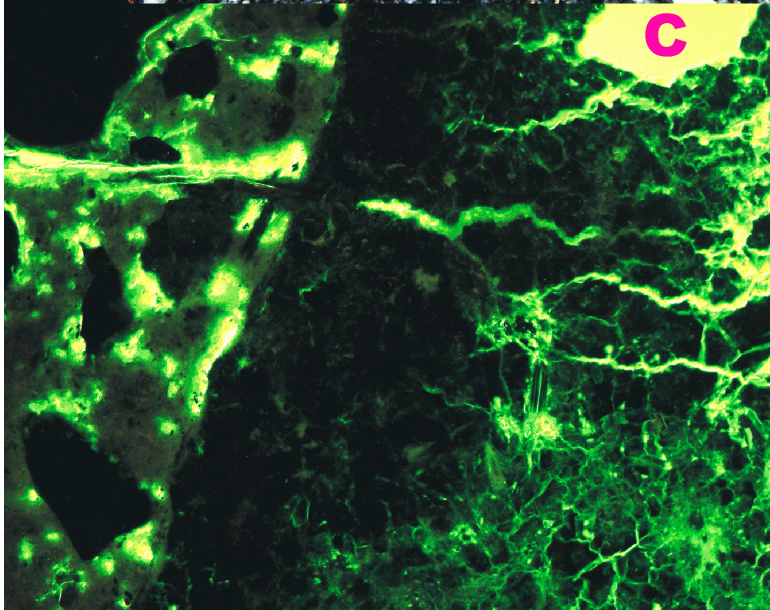
Plate 5a: Alkali-reactive, diagenetically compacted sandstone in plane polarized light (PPL). Sutured quartz grain contacts and enhanced visibility of boundaries between adjacent quartz individuals, and extrusion of ASR-gel into the surrounding paste. Note the detrital muscovite flake at low right of the images' center.



5b: same area as in 5a under crossed polarized light (XPL).



5c: same area as in 5ab under fluorescence (FL). Cracks and interstices are visible in the sandstone interior, and microporosity is clearly enhanced next to the muscovite grain. Magnification 100×.



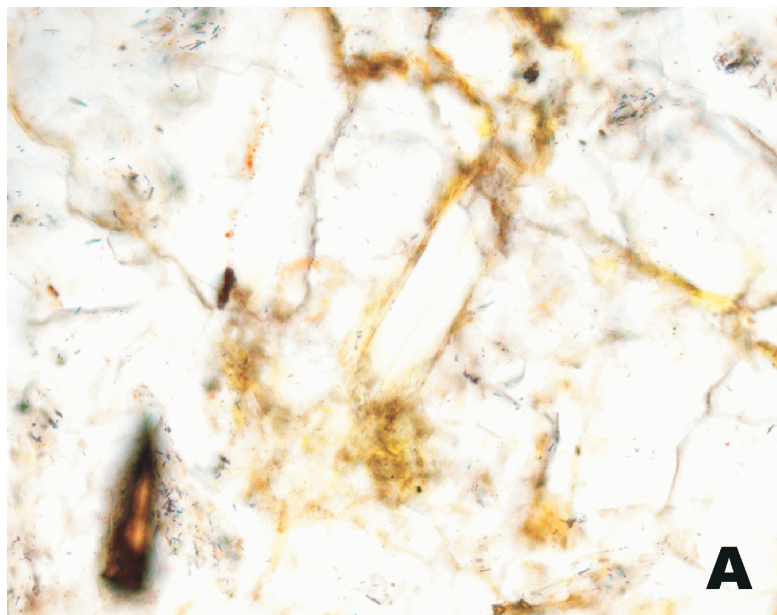
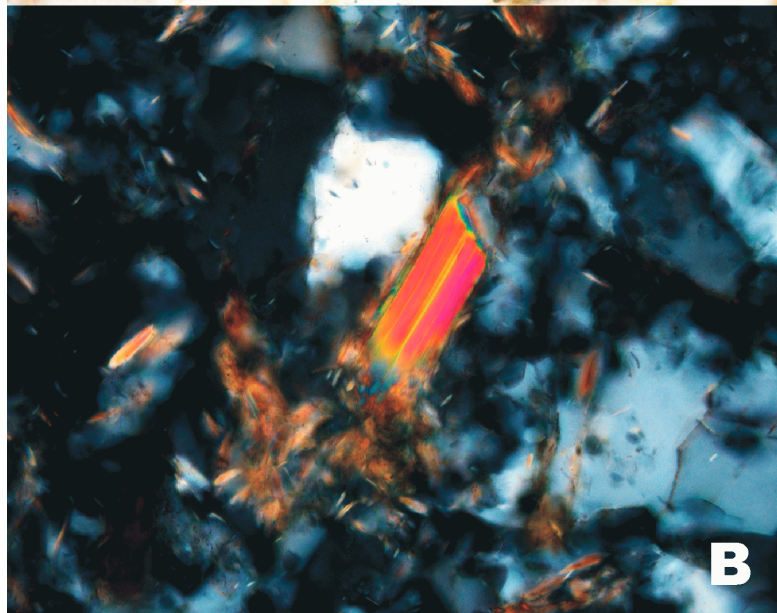
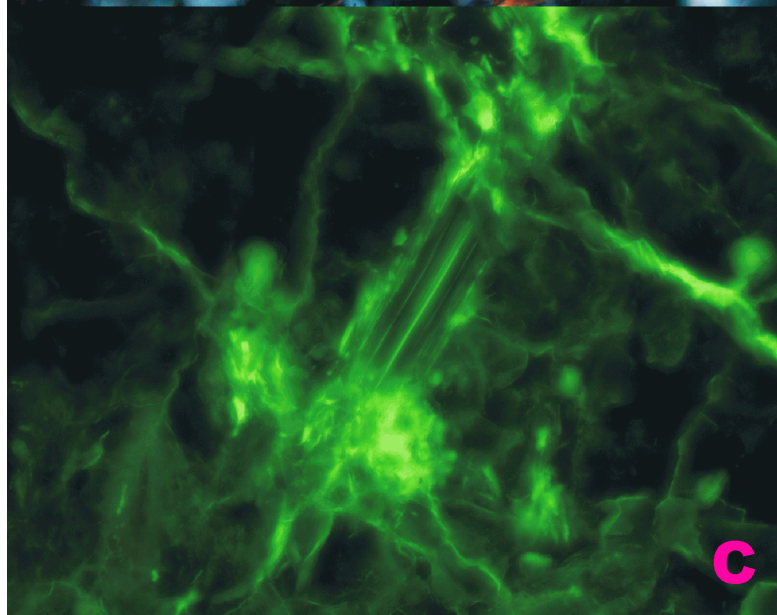


Plate 6a: Details from the muscovite flake in Plate 5 in plane polarized light (PPL). Note the sutured boundaries between adjacent quartz individuals;



6b: same area as in 6a under crossed polarizers (XPL). Sericite flakes can be recognized across the view, but clay minerals, eventually deposited between quartz individuals, are beyond optical resolution.



6c: same area as in 6ab under fluorescence. The interstitial porosity of the sandstone is clearly enhanced near the tips of the muscovite flake in a dumbbell shaped area. (FL). Magnification 400x.

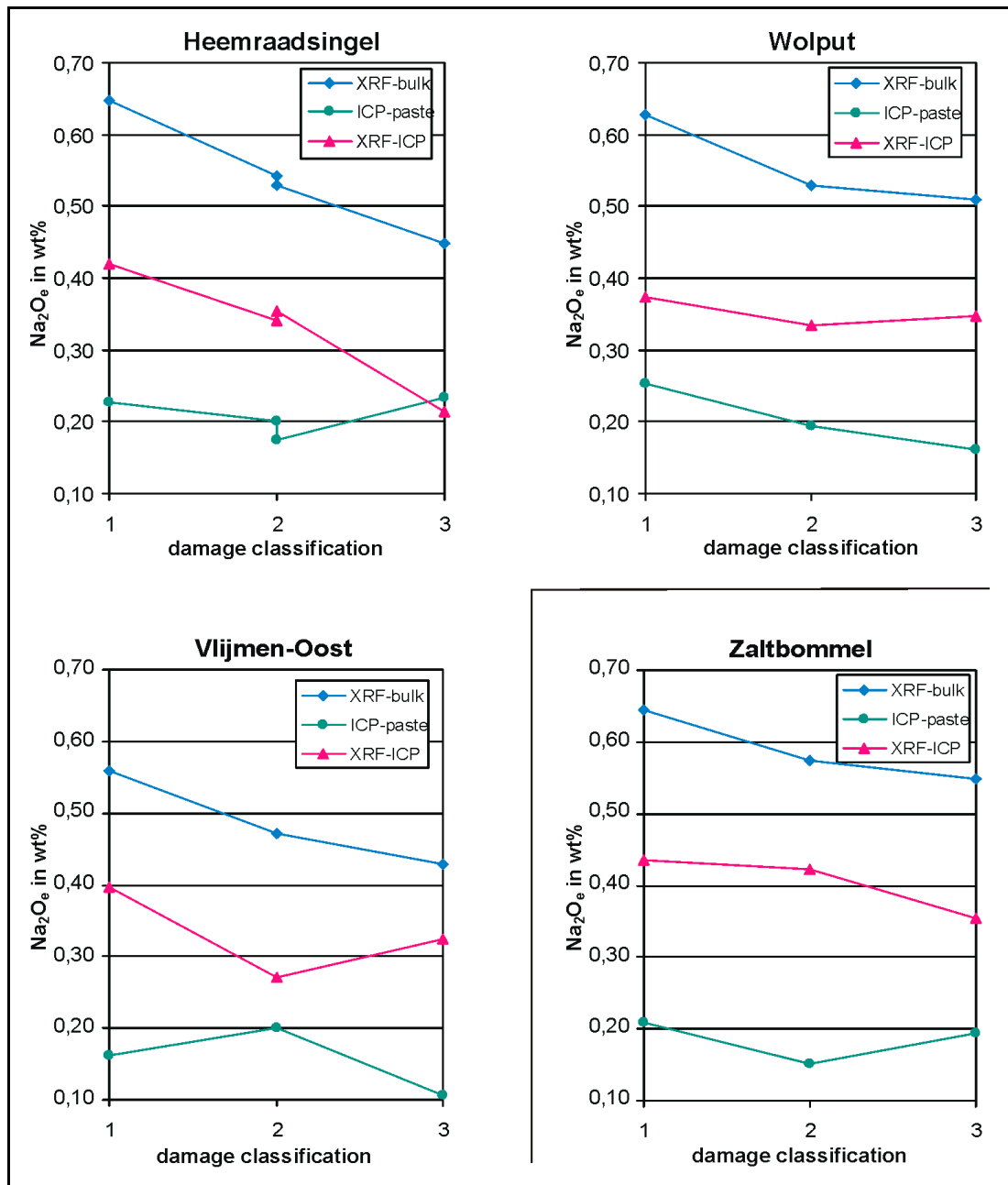
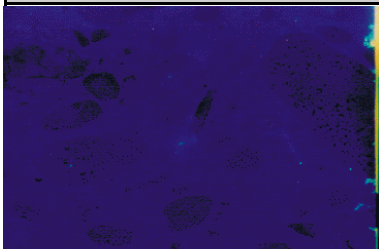
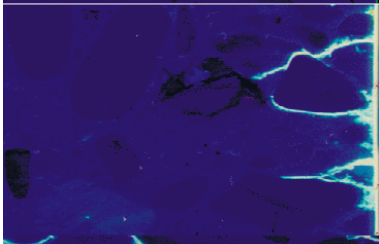
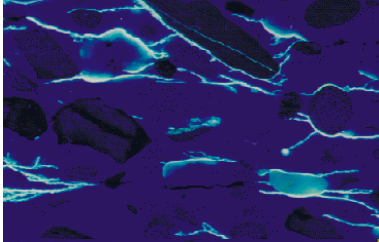
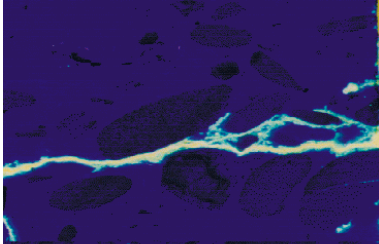
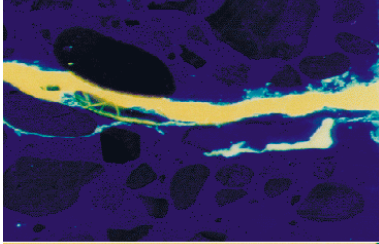
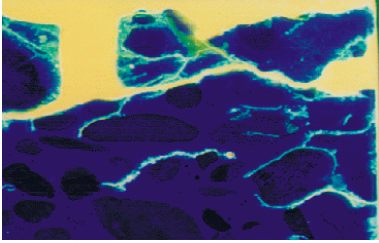


Plate 7: Damage classification versus alkali-contents as measured initially in Chapter 2.

Plate 8: The illustrated damage rating index (DRI) as applied in Chapter 3.

IMAGE	DRI	DESCRIPTION
	0	no cracks visible, pristine concrete
	1	small cracks along the cylindrical core surface (stress relaxation)
	2	small, random, solitary cracks throughout the concrete
	3	one main penetrative crack, parts adhering, coherent concrete
	4	one main penetrative crack, parts separated
	5	incoherent, disintegrated concrete

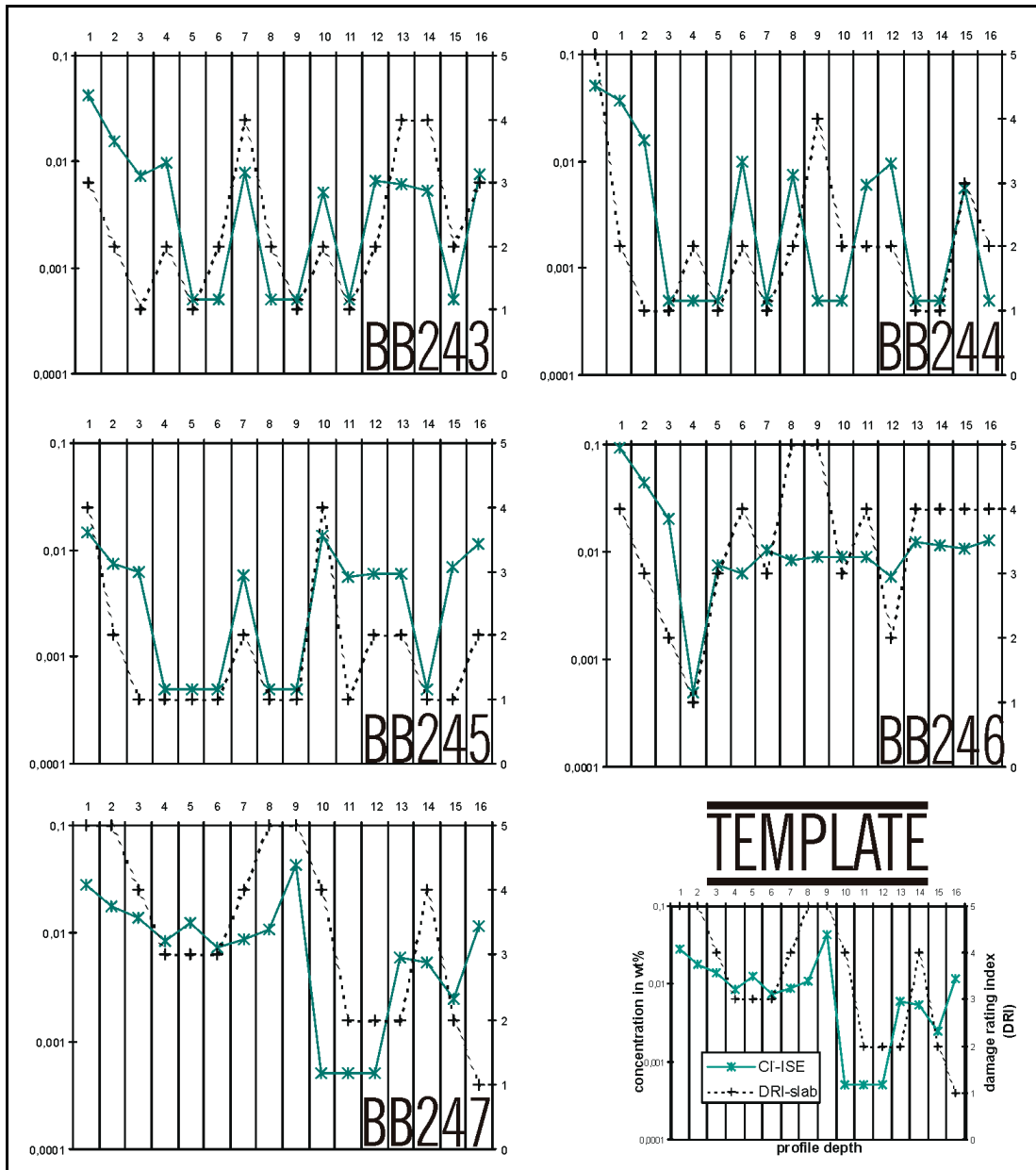


Plate 9: Depth profiles from viaducts Heemraadsingel (BB243-5) and KW5 at Zaltbommel (BB246-7), showing the amount of damage presented as DRI (stippled line; right hand abscissa) versus the chloride content in weight percent (solid, left hand abscissa). Further explanation in Chapter 3.

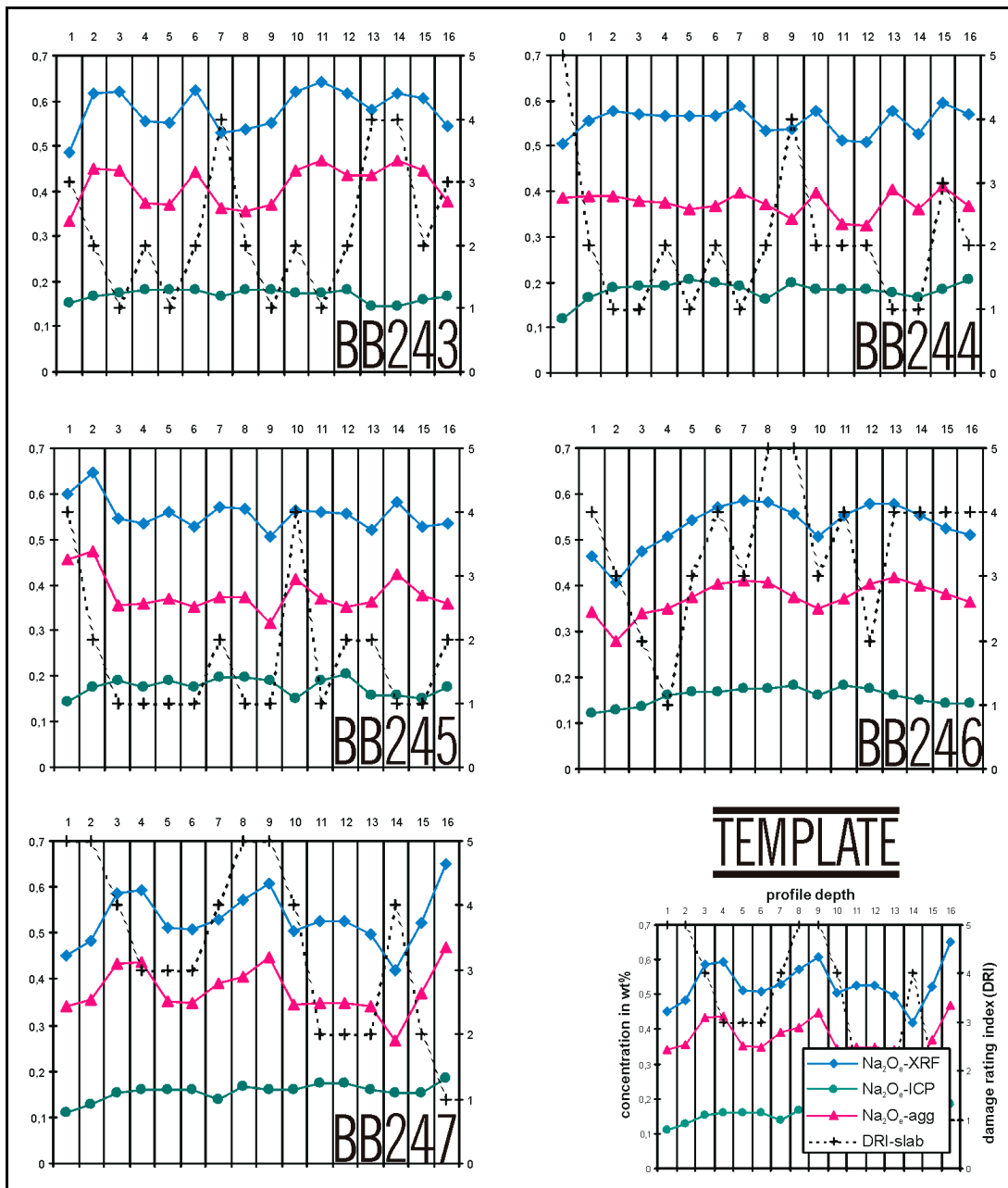


Plate 10: Depth profiles of viaducts Heemraadsingel (BB243-5) and KW5 at Zaltbommel (BB246-7), showing the amount of damage (stippled; right hand abscissa) versus the $\text{Na}_2\text{O}_{\text{eq}}$ in weight percent (different solid colors; left hand abscissa). Further explanation in Chapter 4.

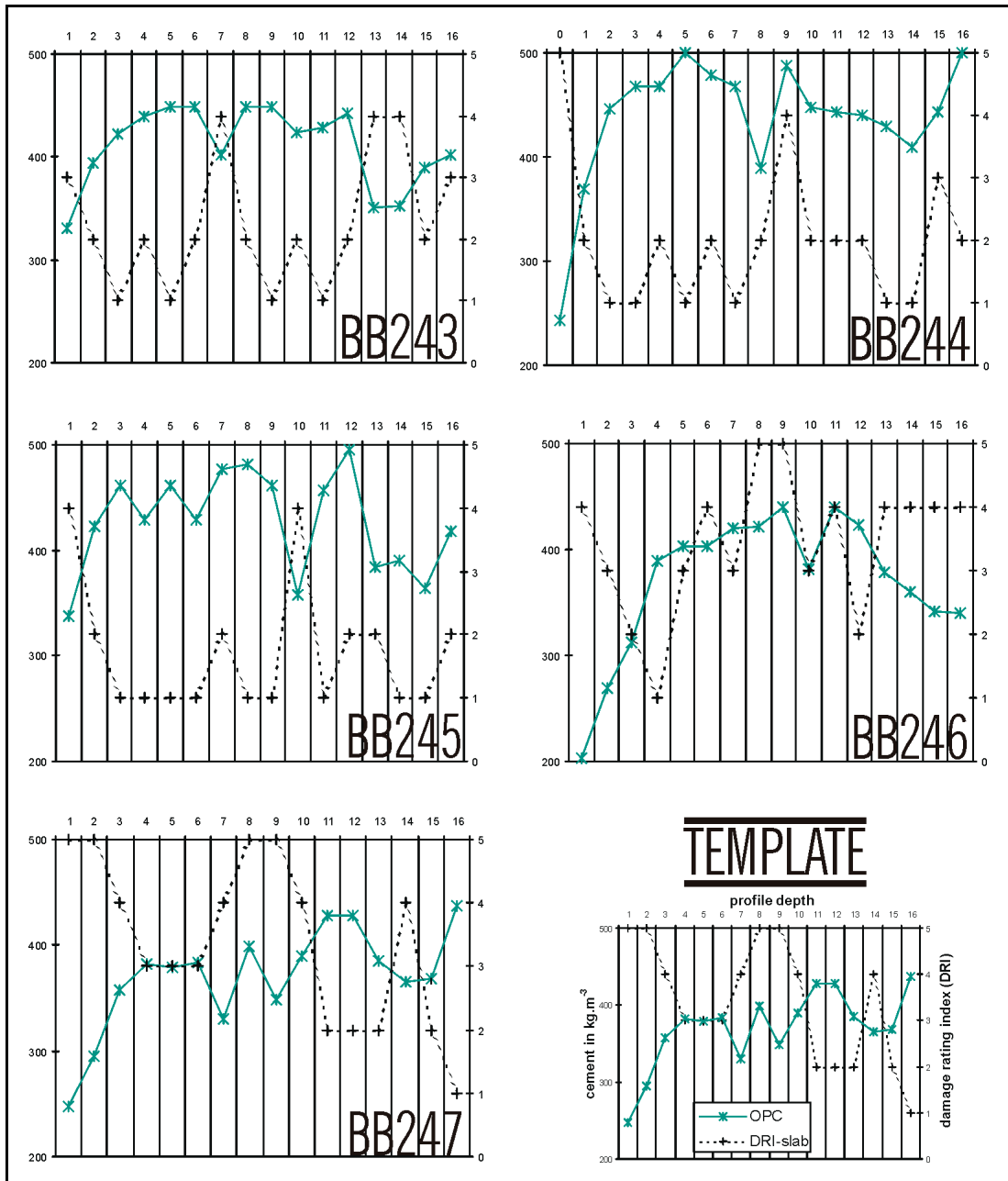


Plate 11: Theoretical cement contents, recalculated from the $\text{Na}_2\text{O}_{\text{eq}}$ -ICP for cement paste (compare with Plate 10). Further explanation in Chapter 4.

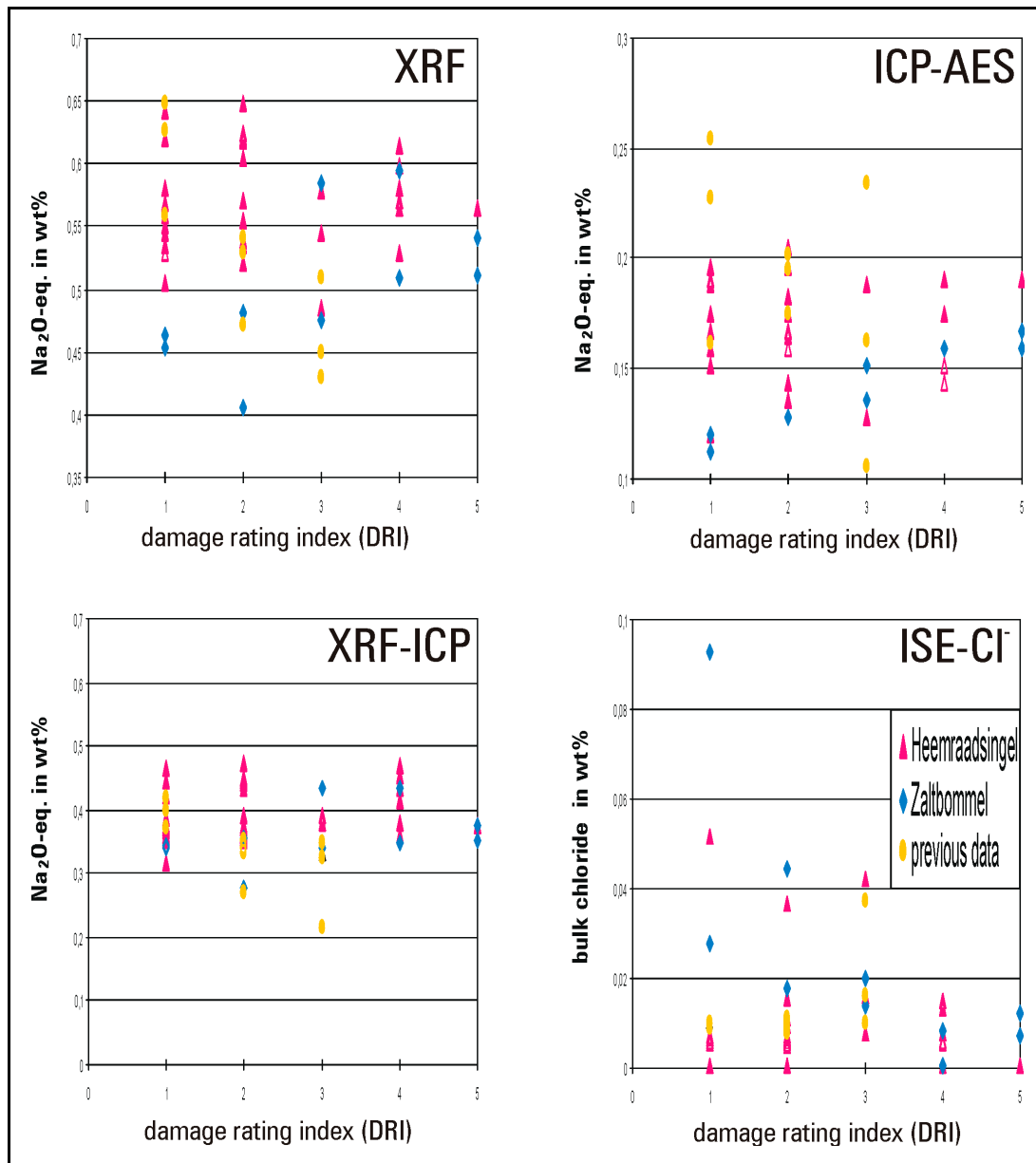


Plate 12: Scattergraphs of the Na₂O_{eq}'s from Plate 10, arranged per DRI. Further explanation in Chapter 4.

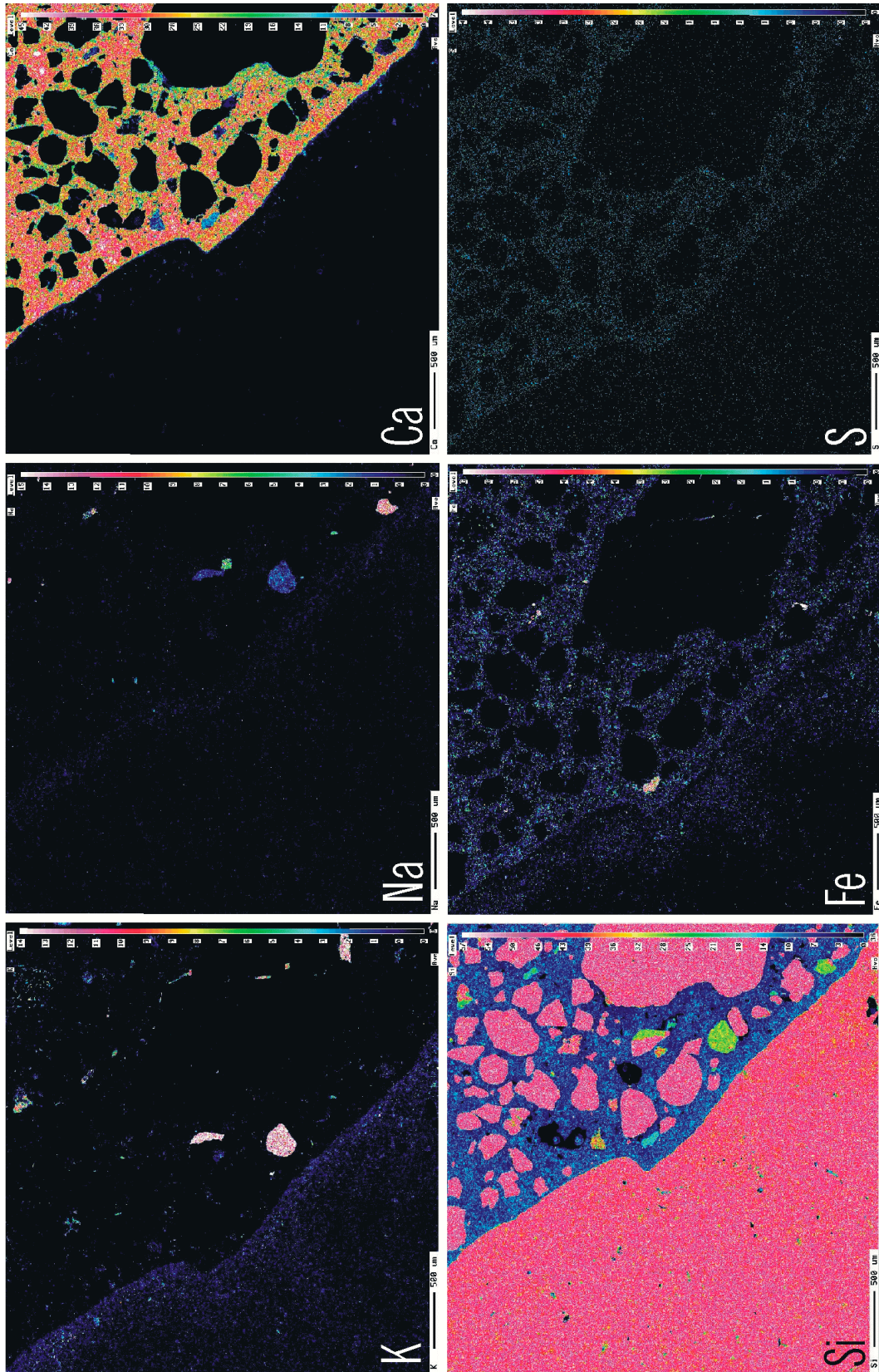


Plate 13: Element maps of intact, uncracked chert. Scale bar is 500µm.

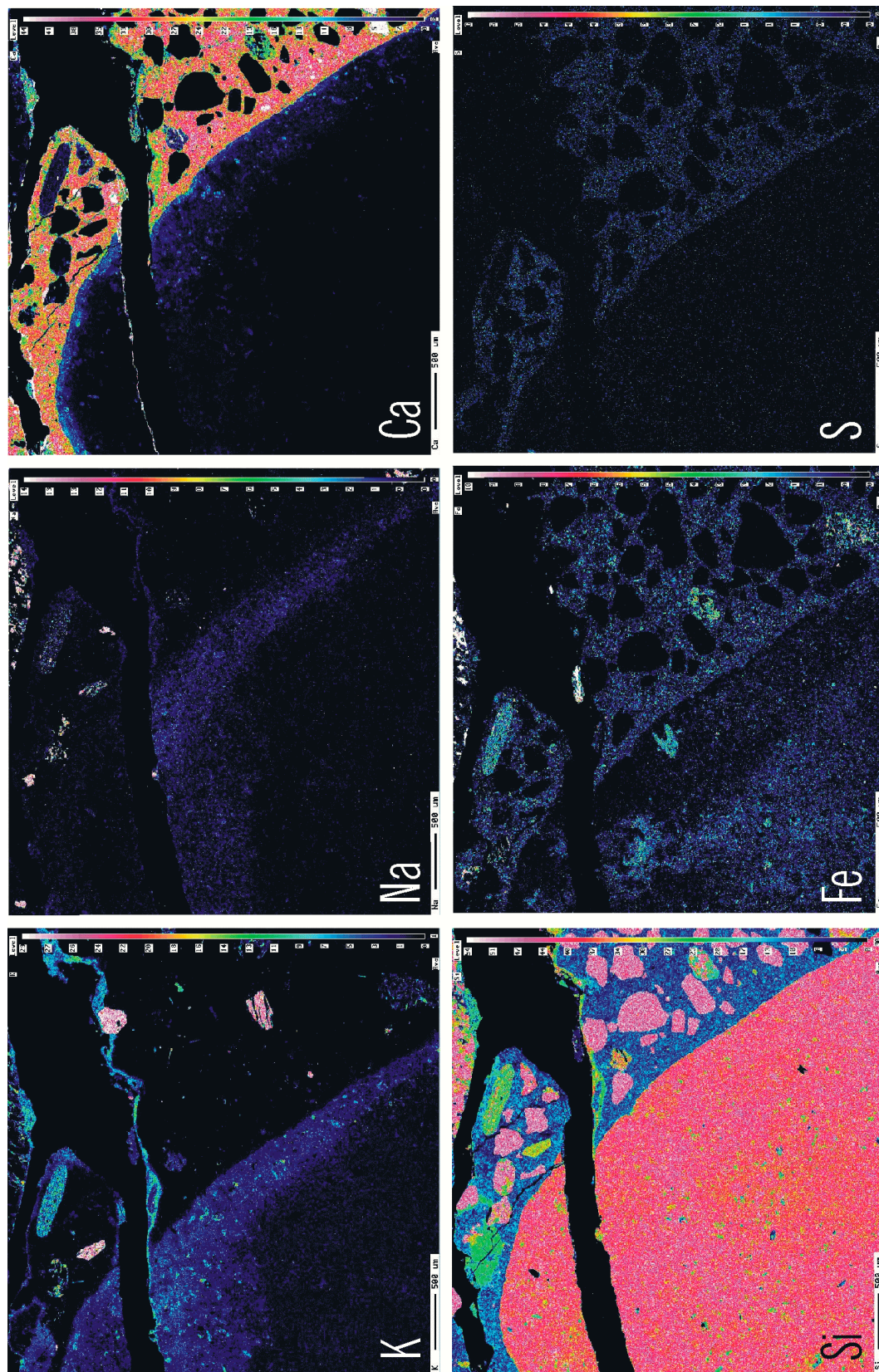


Plate 14: Element maps of the same chert grain as in Plate 13, locally cracked by ASR. Scale bar is 500µm.

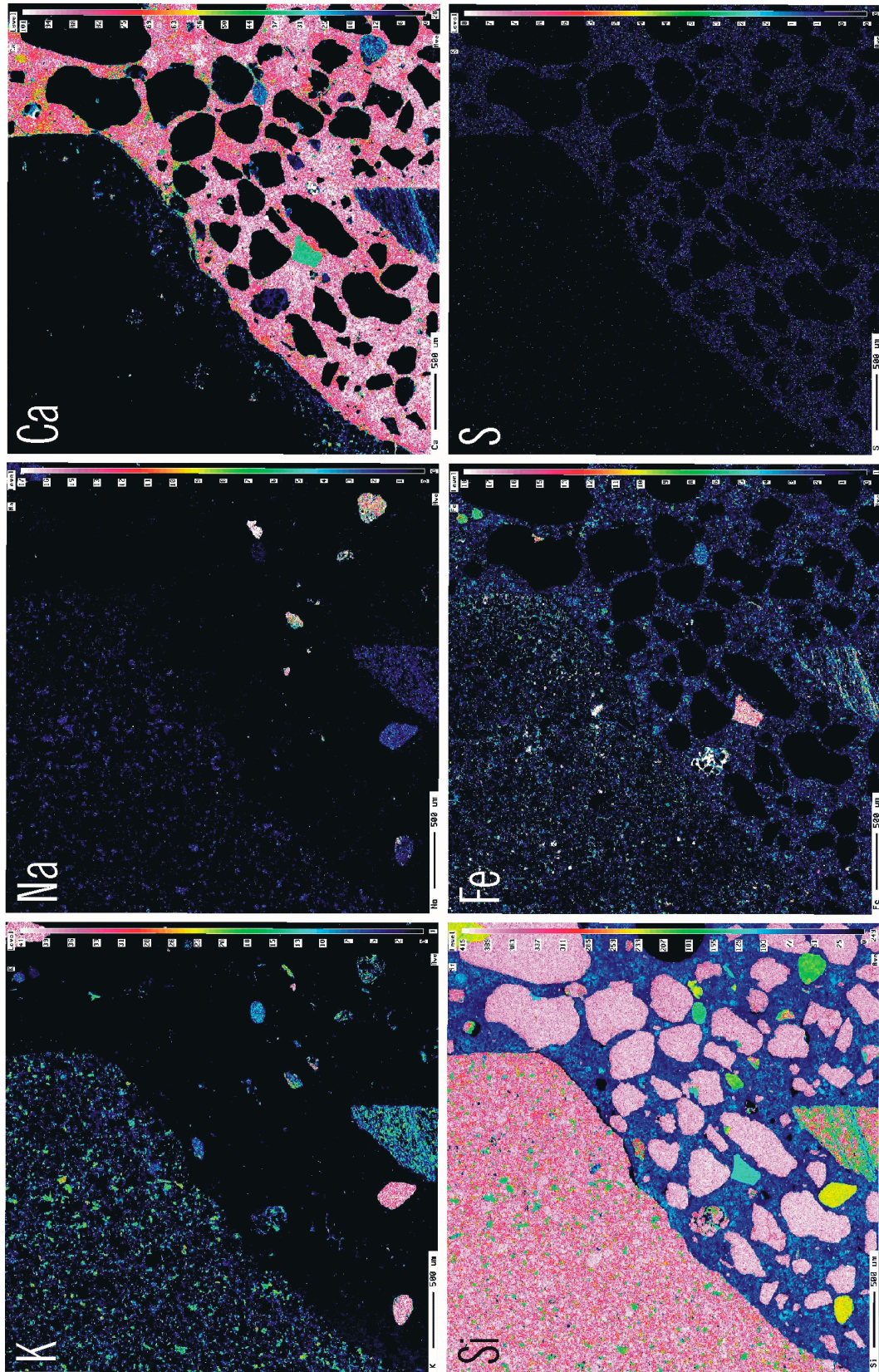


Plate 15: Element maps of intact sandstone. Scale bar is 500µm.

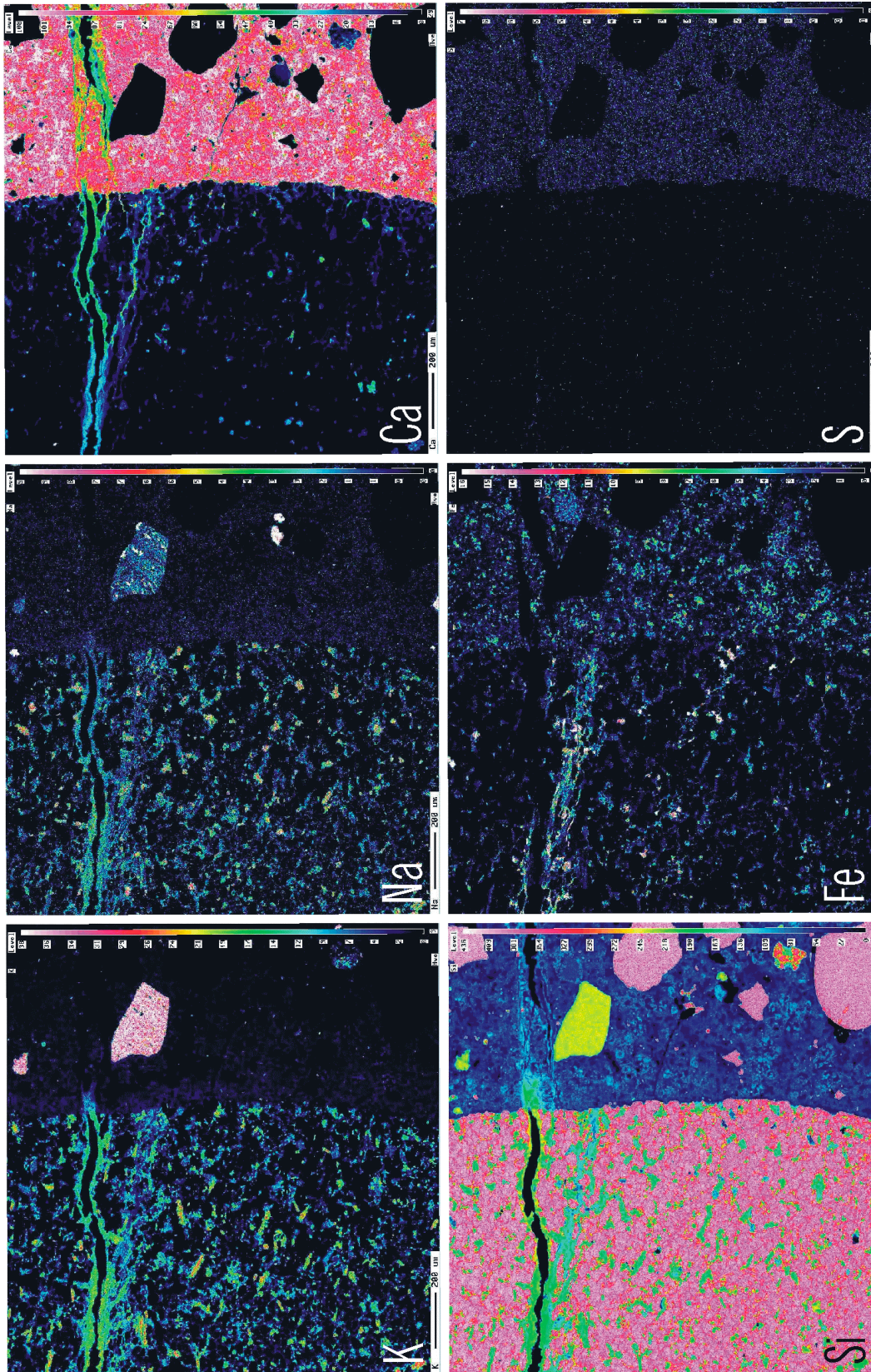


Plate 16: Element maps for a similar sandstone as in Plate 15, locally cracked by ASR. Scale bar is 200µm.